Electrophoretic deposition of nanoparticles for controlled optical properties

Sanaa Shehayeb

THÈSE POUR OBTENIR LE GRADE DE DOCTEUR DE L'UNIVERSITÉ DE MONTPELLIER ET DE L'UNIVERSITÉ LIBANAISE

En Chimie Séparative, Matériaux et Procèdes

École doctorale Chimie Balard-École doctorale de Sciences et Technologies

Unité de recherche Institut de Chimie Séparative de Marcoule (ICSM) et Laboratoire de Catalyse Organométallique et Matériaux (LCOM)

Recepteur Solaire photo-thermique Obtenu par electrophorese des nanoparticules a propriete optique selective

Présentée par Sanaa SHEHAYEB

Le 30 Novembre 2017

Sous la direction de Xavier DESCHANELS et Iyad KARAME

Devant le jury composé de

Lara HAIAOUI, Professeur, American University of Beirut	Présidente-Rapporteur
Ghassan YOUNESS, Professeur, Beirut Arab University	Rapporteur
Bilal NSSOULI, Professeur, CLEA, CNRS-L	Examinateur
Guillaume TOQUER, Maitre de Conference, ENSCM	Examinateur
Xavier DESCHANELS, Chercheur, CEA	Directeur
Iyad KARAME, Professeur, Université Libanaise	Directeur
Leila GHANNAM, Professeur, Université Libanaise	Co-encadrante

UNIVERSITÉ DE MONTPELLIER

"Science knows no country, because knowledge belongs to humanity, and is the torch which illuminates the world."

Louis PASTEUR

Acknowledgements

This work wouldn't have the spirit that it has without the invaluable academic, psychological and support, provided by my thesis supervisors and co-supervisors, colleagues, family and best friends.

I would like first to thank my thesis supervisors Dr. Xavier DESCHANELS (Responsible of LNER laboratory at the ICSM of CEA-Marcoule in France) and Prof. Iyad KARAME (Responsible of LCOM laboratory at the Lebanese University) for their thoughtful encouragement and careful supervision. Their guidance through these three years has empowered me with wide knowledge and better understanding of our subject. I also owe a debt of gratitude to Dr. Guillaume TOQUER (LNER/ICSM) and Prof. Leila GHANNAM (LCOM/LU) for their expert guidance, longtime discussions and tremendous efforts to offer every possible help to ensure a successful understanding and progress of the thesis work. Thank you for sharing the excitement of every discovery and for your unwavering enthusiasm every time I came up with a question. Thank you for your advice, patience and faith in me.

The ICSM is composed of different laboratories where I have found answers and solutions to most of my questions and challenges. I would like to thank all the ICSM family starting by the LNER group members and other laboratories' permanents, engineers and technicians as well as post-docs and PhD students for their technical help and useful discussions. Equally, I would like to thank the EDST research platforms at the Lebanese university for the technical experimental help. I would like to thank particularly: Dr. Diane REBISCOUL (LNER/ICSM) for all the useful discussions as well as for advising and sharing her experience with me. Eng. Cyrielle REY (LNER/ICSM), thank you for all the useful discussions and all the chemical supplies especially the almighty "Isopropanol". Similarly, I would also like to thank Dr. Jeremy CAUSSE and Eng. Alban JONCHERE (L2IA/ICSM) for all the spectroscopy analysis. Dr. Joseph LAUTRU, Dr. Renaud PODOR, and Dr. Michael ODORICO from the L2ME group at the ICSM, adding Bruno CORSO, Xavier LEGOFF and Henri-Pierre BRAU for all your tremendous efforts and the beautiful SEM and AFM images. Finally, I would like to thank Dr. Olivier DIAT (responsible of L2IA group) and L2IA group members for welcoming me at their laboratory to perform several experiments.

It is also my pleasure to thank the administrative department at the ICSM, Mr. Stéphane PELLET-ROSTAING (Director/ICSM) and Mrs. Dominique ALPE-CONCHY (Assistant director/ICSM) for their warm reception at the institute. Similarly, I would like to

thank Mrs. Helene MARTIN, Mrs. Vainina RUSSELLO and Mrs. Mathilde DIAS for their continuous help, cheerful spirit and lovely company.

It is also my pleasure to acknowledge Prof. Lara HALAOUI (Professor at AUB) for honoring me by being the president of the jury of the defense and for accepting to review the work of this PhD. along with Prof. Ghassan YOUNESS (Dean of Faculty of Sciences at BAU). Your valuable comments and advices have added a great value to the work reported. I would also like to thank Prof. Bilal NSSOULI for accepting to participate in the jury.

Moreover, our deepest appreciation goes to the University of Montpellier and the Lebanese National Council of Scientific Research (CNRS-L) for the co-joint funding of the work of this PhD.

I also wish to express my appreciation to many colleagues and friends for the discussion, communication and lovely company: Tamir SUKHBAATAR, Denis HAUCHARD, Suson SANANES I., Cindy COLLAINE, Helene ARENA, Clementine MANSAS, Frederick LACEMON, Sarah HOCINE, Ricardo NAVAM, Carlos ARRAMBIDE C., Moheddine WEHBI, Wissam ZAHREDDINE, Bilal ALASSAAD, Samira ZAHER, Shouaa BOUFAOUR, Nadim EID, Fatima RIDA, Dr. Sanaa N. SHEHAYEB, "French dudes", and all the members of Khota Ashabab for their continuous support.

Every challenging work needs self-efforts as well as guidance and support of those who are very close to our heart. I dedicate this PhD to my sweet and loving family and especially my dad (Saad) and second mothers (Randa and Ola) whose affection, love, encouragement and prayers during day and night made the hardest challenges bearable. Finally, my deepest acknowledgements and dedication goes to my reason of being, my loving husband Mazen, for sharing my wish to complete this PhD and being a constant source of encouragement and support.

To the strongest and kindest soul, to the memory of my mother, engraved in my heart and mind forever. You are my deepest motivation!

Abstract

The production of hot water by using efficient photothermal solar collectors is growing in importance to limit the use of fossil fuels. Black copper (CuO) has proved to be one of the viable solar-selective coatings owing to its nearly intrinsic properties. The formation of a tandem absorber based on CuO thin film deposited onto a highly IR reflecting metallic substrate is processed by electrophoretic deposition (EPD).

In this way, the stabilization of a CuO colloidal suspension is studied previously by adding $Mg(NO_3)_2$ in isopropanol (IPA) or polyethyleneimine (PEI) in water suspension. Both acts as positively charging agents and allow the realization of a cathodic EPD. The colloidal stability as a function of the stabilizing agent content is studied prior to EPD, by dynamic light scattering (DLS) coupled with laser doppler velocimetry.

CuO tandem absorbers are obtained by varying different EPD parameters to control the final thickness and also the morphology. Consequently, the optical selectivity of the tandem material is tuned and optimized. The deposition yield is compared relative to the different applied voltage range, deposition time and nanoparticle concentrations. Homogeneous deposits are obtained for $[CuO]=5x10^{-4}$ g/cm^3 from both suspensions. The optimum applied voltage is found to be 50 V.cm^{-1} for IPA suspension and 2 V.cm^{-1} for H_2O suspension, for deposition times of 30 mins and 120 mins, respectively. The composition and the thickness of the coatings are analysed by Grazing Incidence X-ray diffraction (GIXRD), scanning electron microscopy (SEM) and the density is obtained from energy-dispersive X-ray spectroscopy (EDX). For the previously mentioned optimized conditions, CuO tandem absorbers derived from IPA suspension possess a density of 1.69 g/cm^3 with high surface roughness. In contrast, homogeneous and regular surfaces is obtained from water suspensions having a higher density of 5.7 g/cm^3.

Moreover, absorptance (α) and emittance (ε) are calculated from the reflectance spectra of the UV-Vis-NIR and the Fourier transform InfraRed (FTIR) spectroscopy, respectively. α and ε were combined to determine the efficiency (η) of the tandem material. Tandems obtained from water suspension has η=0.8 -0.87 while from IPA η=0.7. Besides, the applicability of this EPD is checked by performing other deposit of CuO on metallic substrates of different types.

CuO tandems obtained from water suspensions are clearly more prominent to be used as solar selective tandem absorbers due to the high calculated η value reported. The efficiency of such selective tandem absorbers was further enhanced by carbonization (pyrolysis under inert atmosphere) of the polymer (PEI) embedded in the coating. Otherwise, a thin film of SiO_2 nanoparticles was deposited at the surface of the selective tandem absorbers to protect them. Both routes were successfully processed and proved to raise η to 0.9.

Résumé

La production d'eau chaude *via* des capteurs solaires photothermiques est une technique en expansion qui permet de limiter l'utilisation des sources conventionnelles d'énergie (combustibles fossiles, nucléaire…). Le cuivre noir (CuO) s'avère être un matériau possédant des propriétés optiques sélectives intéressantes pour cette application. Ainsi, son utilisation au sein d'un absorbeur sous forme d'un matériau « tandem » est une solution envisagée. Le challenge que nous avons tenté de relever au cours de ce travail, a été de réaliser ce type de matériaux par dépôt électrophorétique (EPD) de nanoparticules de CuO déposé sur un substrat métallique de type wafer de silicium métallisé (platine ou or). Ce substrat « modèle » a été utilisé premièrement car il facilite la mise en œuvre de techniques de caractérisation telles que l'analyse par diffraction X en incidence rasante (GIXRD) ou l'analyse en coupe transversale par microscopie électronique à balayage. Pour ce faire, la stabilisation de la suspension colloïdale de CuO (condition *sine qua non* pour la réalisation d'un dépôt électrophorétique) a été étudiée dans un solvant organique tel que l'isopropanol par ajout de $Mg(NO_3)_2$, ainsi qu'n milieu aqueux en utilisant comme dispersant du polyéthylèneimine. Ces deux adjuvants agissent comme des agents stabilisants et apportent aux nanoparticules une charge positive ce qui permet la réalisation d'un EPD cathodique. Afin d'optimiser la formulation des suspensions, la stabilité colloïdale en fonction de la teneur en stabilisant a été étudiée avant tout dépôt, par diffusion dynamique de la lumière (DLS) couplée à la vélocimétrie laser à effet Doppler.

Différents revêtements contenant le CuO ont été obtenus en faisant varier les paramètres inhérents à l'EPD (temps de dépôt, champ électrique, concentration en nanoparticules) pour pouvoir contrôler l'épaisseur finale ainsi que la morphologie. Par conséquent, la sélectivité optique et le rendement du tandem résultants peuvent être optimisés en jouant sur l'ensemble de ces paramètres. Des dépôts homogènes ont été obtenus pour [CuO] =$5x10^{-4}$ $g.cm^{-3}$ pour les deux milieux. Les meilleures conditions sont 50 $V.cm^{-1}$ // 30 mn pour la suspension d'IPA et 2 $V.cm^{-1}$ // 120 mn pour la suspension en milieu aqueux. La composition et l'épaisseur des dépôts sont analysées par GIXRD, et par microscopie électronique (MEB-EDS). Pour les conditions optimisées, les matériaux tandem obtenus à partir de la suspension CuO/IPA possèdent une densité de 1.69 g/cm^3 avec de la rugosité micrométrique. Au contraire, des surfaces homogènes et régulières sont obtenues en milieu aqueux où les dépôts présentent une densité beaucoup plus élevée autour de 5.7 $g.cm^{-3}$.

L'absorptance (α) et l'émittance (ε) ont été calculées à partir des spectres de réflectance de l'UV-VIS-NIR et de l'Infrarouge lointain, respectivement. L'efficacité (η) du revêtement tandem obtenu en milieu aqueux se situe dans l'intervalle 0.80-0.87 alors qu'elle n'est seulement de 0.7 dans l'IPA. De plus, la faisabilité de l'EPD sur d'autres substrats métalliques plus conventionnels (acier, aluminium, cuivre) en vue d'une application a été explorée. Par ailleurs, l'efficacité des dépôts a pu être améliorée par des post-traitements de deux types. D'une part, en pyrolysant à 400°C sous atmosphère inerte le polymère (PEI) incorporé dans le revêtement. Le carbone résiduel ainsi obtenu à l'issue de cette pyrolyse a permis d'augmenter l'absorptance. D'autre part, en déposant sur la surface des revêtements une couche de nanoparticules de SiO_2 qui joue le rôle de couche anti-réflective tout en permettant de protéger la surface de CuO. Les deux voies ont été réalisées avec succès et le rendement le plus élevé obtenu pour ces revêtements est de 0.9 (valeur comparable aux absorbeurs commerciaux)

Table of Contents

Acronyms

PV: Photovoltaic

FPC: Flat plate collector

STE: Solar Thermal Energy

CSP: Concentrated Solar power

AFM: Atomic Force Microscopy

CE: Counter Electrode

DLS: Dynamic Light Scattering

EDX: Electron Dispersive X-Ray spectroscopy

EPD: Electrophoretic Deposition

RE: Reference Electrode

WE: Working Electrode

IR: Infra-Red

SEM: Scanning Electron Microscopy

PAA: Poly(acrylic acid)

PEI: Poly-ethylenimine

PVA: Poly(vinyl alcohol)

SAXS: Small Angle X-ray Scattering

GIXRD: Grazing Incidence X-Ray Diffraction

ELD: Electrolytic Deposition

Résumé Générale de La Thèse

L'énergie fournie par le soleil en une heure est équivalente à notre consommation annuelle d'énergie. Ainsi, l'énergie solaire peut subvenir à tous nos besoins, si on parvenait à la convertir d'une façon efficace et économiquement viable. Elle peut être exploitée par deux méthodes : la conversion photothermique ou la conversion photovoltaïque. La première technologie consiste à récupérer l'énergie fournie par le soleil pour chauffer un fluide, la seconde consiste à convertir le rayonnement solaire en électricité. Malgré l'exploitation accrue des énergies renouvelables ces dernières années, ce mode de production ne représente que 19 % de l'énergie produite à l'échelle de la planète, dont0.70 % relatif à l'énergie solaire. La plus grande partie de cette énergie est produite par du solaire photothermique (71%), pour le chauffage d'eau et des applications domestiques.

L'énergie thermique basse température se présente comme le moyen le plus intéressant d'exploiter l'énergie solaire. Dans le monde, c'est la chine qui détient le record de consommation d'énergie thermique solaire (65.07 %), suivi par l'union européenne (11.73 %) et les États-Unis (6.74 %). Ce sont les pays en voie de développement qui sont les moins avancés sur ce point dans ce domaine. Cette faible production est dûe au manque de conscience de l'importance de l'énergie solaire dans ces pays et au haut coût élevé des installations de capteurs solaires photothermiques.

Le principe de base de la conversion photothermique de l'énergie solaire consiste à transférer le rayonnement solaire à un fluide caloporteur par l'intermédiaire d'un élément absorbeur sélectif. L'absorbeur sélectif est constitué d'un matériau ou d'un assemblage de matériau qui possède une absorptivité élevée (typiquement $\alpha>0,9$), équivalente à une réflectance basse, sur la bande spectrale d'émission solaire (0.2-2 µm) et une émissivité faible ($\varepsilon<0,1$), c'est-à-dire une réflectance élevée dans la région spectrale de l'infrarouge (2-20 µm) lointain. Il n'existe pas de composés qui possèdent intrinsèquement ces propriétés. Un moyen utilisé pour s'approcher des propriétés d'un absorbeur « idéal », consiste à réaliser un matériel tandem constitué d'un revêtement très absorbant déposé sur un substrat métallique (réflecteur en Infra Rouge).

Les films minces métalliques d'oxydes ont reçu une attention particulière pour des applications dans le domaine du solaire, en raison de leur potentialité pour réaliser des absorbeurs sélectifs, des couches anti réflectives…). Les couches d'oxyde de Cuivre CuO, ou "Cuivre Noir" ont notamment été utilisées pour des applications en tant qu'absorbeur solaire

sélectif du fait de leurs propriétés optiques. Des telles surfaces ont été obtenues par coating (dip-coating, spin-coating) de sels de cuivre (chlorure d'acétate ou d'acétate de cuivre) sur des substrats métalliques Cependant, de telles méthodes nécessitent un post-traitement thermique ou chimique, après le dépôt. Ce traitement peut conduire à la formation d'autres formes de sous-oxydes Cu_2O qui dégrade les propriétés thermiques et optiques de l'absorbeur.

La technique de Dépôt ElectroPhorétique (EPD) est largement utilisée depuis toujours, pour la réalisation de couches céramiques. Plus récemment, l'EPD est utilisée pour le dépôt de revêtements uniformes sur des substrats de formes diverses ; pour la formation des revêtements composites ou encore pour le dépôt de films minces de nanoparticules ou de nanotubes de carbone. Des progrès importants ont été réalisés ces dernières années, sur la compréhension des mécanismes de base de l'EPD, l'expansion des applications traditionnelles de l'EPD et l'exploration des nouveaux domaines d'application à des combinaisons de matériaux.

L'EPD est basée sur la migration de particules chargées par l'application d'un champ électrique et leur dépôt sur l'électrode de signe opposée. L'EPD est considérée comme une technique flexible permettant ainsi le contrôle de l'épaisseur et de la morphologie des films déposés en faisant variés les paramètres du procédé. Il est nécessaire d'avoir une suspension stable, homogène et chargée pour que les particules forment un dépôt. Pour un absorbeur tandem, l'épaisseur de la couche d'absorbeur doit être minutieusement contrôlée pour préserver les propriétés de réflexion du substrat, l'EPD est une technique qui offre une telle possibilité. La plus grande difficulté réside dans l'obtention d'une suspension stable de CuO.

L'objectif de ce travail est la réalisation par EPD d'absorbeurs tandem à base d'oxydes de cuivre pour des applications photo-thermiques à basse température. Les connaissances acquises sur ce système pourront être utilisées sur d'autres systèmes. Un effort particulier a été fait pour trouver les conditions de stabilisation d'une suspension de nanoparticules de CuO en milieu aqueux et dans l'isopropanol. Cette thèse est composée de cinq chapitres principaux, comme suit :

Le chapitre un est divisé en deux parties. La première partie explique le concept général et les procédés utilisés pour produire des absorbeurs sélectifs tandem et en particulier des absorbeurs à base de CuO. L'autre partie présente le procédé général d'EPD, l'influence des paramètres opératoires sur les caractéristiques du dépôt et les différents mécanismes associés à la technique EPD.

Dans le chapitre deux, les différents techniques et les procédures utilisées dans cette étude sont présentées ainsi que les méthodes utilisées pour leur caractérisation.

Dans le chapitre trois sont présentés les travaux réalisés sur la suspension de CuO dans l'isopropanol en utilisant le $Mg(NO_3)_2.6H_2O$ comme stabilisant cationique. Cette suspension a été déposée par EPD pour former un absorbeur tandem sélectif à base de CuO. L'épaisseur de la couche CuO a été contrôlée en faisant varier les paramètres opératoires lors du dépôt par EPD.

Dans le chapitre quatre, la stabilisation d'une suspension de CuO dans l'eau est présentée, en utilisant le polymère cationique (PEI). Cette suspension a été utilisée pour réaliser des absorbeurs tandem par dépôt électrophorétique (EPD). L'influence des paramètres expérimentaux tels que le champ électrique appliqué, le temps de dépôt est présenté, ainsi que l'évaluation de la sélectivité spectrale des films obtenus.

Dans le chapitre cinq est présentée l'influence du substrat utilisé sur la sélectivité des films obtenus par électrodéposition des suspensions CuO/IPA et CuO/H2O. Cette étude prouve l'applicabilité de l'EPD à différents types de substrats (électrode de dépôt), pour former des absorbeurs solaires tandem efficaces. L'influence de post-traitement (recuit thermique, dépôt de couches anti-réflexion) sur la sélectivité est également présentée.

En Conclusion :

L'EPD est un procédé ancien pour l'obtention de films céramiques qui pour la première fois a été mis en œuvre pour obtenir des absorbeurs solaires tandem. CuO est un bon candidat pour cette application car il présente une certaine sélectivité spectrale. Les conditions d'obtention d'une suspension colloïdale stable, prérequis indispensable pour la réalisation d'un dépôt par EPD, ont été optimisées en milieu aqueux par l'ajout d'un polymère cationique (PEI) et en milieu isopropanol par l'ajout d'un stabilisant le $Mg(NO_3)_2.6H_2O$. Les paramètres du procédé EPD (temps de dépôt, champ appliqué…) ont été étudiés afin d'optimiser la sélectivité ainsi que la densification des revêtements. La densité de la couche déposée a été calculée en utilisant l'équation de Hamaker. L'épaisseur du dépôt augmente linéairement en fonction du temps de dépôt et du champ appliqué. Pour le système IPA/CuO, la densité du revêtement augmente en fonction du champ électrique appliqué, variant entre 0.35, 0.49 et 1.69 g/cm3 pour respectivement des champs de 5, 10, 50 $V.cm^{-1}$. Les valeurs d'absorbance (α) et d'émissivité (ε) optimales obtenues sont 0.7 et 0.14 respectivement. Pour le système eau/CuO, comme nous l'avons dit le poly-ethylenimine a été

utilisé comme agent de stabilisation cationique, qui a d'abord un rôle de complexation de Cu^{2+} à la surface de nanoparticules de CuO, puis qui permet de charger positivement ces nanoparticules. La cinétique de dépôt a été étudiée à pH=9. Dans ces conditions, la densité du revêtement calculée en utilisant l'équation Hamaker est de 5.7 g/cm^3. Cette valeur est en accord avec d'autres estimations, 5.9 g/cm^3, faites à partir du logiciel X-film et des analyses obtenues spectroscopie à rayons X à dispersion d'énergie (EDS)).

Finalement, les deux systèmes ont donné des résultats reproductibles, applicables à différents substrats métalliques (Cu/acier inox/Al). Les revêtements tandems obtenus à partir de nanoparticules de CuO dispersées dans l'eau sont plus homogènes et plus denses en comparaison avec les revêtements élaborés à partir des suspensions CuO/IPA. Le rendement maximal obtenu sur les revêtements de type CuO/PEI est de 0.84-0.87, et d'environ 0.7 pour les revêtements CuO/IPA. Une couche protective et anti réflective de SiO_2 de 100 nm d'épaisseur a été déposée sur les revêtements CuO/PEI. Dans ces conditions les propriétés optiques des revêtements ont été améliorées, et le rendement a atteint la valeur de 0.9. Une autre voie d'amélioration a consisté à calciner les revêtements de type CuO/PEI pour transformer le polymère en carbone, afin d'améliorer l'absorbance et de stabiliser le film. Cette optimisation a également conduit à obtenir un rendement proche de 0.9.

General Introduction

The energy that is provided by the sun in one hour is equivalent to our global energy consumption for one year. Thus, solar energy is able to supply all our needs, if it is converted economically and efficiently to renewable energy. It is harnessed either by thermal energy technology or by photovoltaic technology. The former relies on the heat supplied by the sun while the latter converts this solar radiation into electricity. Despite the increased exploitation of renewable energy, still accounts only 19% of the global energy consumption. Only 0.70% of the global renewable enrgy, is solar energy, in which 71% are dedicated to solar thermal energy for water heating and domestic applications (see Figure 1).

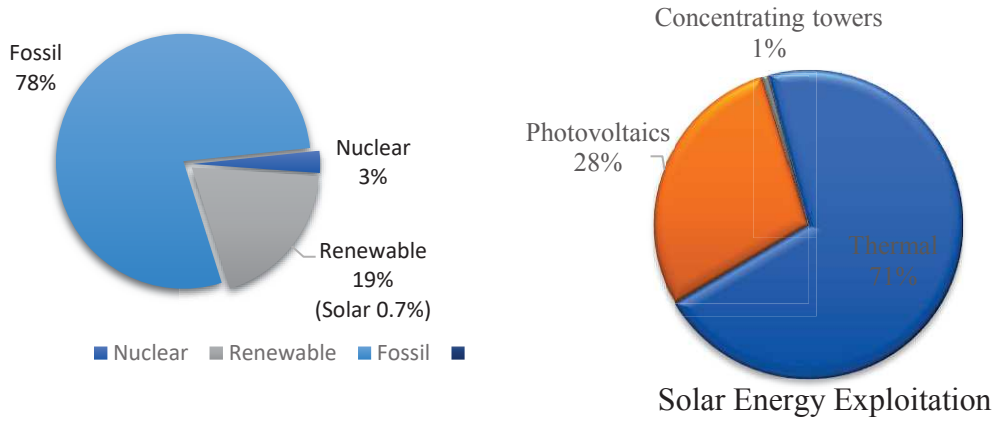

Figure 1: Global energy consumption and solar energy exploitation (retrieved from www.cnrs.fr/sagascience)

Low temperature solar thermal energy presents the most obvious way of harnessing solar energy. It is usually installed on rooftops and used to heat water to supply taps and radiators. The highest solar thermal energy consumption is used by China (65.07 %), followed by the European union (11.73%) and the united states (6.74%), while the lowest consumptions are recorded for underdeveloped countries (see Figure 2). The low consumption in different countries is usually due to lack of awareness of the importance of solar energy and the high cost of installation of solar absorbers.

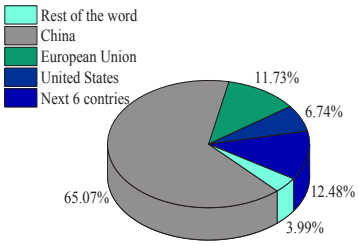

Figure 2: Solar water heaters global consumption around the world. (retrieved from www.cnrs.fr/sagascience)

The basic principle of solar thermal conversion is the transfer of solar radiant energy into heat transfer fluid through an absorber. Selective absorbers for thermal energy conversion requires a high absorptivity or equivalently low reflectance over the spectral range of solar emission (0.5-2 μm) and a low emittance or high reflectance in the mid and far infrared spectral region (2-20μm). Finding a single material whose intrinsic optical excitation spectrum matches the required spectral profile of an ideal absorber has proved to be difficult. Thus, a tandem material consisting of a highly absorbing coating deposited on an IR reflecting metallic substrate, is usually regarded as a solution.

Metal oxide thin films have received great attention due to various applications finding also a significant role in solar energy applications. For decades Copper oxide layers or “Black Copper” have been well investigated as a solar selective absorber thank of their interesting spectral profile. Such surfaces were usually formed on IR reflecting metallic substrates by several processes starting from copper salts (copper acetate or copper chloride). More recent studies have used spin coating, dip coating and many other wet deposition techniques. However, such methods usually require a post deposition step involving thermal treatment that could lead to the formation of other Cu forms that are known to degrade the thermal and optical properties of the absorber.

Until the 1990s, EPD was widely known for ceramic processing. Nowadays EPD continues to attract attention as a processing technique used for the deposition of uniform coatings on substrates of various shapes, for the formation of composite coatings and most importantly for the deposition of thin films of nanoparticles or carbon nanotubes. Key advances have been made toward understanding the basic mechanisms of EPD of nano-structures, expanding traditional applications of EPD and exploring new application areas and new materials combinations.

EPD is based on the migration of charged particles upon the application of an electric field and their deposition to the opposite sign electrode to which they are attracted. EPD is considered as versatile for the ability to control the thickness and morphology of the deposited films by varying simple EPD parameters. The basic principle of a successful EPD is to obtain a charged stable dispersion of the particles to be deposited. In a tandem absorber, the thickness of the absorber layer is important to be controlled in order to preserve the properties of the substrate and the EPD offers such possibility. CuO has proved to be a potential absorber layer in tandem absorbers for its high absorptance value. The formation of a thin CuO coating on a metallic substrate could be achieved by EPD if a stable suspension of CuO could be formed.

Achieving the aim of this PhD project will prove another range of applications for EPD as well as a simple, cost effective and fast way to form copper oxide tandem absorbers for low temperature thermal applications. It will open the path for other traditionally used materials to be formed and processed by EPD. Finding a suitable dispersing medium for CuO will expand the understanding and the research on the stabilization of CuO nanoparticles

The work of this PhD is presented in this thesis composed of five main chapters, briefly explained in the paragraph that follows:

Chapter One is divided into two distinct parts. The first part explains the general concept and the traditional processes used to produce thermal tandem absorbers, in particular CuO tandem absorbers. The second part discusses EPD process in general and its different parameters and mechanisms.

Chapter two presents the different techniques and procedures followed to form spectrally selective coatings by EPD and the methods used for their characterization.

In Chapter three we discuss the stabilization of CuO suspension in IPA using $Mg(NO_3)_2.6H_2O$ as positively charging agent. Then the EPD of this suspension was performed to form spectrally selective CuO tandem absorber. The thickness of the CuO layer was varied by varying different EPD parameters.

Chapter four debates the stabilization of CuO suspension in water using cationic polymer (PEI) followed by the EPD of this suspension. EPD parameters as applied electric field and deposition time are also studied. The spectral selectivity of the deposits was also evaluated.

Chapter five includes the variation of substrate used for both systems (recall the systems). This proves the applicability of EPD to different types of deposition electrodes, in order to form efficient tandem low temperature solar thermal absorbers Then the efficiency of the optimum system was ameliorated either by several post deposition procedures.

Chapter One:

Designing Solar Tandem Absorbers by EPD

1. Introduction

In this chapter, the general concepts of solar thermal energy and electrophoretic deposition technique are presented. In the first part, the composition, the formation and the processing technique of tandem solar absorbers are presented. In the second part, the EPD technique, parameters and mechanisms controlling the deposition process are shown. Finally, the possibility of tailoring a tandem solar absorber of CuO by EPD is discussed.

1.1. Solar Thermal energy

Solar thermal energy (STE) is the direct transformation of solar energy into heat thus it is the most obvious way to use solar energy. Compared to photovoltaics (PV), it presents 72 % of the solar energy technologies around the world. STE finds various applications for industrial and domestic use determined by the operation temperature of the absorber and the mode of conversion of energy. It is classified into high temperature, mid-temperature and low temperature absorbers (see Table 1.1). STE is either directly transformed into heat for water heating or concentrated for higher temperature applications as solar cookers or solar power towers.

Table 1.1: Mode of transformation of energy

Type	Low temperature	Mid temperature	High temperature
T (°C)	~100	100<T<300	T>600
Application	Domestic water heating	Cooking, refrigeration and AC	Electricity production, heat processing
Example	 Flat plate collector	 Solar cooker	 Solar power tower

The most simple and obvious application for the thermal transformation of solar energy is for water heating. The setup of a flat plate collectors (FPC) is represented in Figure 1.1. It is used to supply residential buildings with hot water and heat. Solar radiation is trapped by the outer glass and transformed to the heats the metal tubes containing a coolant (mixture of water and antifreeze) through an absorber. Then when the coolant is sufficiently

heated, it is pumped through a heat exchanger that is connected to a water supply. In order for the fluid to be heated, the light should be efficiently captured by the collector with minimized optical losses at the surface of the absorber.

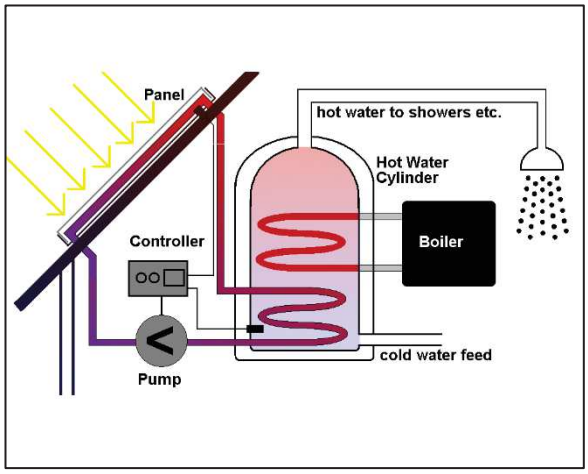

Figure 1.1: Principle of operation of flat plate collectors and storage tank collectors.

A solar selective absorber should efficiently capture solar energy in the high intensity visible and near-infrared spectral regions while maintaining weak thermal infrared radiating properties in the Mid-Far IR. The solar hemispherical spectral irradiance for Air Mass (AM) 1.5 in the wavelength range 0.3 to 4.045μm, the black body radiation spectrum calculated from Planck's law for three different temperatures in the mid-far IR range, and the step function of ideal solar selective coating are presented in Figure 1.2. This shows that selective absorbers are required to have a high absorptance, α (>0.9) (*i.e.* low reflectance) over the spectral range of solar emission (0.5-2.5 μm). A non-selective absorber as a black body will lose the absorber energy as thermal radiation in the IR region. Thus, a selective absorber is required also to have a low emittance, ε (<0.1) (*i.e.* high reflectance) in the mid and far infrared spectral region (2.5-20μm) [2, 3].

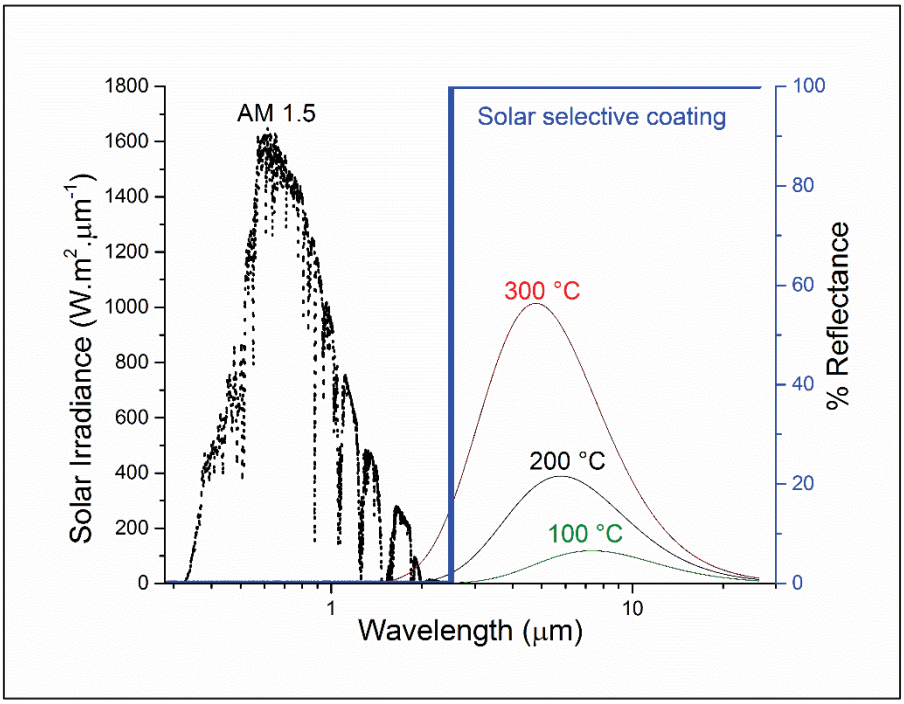

Figure 1.2: Solar hemispherical spectral irradiance for Air Mass (AM) 1.5, black body radiation with increasing temperature, and the step function of ideal solar selective coating.

The solar absorptance α of a surface may be defined as the weighted fraction (by total power density) of the absorbed radiation to that incident on the surface, given by:

$$\alpha = \frac{\int_{0.28}^{2} I_{solar}(\lambda)[1 - R(\lambda)]\, d\lambda}{\int_{0.28}^{2} I_{solar}(\lambda)\, d\lambda} \qquad 1.1$$

Where $R(\lambda)$ is the spectral reflectance of the sample surface and $I_{solar}(\lambda)$ is the normal spectral irradiance, defined by the ISO standard 9845-1 (1992) for air mass (AM) 1.5. The equation 1.1 completely describes the collection ability of the material over a given wavelength range, without any consideration given to the losses due to thermal emittance, hence the lower and the upper limit of the integration correspond to the solar spectrum range between 0.28 and 2 μm, respectively. Besides, the thermal emittance ε of a surface is defined from the weighted fraction (by total power density) of the emitted radiation at a particular temperature to the spectral Planck radiation at the same temperature as the surface:

$$\varepsilon = \frac{\int_{2}^{16} I_{blackbody}(\lambda, T)[1 - R(\lambda)]\, d\lambda}{\int_{2}^{16} I_{blackbody}(\lambda, T)\, d\lambda} \qquad 1.2$$

The formalism of Equations (1.1) and (1.2) is justified by considering the Figure 1.2, which clearly illustrates that there is minimal overlap of the solar spectrum at AM 1.5 (ISO

standard 9845−1, 1992) and the blackbody spectra increasing with the temperature 100, 200 and 300 °C.

The simplified heat balance of a solar collector is therefore given by the following expression [1]:

$$Q_u = S_c.\alpha.E_s - S_a.\varepsilon.\sigma(T_a^4 - T_0^4) - S_a.H.(T_a - T_0) \quad 1.3$$

Where Q_u is the useful energy, S_c the collector's surface (m^2), S_a the absorber surface (m^2), H the thermal losses coefficient by conduction and convection (W. m^{-2}. K^{-1}), E_s the solar radiation flux W. m^{-2}, σ the Stefan–Boltzmann constant (W. m^{-2}. K^{-4}), T_a the temperature of the absorber (K), T_0 the temperature of the environment (K), α the absorptance and ε the emittance. If one considers only the optical losses, *i.e.* the heat losses by conduction and convection are not considered, the efficiency η of the collector is defined having the following expression:

$$\eta = \alpha - \frac{\varepsilon}{XE_s}\sigma(T_a^4 - T_o^4) \quad 1.4$$

Where $X = \frac{S_c}{S_a}$, the factor of concentration is considered equal to 1, for a low temperature photothermal absorber, being exposed to direct solar radiation. At a fixed processing temperature (T_a), this measure tracks the efficiency of the absorber. Thus, one can conclude that it increases by the increasing of α value or by the diminishing of ε value. Ideal cases are obtained when α approaches 1 and ε approaches 0.

Others use the expression 1.5 and 1.6 to express the selectivity of the designed absorber. The problem faced with these expressions is that they don't give a clear interpretation of the absorber's efficiency. For example, if a very low ε is obtained (see equation 1.5) with a moderate α, the calculated selectivity will be very high or not justified (e.g for α=0.6 ε=0.01 the selectivity $\frac{\alpha-\varepsilon}{\alpha}$= 0.98 and $\frac{\alpha}{\varepsilon}$= 60)

$$\text{Selectivity} = \frac{\alpha-\varepsilon}{\alpha} \text{ or } \frac{\alpha}{\varepsilon} \quad 1.5$$

1.1.1. Principles for obtaining solar selective surfaces

The physical factors for obtaining spectral selectivity and solar selective surfaces are; surface texturing, intrinsic material and tandem material.

Surface texturing can increase the solar absorption factor by the surface irregularities of the selective coating (dendrites, roughness) which induce multiple reflections, without substantially increasing the infrared emissivity. This phenomenon called spectral selectivity, is possible only if the irregularities of the surface have a dimension compatible with the incident wavelengths as illustrated in Figure 1.3.

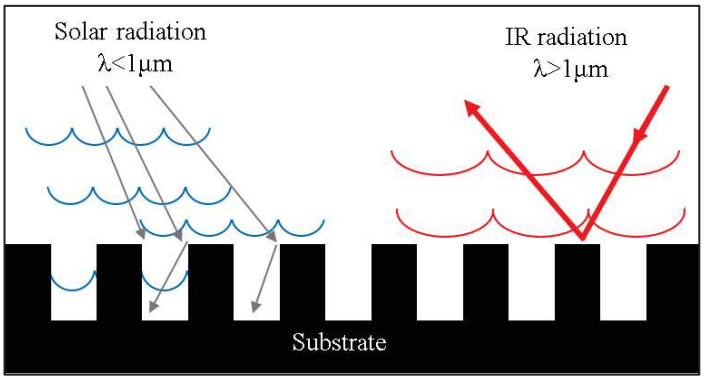

Figure 1.3: Schematic representation of surface texturing.

Intrinsic materials are those whose electronic structure presents a spectral selectivity. However, very few bulk materials possess nearly intrinsic properties. Pure metals present an early transition in the UV-VIS and NIR radiation into high reflectance in the IR. They preserve their reflectance along the IR region. Pure Tungsten is one of the most spectrally selective metals, but as other metals it shows an early transition in the radiation. Semiconductors and carbides have late transition in the UV-VIS and NIR than pure metals but, possess a lower reflectance in the IR region. Well-known examples are Cu_2S and HfC, MoO3-doped Mo (see Figure 1.4).

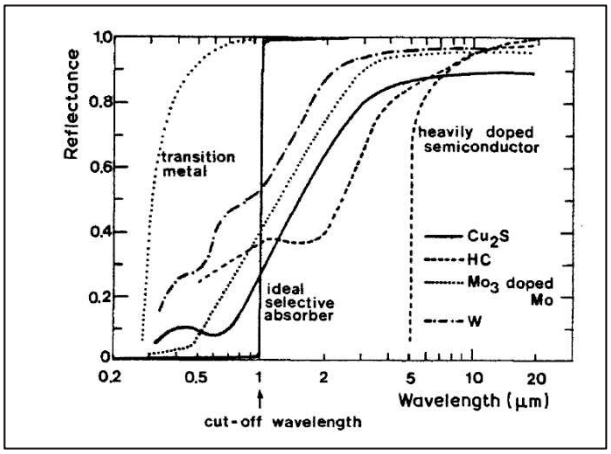

Figure 1.4: Spectral reflectance of metallic tungsten (W), MoO_3 doped molybdenum (Mo), copper sulfide (Cu_2S) and hafnium carbide (HfC) [2].

Since it is difficult to find a single material whose intrinsic optical excitation spectrum matches the required spectral profile of an ideal absorber, a tandem material is usually developed. A tandem is composed of two or more optically selective superimposed materials that complement each other. An absorber-reflector tandem is composed of highly IR reflecting metallic substrate over which a highly solar absorbing coating transparent to blackbody IR radiation is deposited (see Figure 1.5).

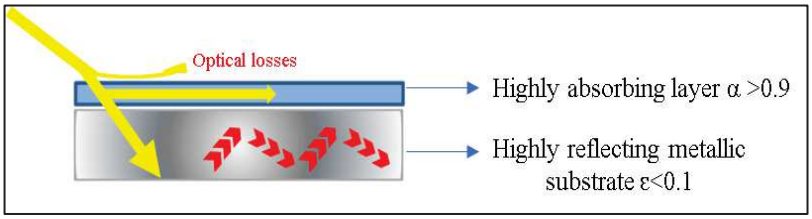

Figure 1.5: Tandem absorber-reflector material.

The metallic substrate of the tandem material, could be copper, aluminum, silver, stainless steel, zinc or molybdenum while, other substrates like platinum and gold are usually avoided due to their high cost [4]. The used substrate should be durable and corrosion resistant. Moreover, the absorbing layer could be formed by various techniques such as electroplating, sputtering, vapor deposition, chemical oxidation or by applying some spectral selective paints. The absorption of the upper layer could be a result of the intrinsic properties of the material (e.g. black paint) or due to texturing created by the processing technique that shift the absorption edge toward higher wavelengths. In the 20th century, selective surfaces of absorber/ reflector tandems were metal-oxide and sulfide layers coated onto various metals. Metal oxides of Copper, Chromium, Zinc and Nickel were generally used. The total reflectance of these layers is presented in Figure 1.6. Selective tandems show low reflectance in the UV-VIS and NIR region (0.8-2 μm) and high reflectance in the Mid-Far IR region (2-20 μm). While non-selective paints for example display low reflectance for the whole range. Selective layers have showed high selectivity by having $\alpha>0.9$ and a low ε. Non-selective layers like black paints have high α (>0.9) and very high ε (>0.9) (see Table 1.2).

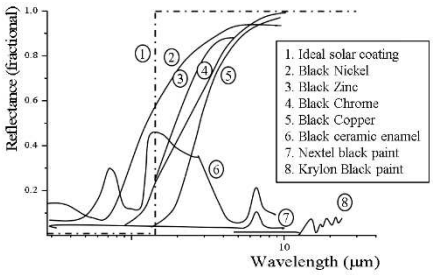

Figure 1.6: Typical reflectance of some selective and non-selective coatings [2]

Table 1.2: Spectral selectivity and processing techniques of traditionally formed tandem absorbers [2]

Coating/Substrate	Process	α/ε
CuO_x/Cu CuO/Au	Chemical oxidation Paint	0.91/0.16 0.8/0.06
CuO_x/Cu	Chemical spray	0.93/0.11
CrO_x/Cr	Electrodeposition	0.97/0.1
NiS-ZnS/Ni	Electrodeposition	0.9/0.1
Nextel black paint	-	0.96-0.98/0.9
Krylon paint	-	>0.95

Nowadays recent advances have been directed toward the creation of a solar selective material which has high selectivity and durability. The processing method should effectively be environmentally and economically friendly as well. Sol-gel techniques have been widely used for this reason [5] and the formation of nanocarbon embedded in dielectric oxide matrixes was also reported by several studies [6] [7] [8]. Along with other metal oxides, Copper oxide or "Black copper" has shown to have nearly intrinsic properties. Compared to other selective absorbers such as black nickel and chrome, CuO is not toxic and presents less hazardous effects on the environment.

1.1.2. CuO absorber reflector tandems

Among the available various metal oxides, Copper oxide (CuO, tenorite) has been extensively studied as a solar selective coating owing to its high solar absorptance and low thermal emittance [9]. It is a p-type semiconductor with a band gap of 1.21-1.51 eV having a monoclinic crystal structure. The other principle oxide is Cuprous oxide (Cu_2O), a n-type semiconductor having a band gap of 2.2-2.4 eV and a cubic structure [10]. Wang et al. [11]

reported the formation of tandem formed of a textured surface composed of crater-like pattern of 0.2-2μm in diameter of carbon-dielectric nano-composite. Cu_2O coatings were formed by spin coating starting from a sol composed of Cu, carbon, and Ti precursors in ethanol. The carbonization of the corresponding coating resulted in the partial reduction of Cu_2O formed into Cu by the residual carbon present. The optimum optical properties with the optimized conditions were α=0.8 and ε=0.08. Cu_2O exhibits a lower solar absorptance compared to CuO especially in the NIR region resulting in a lower absorptance (α). Figure 1.7 shows the UV-VIS and NIR diffuse spectra of Cu_2O, Cu_2O/CuO, and CuO formed on FTO substrates which shows difference of the absorbance between CuO and Cu_2O layers.

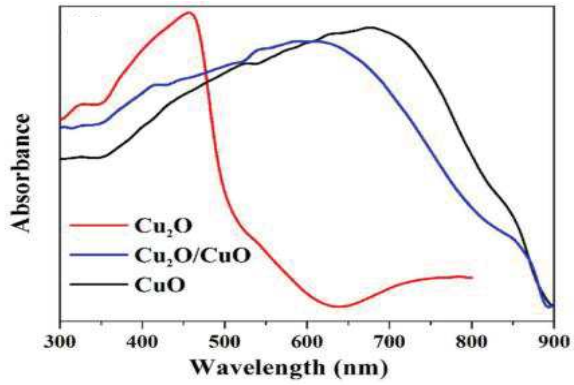

Figure 1.7: UV–vis diffuse reflectance spectra of the pure Cu2O (read line), pure CuO (black line), and Cu2O/CuO (blue line) composite films prepared on FTO substrates [12].

Copper oxide layers have been already investigated as solar selective absorbers. A variety of structures have been widely formed by using different formation techniques. Such surfaces are usually formed on IR reflecting metallic substrates by several processes starting from copper salts (copper acetate or copper chloride) through electrolytic and non-electrolytic processes, given in Table 1.3.

Table 1.3: Processes used to obtain CuO tandem solar absorbers.

Process	α	Ɛ	Reference
Sol-gel	0.92	0.2	[13]
Chemical conversion method	0.94	0.08	[14]
Dc co-sputtering of copper and aluminium	0.73 0.91 (with AR)	0.17 0.18	[15]
Chemical oxidation method	0.7 0.95 0.97	0.01 0.07 0.14	[9] [16] [17]

Cathodic arc deposition	0.93	0.16	[18]
Spraying	0.92	0.1	[19]

The processing methods employed for the production of CuO thin films mostly resulted in the production of Cu_2O or CuS, due to post deposition thermal treatment required. These CuO- composites exhibit lower absorption compared to CuO in the UV-VIS spectrum [12]. Hottel and Unger [19] were able to obtain pure CuO films by spraying a dilute solution of copper nitrate onto an aluminum sheet. Then by heating it above 170^{o}C, CuO films were obtained. They found that the surface roughness plays an important role in enhancing the optical properties of the desired film. Knowing that these surfaces showed degradation at 150^{o}C [17, 21] other authors [13] reported the formation of SiO_2-CuO/SS tandems starting from Silica precursors via sol-gel procedure. The optimized solar parameters (α=0.92, ε=0.2) were exhibited for the thinnest films (one dipping cycle) which consisted of CuO–Cu2O mixture embedded in a partially crystallized silica matrix. Kim et al. [22] have formed a tandem-structure spectrally selective layer by utilizing thermally grown copper oxide nanowires (NWs) and the hydrothermally synthesized cobalt oxide nanoparticles NPs. These tandems were formed to be used as solar selective coatings integrated in the concentrating solar power (CSP) systems. They consisted of a multi-scaled combination of copper NW and cobalt oxide Co_3O_4 NPs embedded between the NWs. The CuO layer having a good visible light absorption, the Co_3O_4 having good near-IR absorbing characteristics and the Cu substrate as IR reflecting substrate. The authors used the "Figure of Merit" (FOM) in order to characterize the efficiency of the tandems, which was found ~0.90. The FOM gives a general verification of the efficiency of a tandem absorber relating the function of α to that of ε. Sathiarg et al., [15] reported the formation of metallic composite films of CuO/Cu/Al_2O_3 by DC co-sputtering. As more Cu pieces were used the formation of CuO was not favored and the film contained Cu metal. The thickness of the optimum coating obtained was 124 nm having the maximum calculated α and ε values 0.73 and 0.17, respectively. The authors then added an anti-reflection (AR) coating of SiO_2 in order to optimize the optical properties, raising the calculated α and ε values into 0.91 and 0.18, respectively. A more recent study by Jeong et al. [20] compared the operation of nanostructured CuO tandems to that of TiNOX, current-state-of-the-art solar absorber. The CuO tandems were formed by wet chemical oxidation method using Cu substrate. They found that CuO nanostructured tandems have

near-equivalent performance to that of TiNOX, having 95-97% overall performance of that TiNOX

1.2. Electrophoretic deposition

"Electrodeposition" term is divided into Electrolytic deposition (ELD) and electrophoretic deposition (EPD). Both are based on the migration of charged species upon the application of an electric field but differ in the suspension identity. The former is based on a suspension of ionic species whereas, the latter is based on a suspension of charged particles.

In EPD, the charged particles are suspended in a liquid medium (aqueous or organic), and migrate toward the opposite sign electrode to which they are deposited. A conventional EPD setup is composed of two electrodes connected to a power supply, one acting as the counter electrode (CE) and the other as working electrode (WE) (see Figure 1.8). Other setups include a third connection for the reference electrode (RE) which allows an accurate measurement of the applied electric field during EPD. Two types of EPD are then identified: anodic and cathodic EPD. The former occurs when negatively charged particles migrate toward the anode (+) while cathodic EPD occurs due to the movement of positively charged particles toward the cathode (-).

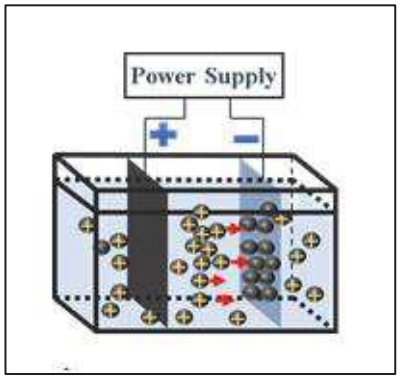

Figure 1.8: EPD setup

The first use of electrophoresis EPD dates back to 1740 by the Indian scientist, Bose, in a liquid-siphon experiment. Later in 1807 Reuss described the movement of clay particles in an aqueous suspension under the application of an electric field. 133 years later, Hamaker conducted a fundamental study on the deposition process resulting in Hamaker equation (see

section 1.2.1) [23]. Nowadays, EPD encompasses a broad range of applications due to the wide range of dimensions in terms of thickness of the deposit that is produced and the complex shapes that could be formed using wide range of materials (see Figure 1.9). This is due to several advantages such as fast deposition, applicability to any solid that is available in the form of a fine powder or charged colloidal suspension, and simple equipment requirement. These advantages can then define EPD as a cost effective, simple and versatile process [24-26].

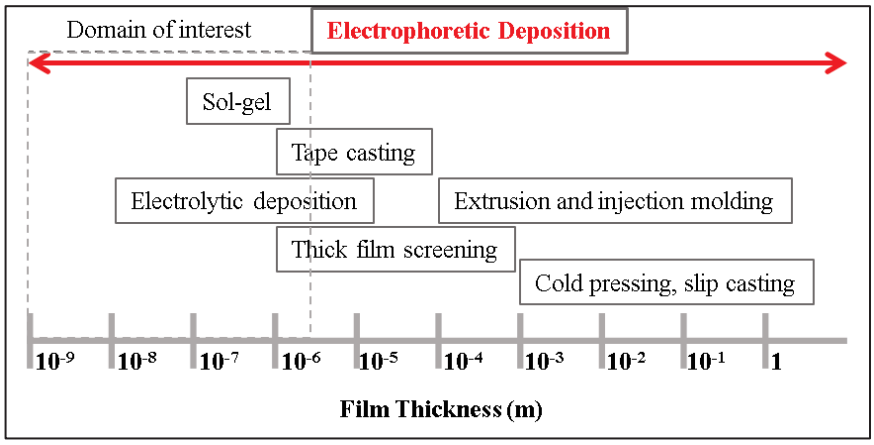

Figure 1.9: Schema representing thickness of films obtained by different processing methods and the domain of interest of using EPD for the work of this PhD

The thickness of the deposit acting as the absorbing layer determines the efficiency of the tandem. The spectral selectivity of the tandem depends largely on the thickness of the deposited layer and EPD with its high versatility allows the control of deposited thickness by varying different parameters. If the deposit is too thick then the absorbed radiation is lost in the IR region in the form of heat, since the role of the substrate will be lost. While if the thickness of the absorbing layer is not enough thick, then the absorptance of the tandem will be very low decreasing its efficiency.

1.2.1. Parameters controlling EPD

The deposition process by EPD requires charged particles suspended in a suitable liquid medium and their subsequent migration upon the application of an electric field. Thus, the success of EPD is determined by two kinds of parameters: those we call EPD parameters

signifying parameters related to the EPD process and physiochemical parameters comprising the parameters related to the suspension used. For a successful EPD there is no rule of thumb or general and fixed values that has to be taken into account but each system has to be studied individually.

The first model used to describe EPD process was suggested by Hamaker [23], who related the deposited yield (m) to the applied electric field (E), the electrophoretic mobility (μ_e), the surface area of the electrode (S), and the particle mass concentration in the suspension (C_s) resulting in equation 1.6:

$$m = Cs.\,\mu e.\,S.\,E.\,t \qquad 1.6$$

Later, Sarkar and Nicholson considered again the Hamaker equation and discussed its applicability for long deposition time. In equation 1.7, the deposited mass is considered directly proportional to deposition time supposing that C_s, μe, S and E are constant. This is true for μe and S since they could be evaluated numerically contrary to C_s and E that vary as the process goes on. The variation of the particle concentration is due to the mass powder consumed during the deposition by EPD. While the variation in E is due to the increased electrical resistance of the deposit compared to the suspension causing a drop in the electric field potential which decreases the motion of charged particles thus preventing further deposition. This change causes the linear fit to deviate from linearity. The variation in mass for short deposition time could be then evaluated, where it is equal to 0 when the deposition starts and then varies with time according to the expression:

$$m(t) = m_0(1 - e^{-kt}) \qquad 1.7$$

Where m_o is the initial mass of powder in suspension (g) and $k=\frac{V}{\mu eSE}$ defined as the kinetic parameter while V is considered constant being the volume of the suspension.

Thus, for short deposition time, the Hamaker equation is directly used without considering the change in C and E during EPD. It is then convenient to convert the Hamaker equation in terms of thickness z instead of deposited mass [27]. We obtain the equation 1.9, where ρ is the density of the deposit:

$$m = \rho.\,S.\,z \qquad 1.8$$

$$z = (Cs.\,\mu e.\,E.\,t)/\rho \qquad 1.9$$

According to equation 1.9, at a constant electric field, C_s, and μ_e, the thickness z is considered directly proportional to the deposition time t. Thus, the slope of the graph of z vs t allows the determination of ρ.

1.2.1.1. Suspension parameters

Suspension features parameter comprise parameters related to the type of suspension, stability, zeta potential, and conductivity, and solid loading of the charged particles. The parameters discussed in this section, concern the formulation of a suspension and the physico-chemical parameters related to its stability.

Solvent

Two types of solvents could be employed as suspending medium, organic or water. Organic suspensions are known to result in high quality coatings due to low conductivity, good chemical stability and wide electrochemical window. But, they possess disadvantages such as high cost, volatility, flammability, low dielectric constant (high electric fields are required). On the other hand, aqueous suspensions have a lower cost, lower environmental load and high dielectric constant thus lower electric field is required. The major limitation of aqueous suspension is the electrolysis of water which yields damaged and low-quality coatings due to the release of H_2 and O_2 gas bubbles at the cathode and anode, respectively.

Particle Size

EPD has been recognized as the most versatile technique for particulate processing in terms of the wide range of dimensions it can be applied to, for example in terms of the thickness of deposits it can produce, as compared to other processing routes and due to its applicability to nanoparticles and nanopowders assembly. Good deposition for a variety of ceramic and clay systems have been reported to occur in the range of 1-20μm while the main problem for larger particles is that they tend to settle due to gravity [24]. However, the last ten years have seen a significant increment of the applications areas where EPD is used with substantial technical advantages for manipulating nanoparticles, CNTs [28], and other nanostructures [29]. The general rule of thumb in EPD is that the particles have to possess a significant surface charge and remain well dispersed and stable to lead to homogeneous and smooth deposition. On the other hand, particle size has shown to have a prominent influence on controlling the cracking of the deposit during drying. Cracking in films deposited from

YBCO small nanoparticles (0.06µm) were reduced compared to those of greater size particles (3µm) [30].

Conductivity of the suspension

It has been pointed out by Ferrari and Moreno [1] [40] that if the suspension is too conductive, particle motion is very low since the current will be mainly carried by the ions present in the medium. While if the suspension is too resistive, the particles charge electronically and stability is lost. Thus, for a successful EPD the electrostatic or electrosteric stabilization of the suspension should be achieved by maintaining a low ionic concentration allowing the suspended particles to be the main current carriers.

Zeta Potential

The zeta potential of the particles is a crucial parameter in EPD and it is directly related to the electrophoretic mobility by Henry's equation (equation 1.10) [31]:

$$\mu = \frac{2}{3}\frac{\varepsilon\zeta}{\eta} f(kr) \qquad 1.10$$

Where $\mathcal{E}$ is the dielectric constant of the dispersion medium, η the viscosity of the solvent, ζ is the zeta potential of the suspension and *f(kr)* is the Henry's coefficient. *f(kr)* depends on the relation between the thickness of the double layer (*1/k*) and the core radius (*r*) of the particle. For non-polar medium *f(kr)* >1 considering Hückel–Onsager case while for polar medium *f(kr)*<1.5, Helmholtz –Smoluchowski case considered; this coefficient is 1.5 and 1, respectively (see

Figure 1.10). For particles in polar media, Smoluchowski's approximation is used where *f(kr)*= 1.5 while for non-polar media the calculation is referred to Huckel's approximation and *f(kr)*= 1.

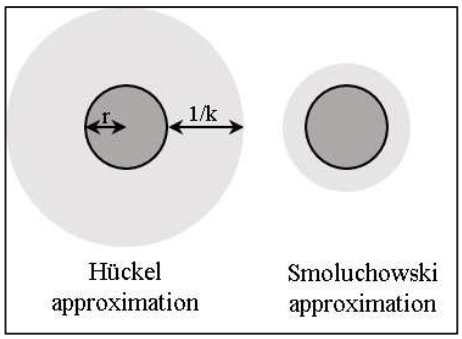

Figure 1.10: Schema illustrating Hückel and Smoluchowski approximations used for the conversion of the electrophoretic mobility into zeta potential.

The electrophoretic mobility is inversely proportional to the viscosity of the suspension. As η increases, μ decreases lowering the motion of the charged particles in the suspension and consequently the ζ value (see equation 2.1). The dielectric constant has a direct effect on the kinetics of the deposition. Too low dielectric constant suspensions fail to cause deposition due to insufficient dissociative power and as a result, particles do not migrate upon the application of an electric field. A high dielectric constant reduces the size of the double layer region and consequently the electrophoretic mobility, due to the high ionic concentration in the liquid [32, 33].

As a result, the magnitude of zeta potential is a key factor in determining the stability of the suspension to be used in EPD. If all the particles in suspension have a large absolute zeta potential (/ζ/) then they will repel each other due to electrostatic interaction and there will be less tendency for the particles to aggregate. However, if particles have low zeta potential values then there will be no force to prevent the particles to come together and flocculate, due to attractive Van der Waals interaction. There is no general rule of thumb for the magnitude of ζ to consider a suspension suitable for EPD. Most references state that particles with zeta potential more positive than +30 mV or more negative than -30 mV are often most of the time stable. However, zeta potential value can be tuned by addition of charging agents such as acids, bases, specific adsorbed ions, surfactants or polyelectrolytes to the suspension [1, 34].

In aqueous solutions, the pH of the suspension plays an important role in determining its stability. Continued addition of alkali solution to negatively charged particles will enhance the negative zeta potential value. While if acid is added to the same suspension then a point will be reached where the charge will be neutralized resulting in zero zeta potential (isoelectric point). Further addition of acid will induce a positive charge towards higher positive zeta potential values.

Stability of the suspension

Suspension stability is characterized by settling rate and tendency to undergo or avoid flocculation. A stable suspension shows no tendency to flocculate, settle slowly and is expected to form dense and strongly adhering deposits. However, if the suspension is too stable, the repulsive forces between the particles will not be overcome by the applied electric field and deposition will not occur. Paradoxically, the suspension should be stable in the bulk but unstable at the vicinity of the electrode to perform suitably EPD.

As a conclusion, the size of the charged particles has to be <20µm otherwise the suspension is subjected to sedimentation. A suspension used for EPD has to possess a moderate conductivity but the ionic concentration has to stay low in solution, otherwise the applied current will be mainly carried by the ions rather than the charged particles. The zeta potential is an indicator of the stability of the suspension and it is directly related to the electrophoretic mobility, dielectric constant, and viscosity of the medium. All these parameters determine the stability of the suspension and the possibility of forming a deposit.

1.2.1.2. EPD parameters

Effect of deposition time

According to Hamaker, the deposit thickness has a linear relationship with time. This phenomenon occurs mainly in the case of constant applied electric field, when the potential difference between the electrodes is maintained constant. However, the electric field influencing electrophoresis decreases with deposition time because of the formation of an insulating layer of ceramic particles on the electrode surface. This prevents further deposition of charged particles resulting in a plateau in the graph of thickness versus time. Charlot *et al.* and Wang *et al.* have proved that the EPD of SiO_2 nanoparticle and ZnO is linear followed by the formation of a plateau for a longer deposition time (see Figure 1.11).

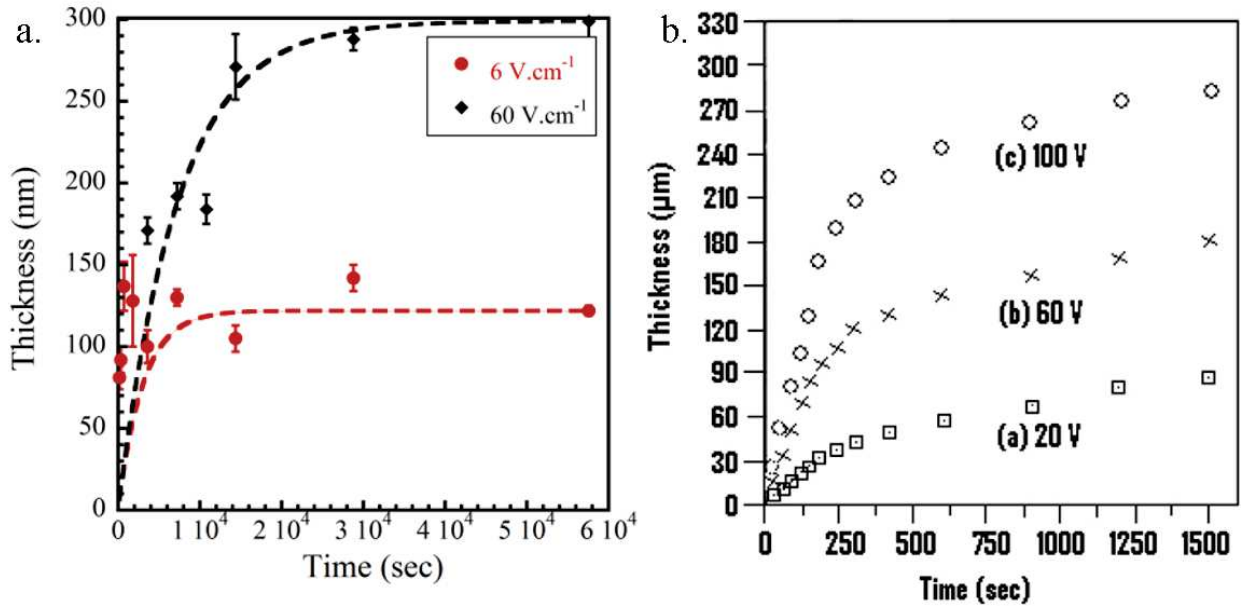

Figure 1.11:Relationship of thickness as a function of deposition time at different applied potentials: b) SiO_2 films on Si electrode in water [27]; b) ZnO films on Cu electrode in IPA [35].

Applied voltage

The applied voltage is directly related to the deposited mass or thickness which normally increases with the increase in applied potential. Although higher number of

particles is deposited at a faster rate but the quality of the deposit suffers with the increase of E. Loosely packed structures of high roughness are usually formed. At high electric fields, the particles migrate fast that they can't find enough time to sit in their best positions to form a closely packed structure and at very low electric field the thickness is very low and the deposit formed possess low adhesion to the electrode. Thus, a careful study should be made to choose the suitable applied electric field.

On the other hand, high applied electric fields could have detrimental effects on the suspension and the deposition electrode. In aqueous suspensions, the increase in E increases the rate of water electrolysis reaction causing a great turbulence beside the deposition electrode due to the formation of gas bubbles preventing particles to deposit or to form a close packed structure. Charlot *et al.* [27] have detected the oxidation of Si electrode during EPD for applied electric field higher than 20 $V.cm^{-1}$. The oxidation of the electrode changes the conductivity of the substrate affecting the homogeneity and density of the deposits. Basu *et al.* [36], have reported that the formation of uniform and homogeneous coatings is achieved, when moderate electric fields of ~15 $V.cm^{-1}$ are applied. A low-quality deposit was obtained for E<10 $V.cm^{-1}$ due to the very slow rate of migration of charged particles. While a non-uniform and a rough coating was also obtained for E>22 $V.cm^{-1}$due to the fast migration of particles resisting the best packing arrangement to produce a uniform and dense coating. Nigishi *et al.* [33] have studied the stability of n-propanol solvents in the absence of any powder as a function of applied electric field. They have found that the current density is proportional to the applied electric field but tends to be unstable for E>50 V. The instability in the current density is known to influence the morphology of deposit formed. All these data act as a guideline to the importance of choosing the applied electric field, to achieve a uniform and well-packed coating.

Concentration of the solid in the suspension

The deposit yield increases with the solid loading of particles in the suspension. It plays a more important role for multi-component EPD where, even if the particle species have the same sign of surface charge, they could deposit at different rates depending on the volume fraction of solids in the suspension. If the volume fraction of solids is high, the powders deposit at an equal rate. If, however, the volume fraction of solids is low, the particles can deposit at rates proportional to their individual electrophoretic mobility [37].

Conductivity of the substrate

Traditionally EPD was performed on electrically conductive substrate and many researchers proved that the uniformity and conductivity of the deposition electrode determined the quality of dense films produced. Peng and Liu have found that the low conductive $La_{0.9}Sr_{0.1}MnO_3$ (LSM) substrate has resulted in a slow deposition and non-uniform green films [38]. Others have also studied the deposition on non-conductive substrates such as NiO-YSZ, providing it has sufficient porosity in order to allow a conductive path through the porous substrate. This proved possible for high applied electric fields >20 V for aqueous suspensions. This was found advantageous since water electrolysis reactions beside the electrode was avoided.

As a result, EPD process is divided into two steps. First, under the application of an electric field, the suspended charged particles migrate towards the deposition electrode of opposite charge. In the second step, the particles accumulate at the electrode and form a coherent deposit (deposition). The migration depends on the bulk properties of the colloidal dispersion (bath conductivity, viscosity, particle concentration, size distribution, and zeta potential). Once the suspension properties are fixed, one can choose the process parameters in order to achieve the desired properties. The rate of migration and deposit yield depends directly on the parameters of the process such as the applied electric field, deposition time and concentration of the particles in the suspension. Finally, deposition is mostly known to occur only on conducting surfaces but recently, non-conductive substrates can also be coated by using EPD [24].

1.2.2. Stabilization of a suspension for EPD

1.2.3. Developing a surface charge on Copper Oxide

In general, the stability of the suspension used in EPD determines the quality of deposits formed. In unstable suspensions, flocculated particles sediment and an irregular thin coating is deposited. In contrast, a well dispersed (*i.e.* stable) suspension form well-ordered uniform film having low surface roughness. At moderate stability (“quasistable”), agglomerated particles are deposited, yielding a high surface roughness and loosely packed deposits (see Figure 1.12).

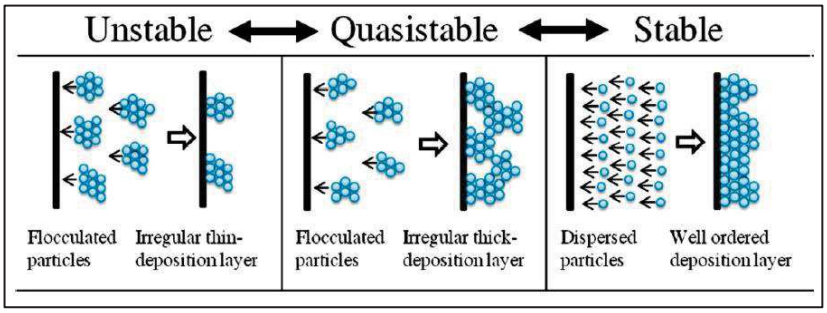

Figure 1.12: schema representing the deposition behavior of charged particles as a function of suspension stability [39].

However, a stable suspension is determined by the dominating repulsive forces between nanoparticles. Starting from a nanopowder, the appropriate dispersing medium could be challenging since metallic oxide nanoparticles tend to agglomerate very fast. Thus, surface groups are added in order to achieve stabilization [40]. Three types of stabilization are reported: “Electrostatic stabilization”, “Steric stabilization” and “Electro-steric stabilization” (see Figure 1.13).

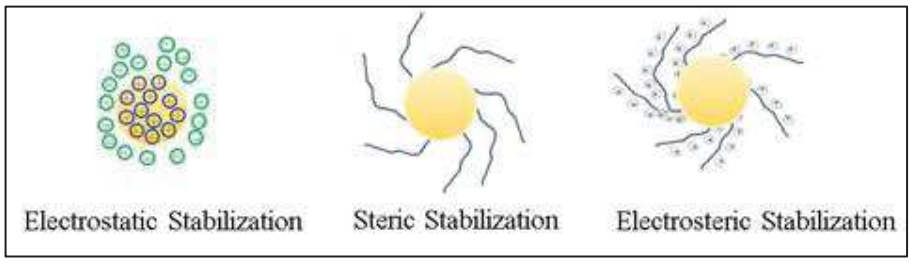

Figure 1.13: Schema representing the different forms of stabilization by polymers.

Electrostatic Stabilization

Electrostatic stabilization of colloids is generally given by the theory of Derjaguin, Landau, Verwey, Overbeek (DLVO). It suggests that the stability of a particle in a solution is dependent on the total interaction energy (Van der Waals attractive forces and repulsive forces). Electrostatic stabilization, results in the repulsion between the particles of the same charge due to the adsorption of charged molecules to the surface of NPs. Adsorption of surfactants onto the powder surface enables the establishment of an electrical double layer around each particle, keeping them apart. The resultant effects on zeta potential and the stability of the suspension depend on the size and structure of the dispersing additives [4,7]

Steric Stabilization

The organic (polymer) or macromolecular (copolymers, dendrimers) ligands are adsorbed on the particle's surface; stabilization occurs due to the physical hindrance created by the adsorbed organic molecules [40].

Electro-steric Stabilization

Electrostatic stabilization is the combination of the two previous mechanisms of stabilization. Polyelectrolytes or charged dispersants (polymers, copolymers or dendrimers) are adsorbed onto the surface of the particles.

1.2.4. How does a deposit form by EPD?

Although EPD is known as one of the classic processing method for ceramics, many mechanisms have been proposed to explain how deposition occurs. It is generally agreed that charged particles first migrate and then deposit. Both steps are controlled by the bulk properties of particle dispersion and the actual field strength. Charged particles have to be stable in the suspension but have to be destabilized at the vicinity of the electrode in order to form a deposit. In other words, there should be a difference in the properties of the suspension in the bulk and at the surface of the electrode, otherwise particles will remain stable and no deposition will occur.

In suspension, a charged particle is surrounded by ions of opposite charge whose concentration is higher than their bulk concentration forming the Electrical double layer (EDL) (see Figure 1.14). Then when an electric field is applied, these ions move to the opposite direction along with the charged particle. Consequently, the deposition occurs if the charged particles are able to be destabilized near the deposition electrode, overcoming the repulsive force dominating between the individual particles with their EDL and the EDL-Electrode repulsion.

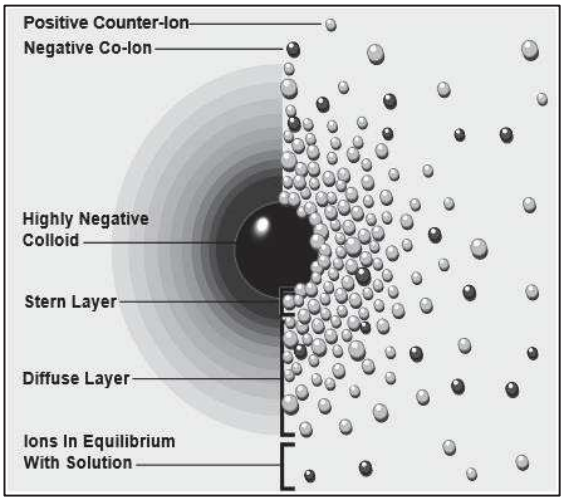

Figure 1.14: Electrical double layer of a charged particle.

However, there are many mechanisms proposed to explain how particles are destabilized beside the electrode leading to the formation of a deposit.

First Hamaker [23, 41] pointed out that a successful EPD requires a stable suspension and the formation of deposit by EPD is identical in nature to the formation of sediment by gravitational forces. They noticed that after certain time, an EPD standing suspension leads to the formation of an adhering sediment in the bottom of the vessel. So, they considered that the electric field is similar to the gravitational force. Its main role is to move the charged particles toward the suitable sign electrode where they accumulate. There, successive movement produces a force which presses the particles together forming an adherent deposit; in the same way, the gravitational force presses the particles on the bottom. Then, interparticle repulsion is overcome by the pressure exerted by other coming particles and the accumulated particles are all pressed together. Later Vanderperre [42] has supported this mechanism by reporting that the zeta potential of charged particles shifts toward the isoelectric point, when the solid loading is increased.

Grillon et al. [43] proposed that deposition occurs due to the neutralization of charged particles upon contact with the deposition electrode, where it becomes static. However, this mechanism is valid starting from very dilute powder suspensions, where the charge of particles is due to salt addition.

Koelmans and Overbeek [44] suggested that the interparticle repulsion decreases due to the increase of the electrolyte concentration near the deposition electrode. This in turn decreases the zeta potential thus inducing flocculation of the particles leading to their deposition. This leads to another supposition which is that the time needed for the deposition

to occur is dependent on the build-up of electrolyte concentration, thus a deposition would not occur before a certain time has passed. But they have found that a deposit occurs as soon as the electric field is applied. However, this mechanism is only plausible when aqueous suspension is used and OH^- ions are released at the electrode due to electrolysis reactions. It is invalid when there is no increase in the electrolyte concentration beside the electrode.

The widely known mechanism was proposed by Sarkar and Nicholson [1], based on the distortion and thinning of the EDL. They considered that charged particles migrate toward the opposite charge electrode with their lithosphere or diffuse double layer containing the counter ion from the liquid. The fluid dynamics and the applied electric field distort the double layer envelop in a way that it becomes thinner ahead and thicker from behind (see Figure 1.15). The cations in the liquid also move to the cathode along with the positively charged particle. The counter ions in the extended "tail" will tend to react with these accompanying cations in high concentration around them. As a result of this reaction, the double layer around the tail will thin so that the next incoming particle (which has a thin leading double layer) can approach close enough for London – van der Waals (LVDW) attractive force to dominate and induce coagulation and deposition. The distortion of the double layer leading to coagulation is plausible considering the high concentration of particles near the electrode (or high collision efficiency). Second, this mechanism works for incoming particles with thin double - layer heads, coagulating with particles already in the deposit.

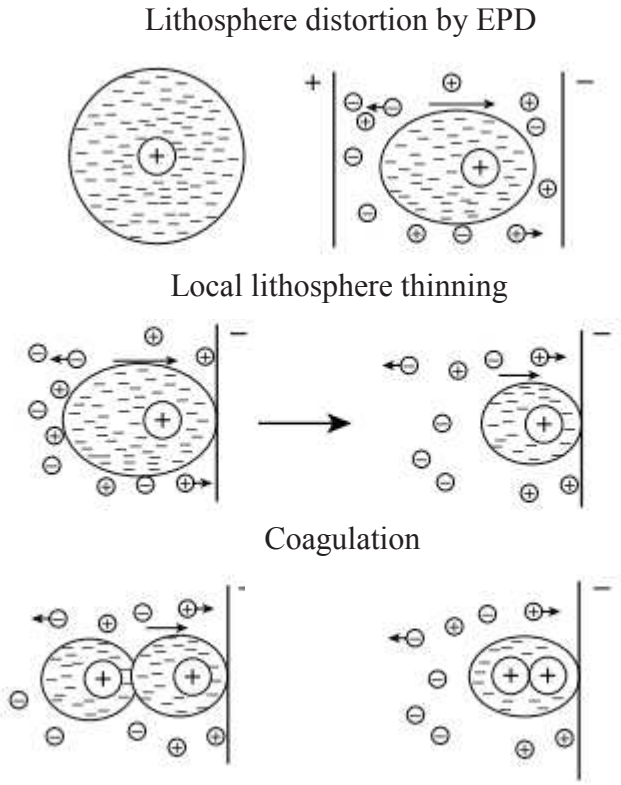

Figure 1.15: Electrical double layer distortion and thinning mechanism [1]

De and Nicholson [45] studied the EPD of Al_2O_3 in ethanol at pH=4. They noted that during cathodic EPD, cations carry the majority of current to the cathode. Contrary to Sarkar and Nicholson, they reported that the real coagulation process is due to the charge depletion at the deposition electrode resulting in local pH change toward the isoelectric point which lowers the zeta potential favoring the coagulation. They demonstrated that the suspension pH increases locally at the cathode toward the isoelectric point of Al_2O_3 (pH_{iep}=7.15) and decreases the ζ of the particles facilitating their coagulation. Besra et al., also verified the pH localization mechanism in aqueous suspension of Al_2O_3 at pH=4.5 [46]. They also observed a decrease in pH at the anode with an increase in the pH at the cathode toward the isoelectric point of Al_2O_3. They also studied the effect of operating under pulsed direct current (PDC) to decrease or eliminate H_2 and O_2 gas bubbles formation at the cathode and the anode, respectively [47]. During PDC the applied electric field is turned off for a certain pulsed width and then turned on. The use of pulsed DC for EPD has proved to control the extent of bubble incorporation and consequently the quality of deposits formed. The application of

continuous DC lead to the incorporation of maximum amount of bubbles in the deposit. Then the amount of gas bubbles incorporated in the deposit decreased with the decrease of the pulse width (T_{off}) during PDC (see Figure 1.16). Two explanations were proposed for this phenomenon. First the possibility that the hydrogen and oxygen formed at the electrode interface might be partly diffused away from the substrate, the reason that prevents them to be incorporated in the deposit. Second the discrete amount of gas generated by electrolysis of water during T_{on} of a pulse is expected to be much less compared to a single continuous DC.

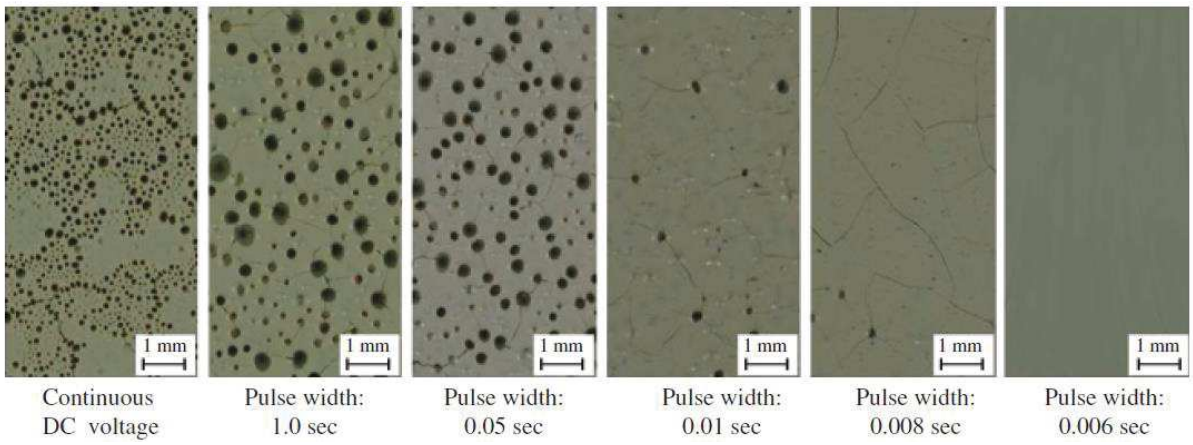

Figure 1.16: Top-view images of as deposited alumina obtained from pulsed EPD (PDC) from a 5 vol% suspension at pH=4.5 on SS substrate for E=40 $V.cm^{-1}$[47].

1.2.5. CuO and EPD

In order to obtain a CuO tandem absorber by EPD one should start from a stable suspension of CuO.

1.2.6. Suspensions of CuO

Many work have been done regarding the synthesis of CuO nanoparticles [37, 48-50] starting from Copper(II) precursors. But mostly studies were based on the application of CuO as nanofluid [48, 51, 52] and few were interested in reporting the stabilization mechanism and the surface properties of CuO (see

Figure 1.4: Spectral reflectance of metallic tungsten (W), MoO3 doped molybdenum (Mo), copper sulfide (Cu2S) and hafnium carbide (HfC) [2].

). The starting reagents of the synthesis of CuO determine its final surface charge. When Copper acetate is used as starting precursor, a carboxylate ion is left adsorbing at the surface of CuO resulting in a pH adjustable surface. At high pH the carboxylate ion is

negative thus positively charged species could adsorb to the surface allowing an electrostatic stabilization of CuO. Mallakpour et al. [53] reported the presence of hydroxyl groups on the surface of CuO (commercial nanopowder) which allows the grafting of neutral polymers as PVA by hydrogen bonding. Other report the chelating mechanism of CuO through surface Cu^{2+} resulting in its stabilization.

Table 1.4: Formation of stable colloids of CuO.

Process	Medium	Dispersant	Reference
Electrostatic	water	Tiron®	[54]
Electrostatic	water	Quaternary ammonium hydroxides	[55]
Steric	n-octane	Oleic acid	[56]
Electrosteric repulsion	water	Sodium polyaccrylate	[57]
Surface modification	n-alkane	Oleic acid or sodium oleate	[58]
Laser ablation	water	-	[59]
Alcothermal method	Ethanol	-	[48]

However, all the reported formed suspension of CuO usually doesn't start from a nanopowder of CuO. The synthesis and stabilization directly occur in solution.

1.2.7. CuO thin films formed by EPD

CuO thin films are widely produced by electrolytic deposition starting from Copper Sulfate or acetate [60] [61] and only few have used EPD. Sullivan et al. [62] and Yin *et al.* [63], for example, have prepared CuO/Al nanothermites by EPD, starting from CuO nanopowder. They also pointed out that this suspension alone in water wasn't stable enough but sufficient for the deposition time they used, thus, they didn't study the suspension stability.

EPD has been used for various applications, but only few publications have been published for the production of photothermal solar receptors. Chen and Boström [28, 64] have used EPD for the formation of CNTs films as photothermal solar receptors. They reported EPD as fast, simple and inexpensive method for the production of commercial solar absorbers.

Conclusion

A selective photothermal absorber has to possess $\alpha>0.9$ and $\varepsilon<0.1$. Absorber-reflector tandem solar absorbers allow the formation of such selective surfaces. CuO tandems have been widely formed by a variety of methods which resulted in selective tandem absorbers. Previous reported methods required an additional post deposition step to obtain the final oxide layer and in other cases large starting precursor concentration and processing time are required. We argue that EPD allows the deposition of homogeneous layers of controlled morphology and thickness by tuning parameters such as voltage and deposition time. The starting solid loading is low and in some cases no post deposition process is required. However, a key parameter of EPD is a stable suspension of charged particles and a uniform and conductive deposition electrode. EPD allows the deposition of particles with various sizes and shapes but few studies have focused on the nanometric range.

As a conclusion, EPD presents a challenging new processing route for the formation of tandem solar absorbers. CuO is a good candidate as the absorbing film of the tandem but in order to form this tandem by EPD a charged and stable colloidal suspension of CuO should be prepared. Then the surface and thickness of the tandem then could be controlled by varying different EPD parameters as deposition time and applied electric field. This approach explores a suitable stabilizing medium for CuO nanoparticles which expands the few studies done and extend more the application of EPD at the nanoscale range. In the coming chapters CuO tandem absorbers are attempted to be formed by EPD.

References

[1] J. Spitz, A. Aubert, J.M. Behaghel, S. Berthier, J. Lafait et J. Rivory Rev. Phys. Appl. (Paris), 141 (1979) 67-80

[2] W.F. Bogaerts, C.M. Lampert, Journal of Materials Science, 18 (1983) 2847-2875.

[3] B.E. Russ, J.B. Talbot, Journal of the Electrochemical Society, 145 (1998) 1245-1252.

[4] R.E. Peterson, J.W. Ramsey, Journal of Vacuum Science & Technology, 12 (1975) 174-181.

[5] A. Amri, Z.T. Jiang, T. Pryor, C.-Y. Yin, S. Djordjevic, Renewable & Sustainable Energy Reviews, 36 (2014) 316-328.

[6] G. Katumba, G. Makiwa, T.R. Baisitse, L. Olumekor, A. Forbes, E. Wäckelgård, physica status solidi (c), 5 (2008) 549-551.

[7] D. Katzen, E. Levy, Y. Mastai, Applied Surface Science, 248 (2005) 514-517.

[8] A. Charlot, O. Bruguier, G. Toquer, A. Grandjean, X. Deschanels, Thin Solid Films, 553 (2014) 157-160.

[9] M. Serra, D. Sainz, Solar Energy Materials, 13 (1986) 463-468.

[10] C. Ji, I.P. Shapiro, P. Xiao, J. European Ceram. Soc., 29 (2009) 3167-3175.

[11] K.K. Wang, S. Khan, G.Z. Yuan, C.Z. Hua, Z.Z. Wu, C.L. Song, G.R. Han, Y. Liu, Solar Energy Materials and Solar Cells, 163 (2017) 105-112.

[12] Y. Yang, D. Xu, Q.Y. Wu, P. Diao, Scientific Reports, 6 (2016).

[13] E. Barrera-Calva, J. Mendez-Vivar, M. Ortega-Lopez, L. Huerta-Arcos, J. Morales-Corona, Olayo-Gonzalez, Research Letters in Materials Science, 2008 (2008) 5.

[14] X. Xiao, L. Miao, G. Xu, L. Lu, Z. Su, N. Wang, S. Tanemura, Applied Surface Science, 257 (2011) 10729-10736.

[15] T.S. Sathiaraj, Indian Journal of Pure & Applied Physics, 45 (2007) 613-617.

[16] S. Karthick Kumar, S. Suresh, S. Murugesan, S.P. Raj, Solar Energy, 94 (2013) 299-304.

[17] A. Scherer, O.T. Inal, A.J. Singh, Solar Energy Materials, 9 (1983) 139-158.

[18] A. Marquez, G. Blanco, M.E.F. de Rapp, D.G. Lamas, R. Tarulla, Surface & Coatings Technology, 187 (2004) 154-160.

[19] H.C. Hottel, T.A. Unger, Solar Energy, 3 (1959) 10-15.

[20] D. Jeong, J. Lee, H. Hong, D. Choi, J.-W. Cho, S.-K. Kim, Y. Nam, Solar Energy Materials and Solar Cells, 169 (2017) 270-279.

[21] A. Scherer, O.T. Inal, R.B. Pettit, Journal of Materials Science, 23 (1988) 1923-1933.

[22] T.K. Kim, B. VanSaders, J. Moon, T. Kim, C.H. Liu, J. Khamwannah, D.W. Chun, D.Y. Choi, A. Kargar, R.K. Chen, Z.W. Liu, S.H. Jin, Nano Energy, 11 (2015) 247-259.

[23] H.C. Hamaker, Transactions of the Faraday Society, 35 (1940) 279-287.

[24] L. Besra, M. Liu, Progress in Materials Science, 52 (2007) 1-61.

[25] A.R. Boccaccini, S. Keim, R. Ma, Y. Li, I. Zhitomirsky, Journal of the Royal Society Interface, 7 (2010) S581-S613.

[26] A.R. Boccaccini, J.A. Roether, B.J.C. Thomas, M.S.P. Shaffer, E. Chavez, E. Stoll, E.J. Minay, Journal of The Ceramic Society of Japan, 114 (2006) 1-14.

[27] A. Charlot, X. Deschanels, G. Toquer, Thin Solid Films, 553 (2014) 148-152.

[28] Z. Chen, T. Boström, Solar Energy Materials and Solar Cells, 144 (2016) 678-683.

[29] A.R. Boccaccini, J.A. Roether, B.J.C. Thomas, M.S.P. Shaffer, E. Chavez, E. Stoll, E.J. Minay, Journal of the Ceramic Society of Japan, 114 (2006) 1-14.

[30] N. Sato, M. Kawachi, K. Noto, N. Yoshimoto, M. Yoshizawa, Physica C, 357 (2001) 1019-1022.

[31] D.C. Henry, Proceedings of the Royal Society of London Series a-Containing Papers of a Mathematical and Physical Character, 133 (1931) 106-129.

[32] R.W. Powers, J. Electrochem. Soc., 122 (1975) 490-500.

[33] H. Negishi, H. Yanagishita, H. Yokokawa, Electrophoretic deposition of solid oxide fuel cell material powders, Electrochemical Society Inc, Pennington, 2002.

[34] M. Zarbov, I. Schuster, L. Gal-Or, Journal of Materials Science, 39 (2004) 813-817.

[35] Y.C. Wang, I.C. Leu, M.H. Hon, Journal of the American Ceramic Society, 87 (2004) 84-88.

[36] D. Das, R.N. Basu, Materials Research Bulletin, 48 (2013) 3254-3261.

[37] A. El-Trass, H. ElShamy, I. El-Mehasseb, M. El-Kemary, Applied Surface Science, 258 (2012) 2997-3001.

[38] Z.Y. Peng, M.L. Liu, Journal of the American Ceramic Society, 84 (2001) 283-288.

[39] Y.S. Joung, C.R. Buie, Langmuir, 27 (2011) 4156-4163.

[40] R. Moreno, B. Ferrari, Nanoparticles Dispersion and the Effect of Related Parameters in the EPD Kinetics, in: J.H. Dickerson, A.R. Boccaccini (Eds.) Electrophoretic Deposition of Nanomaterials, Springer New York, New York, NY, 2012, pp. 73-128.

[41] H.C. Hamaker, E.J.W. Verwey, Transactions of the Faraday Society, 35 (1940) 0180-0185.

[42] L. Vandeperre, O. Van der Biest, F. Bouyer, A. Foissy, American Ceramic Society Bulletin, 77 (1998) 53-58.

[43] F. Grillon, D. Fayeulle, M. Jeandin, Journal of Materials Science Letters, 11 (1992) 272-275.

[44] H. Koelmans, J.T.G. Overbeek, Discussions of the Faraday Society, (1954) 52-63.

[45] D. De, P.S. Nicholson, Journal of the American Ceramic Society, 82 (1999) 3031-3036.

[46] L. Besra, T. Uchikoshi, T.S. Suzuki, Y. Sakka, J. European Ceram. Soc., 30 (2010) 1187-1193.

[47] L. Besra, T. Uchikoshi, T.S. Suzuki, Y. Sakka, Journal of the American Ceramic Society, 91 (2008) 3154-3159.

[48] T. Kida, T. Oka, M. Nagano, Y. Ishiwata, X.-G. Zheng, Journal of the American Ceramic Society, 90 (2007) 107-110.

[49] Y.F. Lim, J.J. Choi, T. Hanrath, J. Nanomater., (2012).

[50] I. Singh, R.K. Bedi, Solid State Sciences, 13 (2011) 2011-2018.

[51] D.P. Kulkarni, D.K. Das, G.A. Chukwu, Journal of Nanoscience and Nanotechnology, 6 (2006) 1150-1154.

[52] D.P. Kulkarni, D.K. Das, S.L. Patil, Journal of Nanoscience and Nanotechnology, 7 (2007) 2318-2322.

[53] S. Mallakpour, M. Dinari, E. Azadi, International Journal of Polymer Analysis and Characterization, 20 (2015) 82-97.

[54] M. Guedes, J.M.F. Ferreira, A.C. Ferro, Journal of Colloid and Interface Science, 330 (2009) 119-124.

[55] M. Guedes, A.C. Ferro, J.M.F. Ferreira, Stabilisation of CuO aqueous suspensions, in: P.M. Vilarinho (Ed.) Advanced Materials Forum Iii, Pts 1 and 2, 2006, pp. 1369-1373.

[56] J.Y. Jeng, J.C. Liu, J.H. Jean, Journal of the American Ceramic Society, 90 (2007) 3676-3679.

[57] A.h. Qiang, L.m. Zhao, C.j. Xu, M. Zhou, Journal of Dispersion Science and Technology, 28 (2007) 1004-1007.

[58] C.-C. Li, M.-H. Chang, Materials Letters, 58 (2004) 3903-3907.

[59] A.E. Tyurnina, V.Y. Shur, R.V. Kozin, D.K. Kuznetsov, V.I. Pryakhina, G.V. Burban, Phys. Solid State, 56 (2014) 1431-1437.

[60] V. Dhanasekaran, T. Mahalingam, R. Chandramohan, J.-K. Rhee, J.P. Chu, Thin Solid Films, 520 (2012) 6608-6613.

[61] J.S. Sagu, T.A.N. Peiris, K.G.U. Wijayantha, Electrochemistry Communications, 42 (2014) 68-71.

[62] K.T. Sullivan, M.A. Worsley, J.D. Kuntz, A.E. Gash, Combustion and Flame, 159 (2012) 2210-2218.

[63] Y. Yin, X. Li, Y. Shu, X. Guo, H. Bao, W. Li, Y. Zhu, Y. Li, X. Huang, Materials Chemistry and Physics, 194 (2017) 182-187.

[64] Z. Chen, T. Boström, Solar Energy Materials and Solar Cells, 157 (2016) 777-782.

Chapter Two:

Materials and Experimental Methods

2. Introduction

This chapter presents the different methods used to analyze the starting material for the EPD process, and the characterization methods followed to characterize the starting CuO nanopowder and calculate the spectral selectivity of the tandem absorbers to be formed

2.1. CuO Nanopowder

2.1.1.a. TEM Analysis

CuO nanopowder <50nm was obtained from Sigma Aldrich having black color. The TEM micrograph of CuO nanoparticles is presented in

Figure 2.1. The CuO nanoparticles have a spherical-oval shape. The size of the nanoparticles varies between 11.5 and 32 nm having an average size of 21.5±7.24 nm.

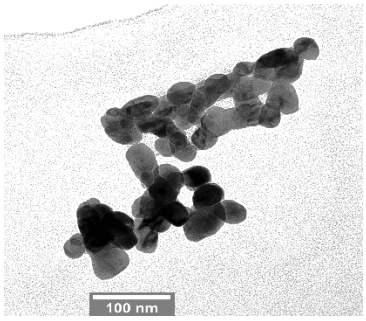

Figure 2.1: TEM micrograph of CuO nanopowder.

2.1.1.b. Thermal analysis of bulk CuO

CuO is the highest oxidized form of Cu thus it is stable under air and further transformations in response to high temperatures are avoided. To verify this, TGA analysis was performed under Oxygen, which showed CuO nanopowder to be pure and stable up to as high temperatures as 900°C (see Figure 2.2a).On the other hand, under Argon atmosphere, the TGA analysis of CuO nanopowder showed one step degradation at 850°C which corresponds to 10% loss of CuO into Cu_2O and O_2 (see Figure 2.2b).

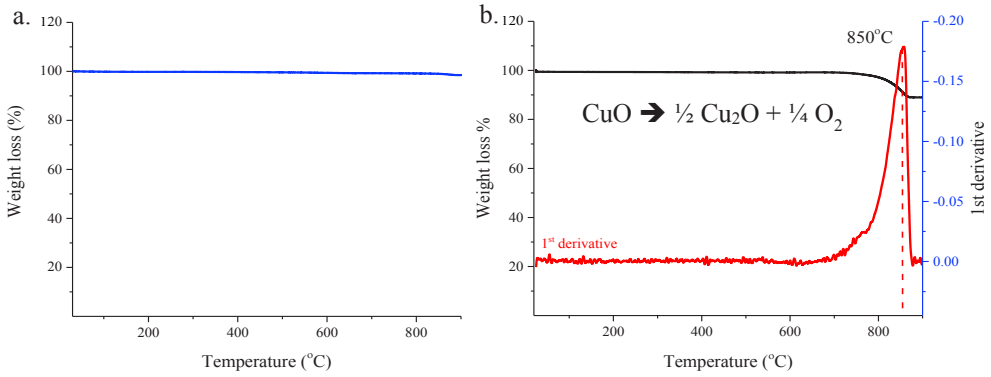

Figure 2.2:TGA thermogram of pure CuOnanopowder performed under a) Oxygen, b) Argon atmosphere

CuO belongs to the monoclinic crystal system while Cu_2O crystalizes in cubic structure which allows the differentiation of these two copper oxides by XRD. In order to study and understand the reduction of CuO under thermal treatment, the XRD diagram of CuO was recorded directly upon thermal treatment in the XRD chamber between 30°C and 900°C under Argon atmosphere (see Figure 2.3). The XRD patterns of CuO, at the beginning of the experiment until 750°C, show intense diffraction peaks at 35.5° and 38.4° corresponding to (-111) and (111) planes of CuO, respectively. At 850°C, a small hump emerge at 11.11°, 36° and 43°corresponding to (110), (111), and (200), and (311) of Cu_2O, respectively. As temperature increases to 950°C, the intensity of the XRD peaks corresponding to Cu_2O increases and as the sample cools down at the end of the experiment, the intensity of Cu_2O planes (111) exceeds those of CuO. Thus, according to the TGA and XRD analysis, the present CuO nanoparticles are reduced to Cu_2O starting at 850°C corresponding to the results of the TGA analysis.

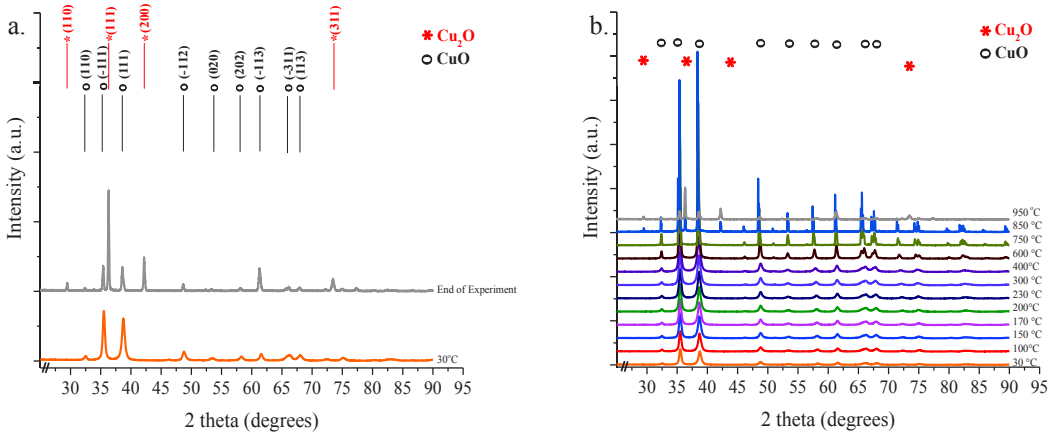

Figure 2.3: XRD pattern of CuO a) at the begining and end of thermal treatment, b) durning the thermal treatment between 30 and 900°C.

2.1.2. LUDOX Suspensions

For the proceeding experiments, commercial SiO_2 LUDOX suspensions (AS-40%, TM-50%, and HS-40%) were used where particles are dispersed in alkali medium (pH=9-10). According to the supplier the average particle diameter is 22-25, 22, and 12 nm, respectively. Upon several dilutions sizes were verified by dynamic light scattering (Zetasizer NanoZS Malvern series).

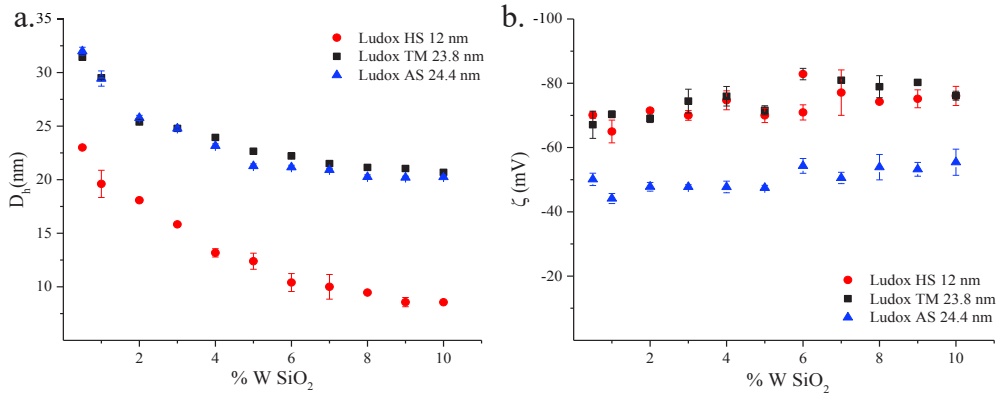

Figure 2.4 shows the average hydrodynamic diameter (D_h) and the zeta potential (ζ) as a function of % W of the nanoparticles in the suspension. D_h decreases exponentially with increasing %W for all SiO_2 suspensions which proves that repulsive forces are dominating. The estimated nanoparticle size is found equal to 24, 23, and 12 nm approximately with a polydispersity of 0.2. The measured ζ_p is negative for all SiO_2 suspensions attaining an

average value of 70 mV for 12 and 22 nm suspensions while an average of 50 mV was obtained for LUDOX AS suspension. The difference between LUDOX TM and HS on one side and LUDOX AS on the other side is due to difference of cation in the suspension being Na^+ for the former and NH_4^+ for the latter.

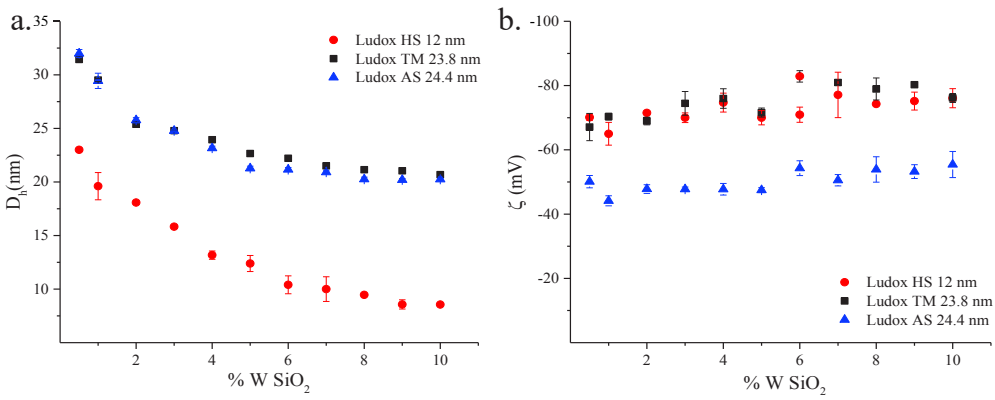

Figure 2.4:Hydrodynamic diameter (D_h) and zeta potential (ζ_p) of SiO_2 suspension.

By Small Angle X-ray Scattering (SAXS) the sizes of the SiO_2 nanoparticles were verified to be 15.4 nm for LUDOX HS, 23.8 nm for LUDOX TM and 24.4 nm for LUDOX AS, corresponding to the sizes provided by the supplier.

2.2. EPD Setup

Electrophoretic experiments are conducted using a PS 9009 TX electrophoresis power supplier provided by APELEX. It enables a voltage from 10 to 3000 V with a maximum current of 300 mA by steps of 10 V. The deposition cell is only based on two electrodes: the working electrode (WE) and the counter electrode (CE). For EPD at 5 $V.cm^{-1}$ and in aqueous suspension, experiments were conducted in potentiostatic conditions using a VersaSTAT 4 potentiostat controlled by the Versastudio software (Princeton Applied Research®), based on three conection electrode CE, WE and a reference electrode (RE). This instrument supplies absolute compliance voltage of 12 V at full rated current. The software yields electrochemical cell features (current, resistance, time, apparent applied potential) (see Figure 2.5). Before every EPD experiment a uniform and conductive clean deposition electrode or working electrode was prepared, then dipped in the corresponding PEI/CuO water suspension prepared followed by variation of different EPD parameters. Then before 10s of the end of EPD and while the applied potential is still ON, the beaker containing the suspension is

lowered quickly. The working electrode was then removed and dipped 2 times in a small beaker containing water then in a beaker containing ethanol. Then the deposit is left to dry vertically in an individual box for at least two days before further analysis.

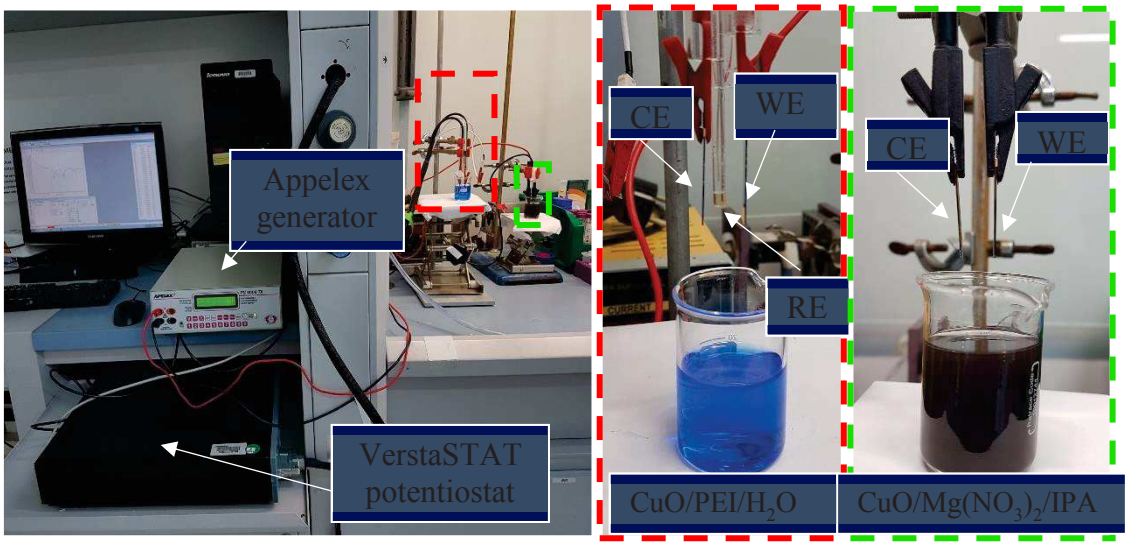

Figure 2.5: EPD setup showing both types of suspensions used.

2.3. Characterization of the suspension

Prior to deposition, the suspension is characterized using Malvern's zeta sizer Nano series (see Figure 2.6). It allows the measurement of hydrodynamic size (D_h) using "Dynamic light scattering" and the measurement of electrophoretic mobility (μ_e) using "Laser Doppler velocimetry". Then zeta potential could be calculated from the measured value of μ_e. Both methods are explained in the following section. All the proceeding explanations are extracted from the technical notes present at Malvern technologies website.

Figure 2.6: Malvern zeta sizer nanoseries (ZS90).

2.3.1. Laser Doppler Velocimetry

After determining the electrophoretic mobility, the zetasizer uses the electrophoretic mobility to calculate the zeta potential by Henry's equation:

$$\mu = \frac{2}{3}\frac{\varepsilon_0 \varepsilon_r \zeta}{\eta} f(kr) \qquad \text{(Equation 2.2.)}$$

Where $\varepsilon_0$the permittivity of vacuum, ε_r the relative permittivity of the solvent, η the viscosity of the solvent, f (kr) is Henry's coefficient, which depends on the relation between the thickness of the double layer (1/k) and the core radius (r) of the particle. For a point charge (kr>>1, Huekel–Onsager case) or a flat surface (kr<<1.5, Helmholtz –Smoluchowski case) this coefficient is 3/2 and 1, respectively.

Figure 2.7 presents a typical measurement system for zeta potential made up of six main components. The most important is the laser (1) which is used to provide a light source to illuminate the particles within the sample, which absorbs at (λ=632 nm). For zeta potential measurements this light source is split to provide an incident and reference beam. The reference beam is also 'modulated' to provide the doppler effect necessary. The laser beam passes through the center of the sample cell (2), and the scattering at an angle of 17° is then detected. When an electric field is applied to the cell, any particles moving through the measurement volume will cause the intensity of light detected to fluctuate with a frequency proportional to the particle speed. Then the detector (3) sends this information to a digital signal processor (4). This information is then passed to a computer (5), where the Zetasizer Nano software produces a frequency spectrum from which the electrophoretic mobility and hence the zeta potential information is calculated. An attenuator (6) is used to regulate the intensity of the laser passing through the sample in order to improve light scattering favoring sample analysis. To correct any differences in the cell wall thickness and dispersant refraction compensation optics (7) are installed within the scattering beam path to maintain alignment of the scattering beams.

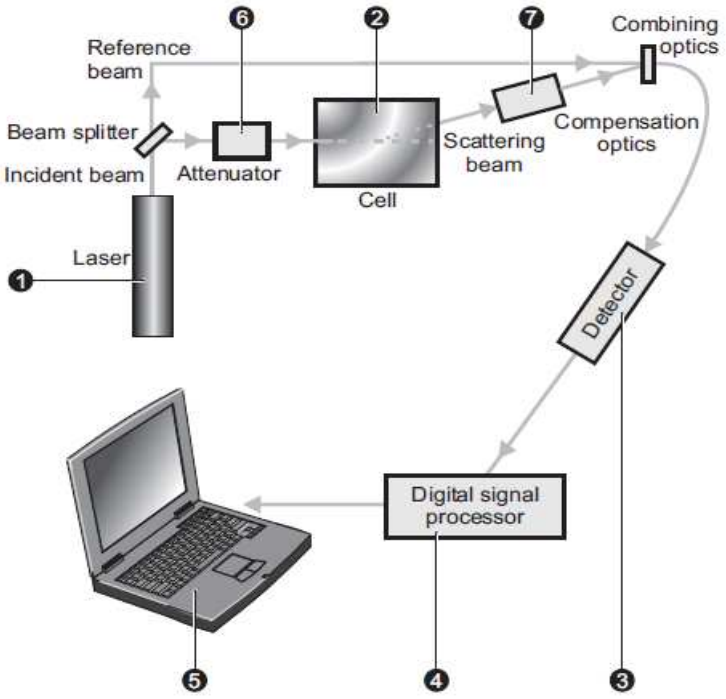

Figure 2.7: procedure followed to measure zeta potential. (retrieved form www.malverninstruments.com)

The classical measurement cell of the electrophoretic mobility is the folded capillary cell which is composed of two electrodes, at either end to which a potential is applied. Universal Dip cell is also widely used, the measurement concept is the same but the measurement electrodes are only 2 mm apart and positioned directly in the measurement zone. Particles move towards the electrode of opposite charge, then their velocity is measured and expressed in unit field strength as their mobility (see Figure 2.8). In both cases ~1 mL of suspension is only needed.

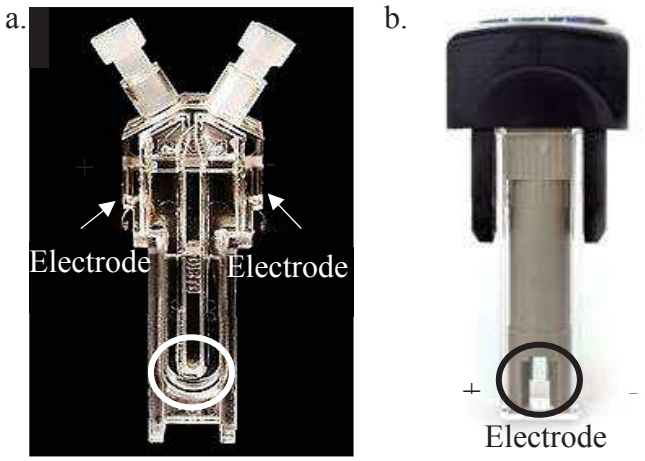

Figure 2.8: A classical micro-electrophoresis measurement cell: folded capillary cell and dip cell

The interpretation of stability of the colloid in response to the zeta-potential values are presented in Table 2.1.

Table 2.1: Stability criteria of suspensions depending on the ζ value.

Zeta potential [mV]	Stability behavior of the colloid
0 to ±5	Rapid coagulation or flocculation
10 to ±30	incipient instability
±30 to ±40	Moderate stability
±40 to ±60	Good stability
More than ±61	excellent stability

2.3.2. Dynamic Light Scattering

Dynamic Light scattering is a non-destructive technique for measuring size of particles in suspension. The speed of particles undergoing Brownian motion is measured which is influenced by the particle size, sample viscosity, and temperature. The temperature should be accurately measured for the viscosity value. During the measurement the temperature should be stable in order to ensure accurate size interpretation. The velocity of the Brownian motion is defined by the translational diffusion coefficient (D). "D" could be converted into particle size using the Stokes-Einstein equation:

$$D_h = \frac{kT}{3\pi\eta D} \qquad \text{(Equation 2.2.)}$$

Where D_h is the hydrodynamic diameter, k is Boltzmann's constant, T is the absolute temperature, η is the viscosity and D the diffusion coefficient.

Then $D_{h\ is}$ defined as the diameter of a hard sphere that diffuses at the same speed as the particle or molecule being measured. It will depend not only on the size of the particle "core", but also on any surface structure, as well as the type and concentration of any ions in the medium. The ionic concentration affects the particles migration speed by varying the thickness of the double layer, called Debye length (k^{-1}). A low concentration ionic medium will produce an extended double layer of ions around the particle, reducing the diffusion speed and resulting in a larger, apparent hydrodynamic diameter. Higher ionic concentration media (≥10mM) will compress the electrical double layer and reduce the measured hydrodynamic diameter. On the other hand, the surface structure of the adsorbed polymers could also affect the hydrodynamic diameter. A polymer adsorbed at the surface and projected into the suspension will increase the thickness of the double layer. In contrast if the polymer is lying flat on the surface the double layer will be thinner. However, for a non-spherical particle, DLS will give the diameter of a sphere that has the same average translational diffusion coefficient as the particle being measured.

A minimum volume of 12 µl and a maximum of 1 ml of suspension to be characterized is introduced into a disposable polystyrene cuvette, then positioned in the sample port in the apparatus. The range of sizes that could be measured by this type of apparatus is between 0.3 nm and 10 µm.

2.4. Characterization of tandem absorbers

2.4.1. Scanning Electron Microscopy and Atomic Force Microscopy

The formed coatings are characterized by an Environmental scanning electron microscopy (ESEM). Analyses are obtained with a FEI Quanta FEG 200 ESEM coupled with an energy dispersive X-ray micro analyzer (EDX) Bruker X-Flash 4010 SDD. ESEM observations and EDX analyses are performed at an operating voltage varying between 2 and 30 kV under a N_2 gaseous partial pressure of 10 Pa. ESEM is used to characterize the deposit microstructure (from the top-view images) and also to determine the deposit thickness from the cross-section view of the working electrode. FIJI program was used to measure the average thickness of the obtained films by measuring 20-50 points per image. The average thickness is automatically generated by the system with the corresponding standard deviation.

For fundamental studies, Pt or Au metallized silicon wafers, are used since they possess a suitable conductivity for EPD offering a smooth surface with easy handling. Prior to the deposition, the AFM analysis of the electrode revealed a root mean square (RMS) roughness of 0.66 nm for Pt Si wafer and 1.02 nm for Au Si wafer (See Figure 2.9a and Figure 2.10a). Thus, with such smooth electrode surface any topology measurements after deposition are considered due to the deposited nanoparticles. To verify the thickness of the Pt layer on the Si wafer the commercial substrate was cut in the middle by a diamond graving pen and then analyzed by SEM in a cross-section view (see Figure 2.9b and Figure 2.10b). The thickness of the Pt layer deposited on Si wafer is 114 ± 14 nm, a very thin layer of Ti is used to allow the sticking of Pt layer but is not well observed by the SEM analysis. For the Au Si wafer a greater contrast is observed between the Ti layer used to accroach and the Au top layer. The thickness of the Au layer measures ~100 nm and the Ti layer ~50 nm

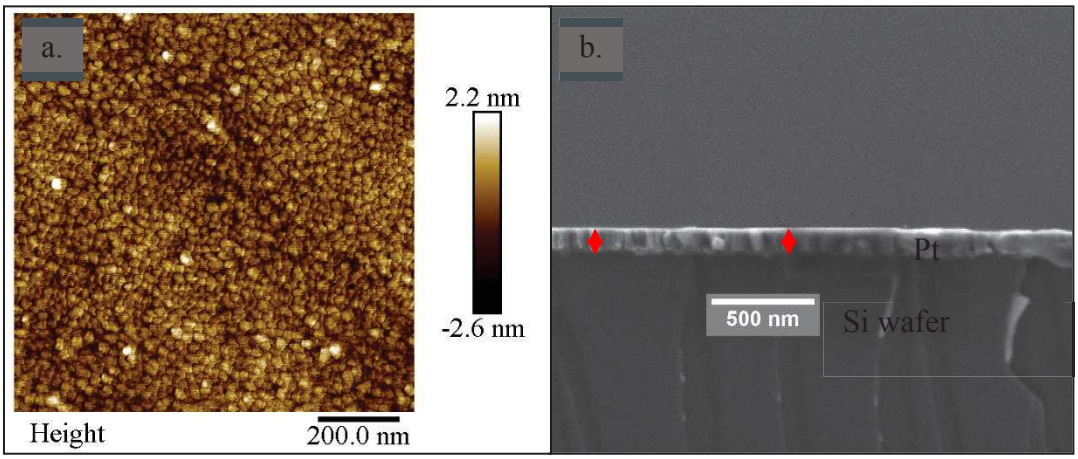

Figure 2.9: Pt Si wafer Working electrode characterization: a) AFM image. b) SEM cros-section of Pt Si wafer (WE) prior to EPD.

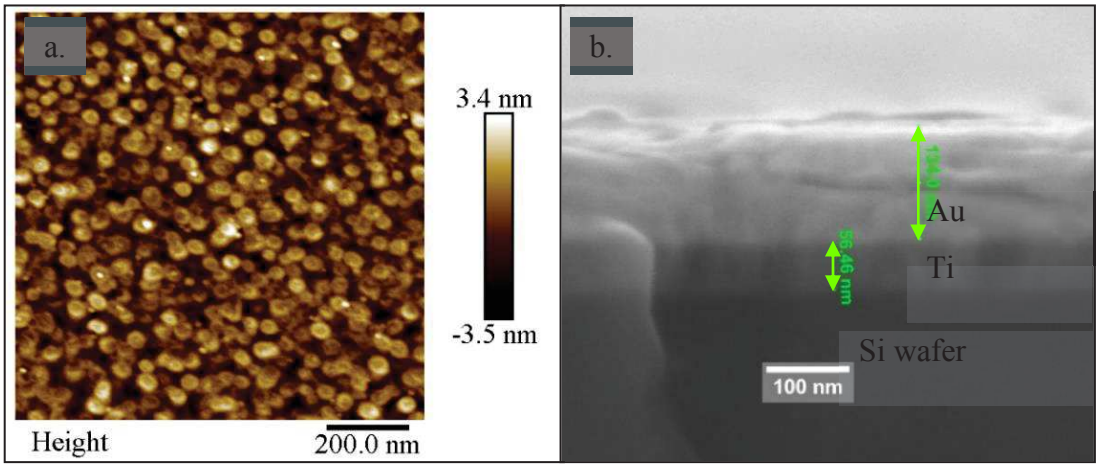

Figure 2.10: Au Si wafer Working electrode characterization: a) AFM image. b) SEM cros-section of Pt Si wafer (WE) prior to EPD.

All the substrates to be used as working and counter electrode were cut into rectangular shapes (2.5 cm*2 cm) and then washed by ethanol in an ultrasonic bath for 10 minutes. Then the substrates were directly dried under Nitrogen flow. For other metallic substrates as pure Pt, Cu, SS (inox steel) and Al, industrial cleaning methods were followed. The corresponding substrate was first connected to the negative pole of the generator by a connecting crocodile. Then a counter electrode of Pt was placed on the opposite pole. Both were then dipped in a commercial solution of UNICLEAN and a current of 0.5A was passed for 1 min. The formation of gas bubbles due to the imposed current cleans the corresponding substrate. Then the substrate was removed and dipped in H_2SO_4 solution followed by washing with water and drying under Nitrogen or Argon flow. To have a homogeneous current passing through the electrode, a Copper scotch of 0.2 cm in width was stuck to the upper part in contact with the crocodiles.

2.4.1.a. EDX

2.4.1.b. X-film-EDX

X-film software allows the determination of thin film thickness and composition using Energy Dispersive X-Ray [1]. Applying several energies of the primary electron beam (E_0) allows the variation of depth of the penetration into the material. This allows the measurement of the K-ratio of the rays of various elements present in the multi-layer. The values of thickness and composition are obtained thanks to the experimental values corresponding to the curves "k ratio = f (E_0)" fit closest to the experimental points. The

obtained expression from the software is "ρz (mg/cm^2)", then for the measured experimental value of thickness z (μm) the density ρ (g/cm^3) could be calculated.

2.4.2. Diffuse Spectroscopy

2.4.2.a. UV-VIS-NIR Spectroscopy

The absorptance in the UV-VIS and NIR region was determined using a Shimadzu UV 3600 spectrophotometer equipped with an integrating sphere of 50 mm diameter to be used in the wavelength range of 0.28-1.8 μm. The UV-3600 (shimadzu) has two different sources, a halogen lamp for the visible range and a deuterium lamp for the field UV. An integration sphere covered with barium sulfate ($BaSO_4$) is integrated into the optical system of the device (see Figure 2.11). To perform the measurement with this sphere, a baseline scan is first performed where the $BaSO_4$ pellet is placed on the sample and reference holder. For a sample scan, the sample is then positioned as shown in the figure. The total reflectance curve (between 0.28-1.8 μm) is then used to calculate the α value of formed tandems.

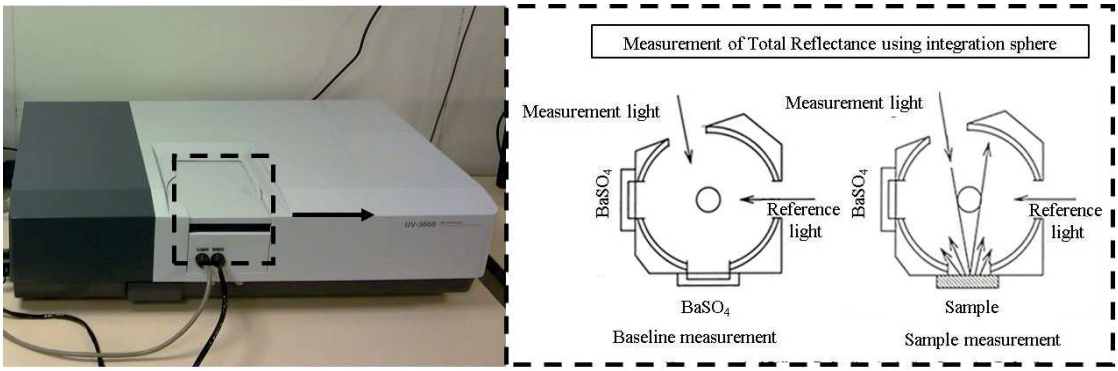

Figure 2.11: UV-VIS-NIR spectrometer (UV-3600 shimadzu) with integration sphere connected

2.4.2.b. Mid-Far IR Spectroscopy

The infrared reflection spectra are obtained from a sphere of integration (PIKE) covered with gold. This sphere is connected to the optical system of a Spectrum-100 FT-IR (Perkin Elmer) (see Figure 2.12). the sample is placed directly facing the integration sphere. The reflectance measurements are carried out over a wavelength range from 2.5-15 μm. The total reflectance curve is later used to calculate the emittance value.

Figure 2.12: Perkin elmer

2.4.3. Metallic substrates as deposition electrodes

The basic principle of a CuO tandem absorber-reflector system is the employment of an IR reflecting substrate on which CuO is deposited. Such surface should possess high % R in the mid-far IR region thus low emissivity ($\varepsilon<0.1$). The total reflectance (%R) of naked substrates are showed in Figure 2.13, where all metallic and metallized substrates present high reflectance in the IR region and similar calculated emittance of ~0.01. On the other hand, these substrates present different reflectance in the UV-VIS and NIR where the lowest reflectance is reported for Cu substrate ($\alpha=0.49$), SS ($\alpha=0.33$) and Au ($\alpha=0.31$). While Pt ($\alpha=0.28$), Au Si wafer ($\alpha=0.25$), Pt Si wafer ($\alpha=0.24$), and Al($\alpha=0.19$) presents higher %R. The difference in the % R between different substrates is due to the intrinsic properties of each material where each substrate has a specific cut-off wavelength which determines the limit of absorption in the UV-VIS and NIR region. Thus, the role of the absorbing CuO layer is to shift this cut-off wavelength to the right resulting in higher absorption.

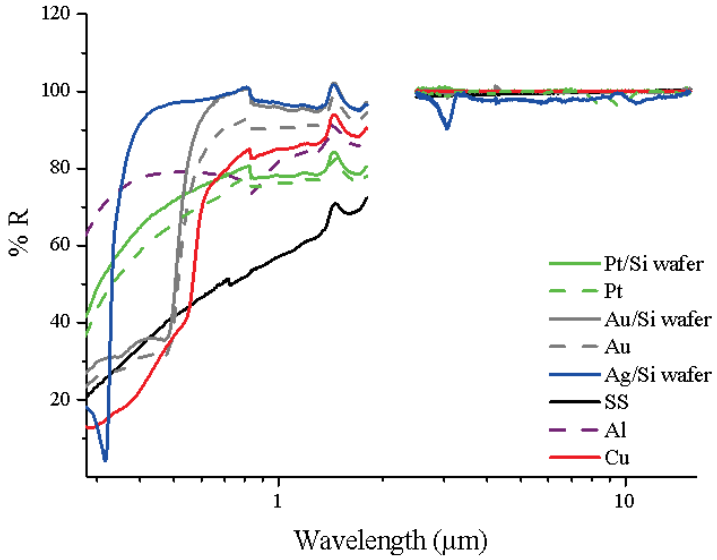

Figure 2.13: %R of naked substrates used for EPD.

Choosing a suitable working electrode (WE) for EPD is one of the critical parameters since it's uniformity and conductivity play an important role in the homogeneity and density of the deposits obtained by EPD. In our laboratory, we prefer using metallized Si wafer (Au, Pt) since they maintain the optical properties of a metallic substrate (pure Au and Pt), possess acceptable conductivity and allows easy handling for cross-section analysis by SEM. But since such substrates are expensive and not promising for industrial use, we have attempted to form CuO tandem absorbers using industrially used substrates such as Aluminum (Al1050), Stainless Steel (SS316L), Copper (Cu). The use of these substrates will be studied for both IPA and water suspensions.

Table 2.2: Spectral properties and resistivity of naked substrates.

Substrate	α	ε	Resistivity (Ω.cm)
Pt/Si wafer	0.24	<0.01	-
Pt	0.28		94.10^{-9}
Au/Si wafer	0.31		-
Au	0.25		22.10^{-9}
Ag/Si wafer	0.036		-
Al 1050	0.19		26.10^{-9}
Cu	0.49		17.10^{-9}
SS 316L	0.33		74.10^{-4}

2.4.4. GIXRD

In the case of thin films using routine Θ/2Θ scan, a weak signal from the film is observed with an intense signal from the substrate. Then to avoid the intense signal from the substrate, a thin film scan could be performed or a 2Θ scan with fixed grazing angle of incidence, Θ. Usually the lower the grazing angle, the shallower the penetration beam is.

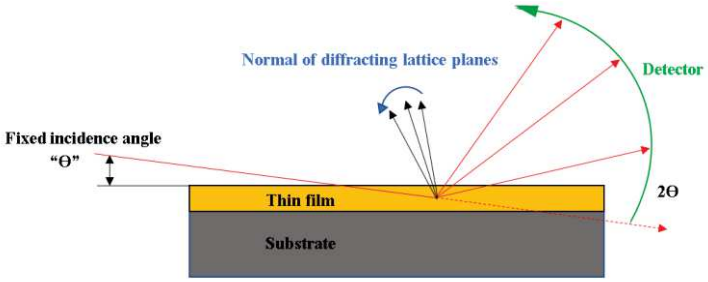

Figure 2.14: Thin film scan: 2Θ scan with fixed Θ.

Then the response to the beam depends on the incident angle value compared to that of the characteristic critical angle of the material. In order for the characteristic peaks to appear Θ should be slightly greater than Θ_c. The critical angle is calculated from the electronic density (ρ_e) using equation 2.7:

$$\Theta_c=\sqrt{\frac{\rho_e}{14.4}} \qquad \text{(Equation 2.7)}$$

Table 2.3: Calculated Θ_c.

	Pt	Au	Cu	CuO	Cu_2O
Θ_c (°)	0.55	0.56	0.41	0.3	0.22

However, As the beam penetrates the material, it gets absorbed so the beam intensity is then reduced. The density and the property of the deposited material deposited affects largely the penetration depth of the beam. For example, in some cases, even if $\Theta_i > \Theta_c$, the attenuation length wouldn't be sufficient to penetrate the material and provide the corresponding XRD peaks.

Table 2.4 shows X-ray attenuation length for a ~1.5 µm CuO thin film on Pt Si wafer varying with the corresponding Θ_i. According to Table 2.3, Θ_c =0.3of CuO but at 0.3 according to Table 2.4 only the extreme surface is observed (3.51 nm). And as Θ_i is increased, the penetration into the deposit increases expected to result in more intense signals.

Table 2.4: X-ray attenuation length.

Θ_i (°)	X-ray attenuation length(nm) at 8050.92 eV and ρ=5.7g/cm^3
0.3	3.51
0.4	532.8
0.5	1065
1	2086

Conclusion

This chapter allows a closer understanding to the different techniques used to characterize the suspensions prior to deposition. the experimental procedure of EPD technique is also explained. Finally, the characterization techniques used to evaluate the spectral selectivity and properties of the absorber are also discussed.

References

[1] X. Llovet, C. Merlet, Microscopy and Microanalysis, 16 (2010) 21-32.

Chapter Three:

Electrophoretic deposition of CuO in Isopropanol

3. Introduction

Many efforts have been done to create a rule of thumb on forming a suitable suspension to be used for EPD. It has been generally accepted that the most important characteristics of the suspension are moderate zeta potential, high stability and low viscosity. In order for the deposition step to occur, charged particles have to overcome the inter-particle repulsive forces and be destabilized beside the electrode. Thus, if the value of the zeta potential is too high then no deposition will occur. The possibility of attaining the combination of all these properties renders EPD of an unstudied powder system (such as CuO) complex requiring an individual study. One of the challenging aspects of using commercial CuO nanopowder, is finding the suitable stabilizing medium since it sediments in water [1], dissolves in highly acidic solutions [2] and is slightly stable in alcohols [3]. The traditional approach of choosing a suitable suspending medium for EPD is based on using easily accessible industrial solvents such as acetone and alcohols (Ethanol, Isopropanol, etc.). Along with water these solvents are the preferred media since their polar feature facilitates the migration of charged particles upon the application of an electric field. The appropriate media to disperse the nanoparticles has to display a significant dielectric constant and also a wide electrochemical window. Among the available solvents, isopropanol (IPA $\mathcal{E}$=18.3, 25^{o}C) is widely used in EPD and more precisely for the stabilization of ZnO nanoparticles and phosphor particles in the presence of $Mg(NO_3)_2.6H_2O$ as a stabilizing agent [4-8].

Moreover, deposits formed for low temperature solar receptors must meet certain requirements in order to achieve a tandem effect between the deposit and the substrate. The deposit thickness, the packing density and the deposit morphology should be optimized in order to ensure maximum absorption of sunlight, yet preserving the optical properties of the substrate. On the other hand, the deposit must have sufficient adhesion strength to withstand handling during manufacturing and application.

In this chapter, CuO stabilization is studied in IPA by the addition of $Mg(NO_3)_2.6H_2O$ as a stabilizing agent [4-8]. Deposit thickness and morphology is controlled by varying different parameters such as applied electric field, deposition time and nanoparticles concentration. Finally, the spectral selectivity of the obtained deposits as a function of different deposition parameters is reported.

3.1. Stabilization of CuO in isopropanol

Isopropanol is widely used as a solvent for different suspensions used in EPD. It has a moderate dielectric constant ($\mathcal{E}$ =18.3, 25°C) and a quite wide electrochemical window. However, the idea of using IPA as a stabilizing medium for CuO was inspired from the reported studies of Talbot *et al.* [6-8], on the effect of the presence of $Mg(NO_3)_2$ on the EPD of phosphors in IPA. They suggested that the slight dissociation of magnesium nitrate, maintains a positive charge on the suspended particles resulting in a higher stability. Then, due to the presence of water impurities, minor electrolysis reactions occur forming $H_{2(g)}$ and $OH^-_{(aq)}$ species at the cathode. As a result, the combination of these electrochemical and precipitation reactions forms a deposit of $Mg(OH)_{2(S)}$ at the cathode which plays the role of binder material (see equations 3.1-3). The source of water is the solvent itself, the hydrated magnesium nitrate as well as any water adsorbed from the atmosphere.

$$Mg(NO_3)_2 \rightarrow MgNO_3^+ + NO_3^- \ (K_d = 1.5x10^{-4}\ M) \qquad (3.1)$$

$$2H_2O + 2e^- \leftrightarrow H_{2(g)} + 2OH^- \ (E^\circ = -1.025V\ vs.\ Ag/AgCl) \qquad (3.2)$$

$$Mg(NO_3)^+ + 2OH^- \rightarrow Mg(OH)_{2(s)} + NO_3^- \qquad (3.3)$$

In order to observe the effect of $Mg(NO_3)_2$ on the stability of CuO in IPA, the concentration of CuO was fixed. For 0.1wt% suspension and above, the color of the suspension was dark black which causes the heating of the sample during light scattering measurements (DLS, Doppler velocimetry) due to the absorption of the laser by the black color. This change in temperature causes improper measurement. As a result, 0.05 wt% is considered as an intermediate concentration compared to 0.1 wt % where the sample can't be studied profoundly. At this concentration, the suspension stands still for ~30 mins and light scattering measurements could be applied. To investigate the role of $Mg(NO_3)_2$ in the suspension, the zeta potential values ζ(mV) and the hydrodynamic diameter D_h(μm) of particles were analyzed as a function of $[Mg(NO_3)_2]$ (see Figure 3.1). In the absence of $Mg(NO_3)_2$, CuO nanoparticles are unstable in IPA and have a hydrodynamic diameter (D_h) of ~1μm and a zeta potential (ζ) of -8.2 mV. As $Mg(NO_3)_2$ (1.5×10^{-6} g/cm^3) is added to the suspension, the zeta potential value is shifted to positive, implying that $Mg(NO_3)^+$ surrounds the surface of CuO nanoparticles. Then, as $[Mg(NO_3)_2]$ increases, the magnitude of the zeta potential increases reaching a maximum value of $/\zeta/ = 35 \pm 5$ mV for $[Mg(NO_3)_2] = 1.5 \times 10^{-5}$-$1.5 \times 10^{-4}$ g/cm^3. Then for further increase in $[Mg(NO_3)_2]$ the zeta potential value decreases

reaching its minimum of ~5 mV for $[Mg(NO_3)_2] = 1.5 \times 10^{-3}$ g/cm^3. Similarly, same variation of the measured hydrodynamic diameter of CuO nanoparticles in observed. As the concentration of $Mg(NO_3)_2$ increases, the apparent hydrodynamic diameter decreases reaching its minimum for $[Mg(NO_3)_2]$ in the range of [10^{-5}-1.5 x 10^{-4} g/cm^3]. At higher concentration, large agglomerates are formed (>2000nm).

The increased addition of $Mg(NO_3)_2$ increases the conductivity of the suspension due to the high amount of free ions present in the medium, which become the main current carrier. This results in reduced electrophoretic mobility and consequently reduced zeta potential (see chapter 1) [9, 10].

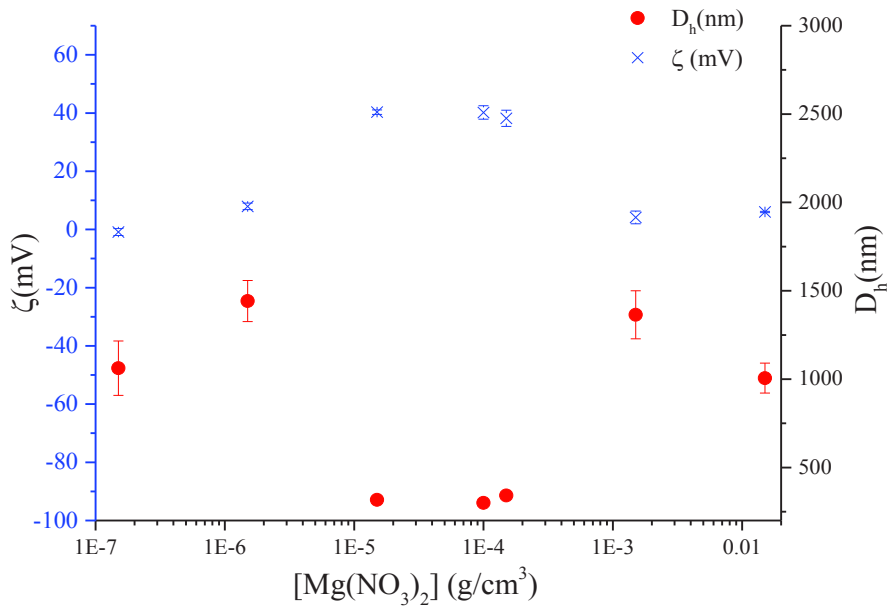

Figure 3.1: zeta potential ζ(mV) and hydrodynamic diameter D_h(nm) of CuO-IPA suspension as a function of the present $[Mg(NO_3)_2]$ (g/cm^3).

For the following, the $Mg(NO_3)_2$ concentration is fixed at 1.5 x 10^{-4} g/cm^3 because it lies in the range of concentration where the hydrodynamic diameter achieves the lowest value, indicating that the formation of large clusters is prevented and the stabilization of colloid is achieved. On the other hand, for this range of concentration, the highest measured but moderate magnitude of zeta potential value is reached, implying that the electrophoretic mobility is high too, thus deposition will occur.

3.2. Electrophoretic deposition of CuO in IPA

For organic solvents, a high electric field is usually applied to promote the migration of charged nanoparticles. The wide electrochemical window of organic solvents allows the application of high electric fields without their dissociation during EPD. In contrast, very low applied electric fields are used for water suspensions in order to avoid electrolysis reaction at the electrodes (see Chapter 1)

The EPD setup was formed using two connection electrodes (CE and WE) for EPD experiments for $E \geq 10 V.cm^{-1}$ and three connection electrodes (CE, RE(Ag/AgCl), and WE) were used for $E=5 V.cm^{-1}$. For fundamental studies metallized Au Si wafers were used as WE or deposition electrode offering that characteristics of conductive substrate facilitating the analysis later by cross-section in SEM. Pure Pt foil of the same area of Au Si wafer was used as counter electrode (CE). The distance between the electrodes was fixed at 1cm and the RE was placed in between the two electrodes when three connections are used.

The suspension was prepared by adding 5 x 10^{-4} $g/cm^3$of CuO to 100 mL IPA containing 1.5 x 10^{-4} g/cm^3 $Mg(NO_3)_2.6H_2O$. The suspension was then stirred mechanically for 5 mins then submitted to ultrasound for 20mins followed by mechanical stirring overnight. Then, before each EPD experiment the suspension was submitted to ultrasonic irradiation for 15 mins followed by mechanical stirring for 5 mins. The applied electric field was varied between 5 and 100 $V.cm^{-1}$ to determine the optimum applied electric field. Then the deposition time was varied between 5 and 60 mins.

3.2.1. Effect of $Mg(NO_3)_2$ as a binder material

The pictures of CuO deposits obtained by the EPD of CuO /IPA suspension with and without $Mg(NO_3)_2$ are shown in Figure 3.2 with the corresponding EDS analysis. The inserted pictures in figure 3.2 a and b represents the photographs of the formed deposits on Au Si wafer. In the absence of $Mg(NO_3)_2$, the yellow color of Au substrate is almost the same (Figure 3.2a, insert) which means that a very thin layer of particles has been formed. The analysis of the deposit by SEM and EDX shows a deposit of clusters of CuO scattered on the substrate of varying size between 1 and 10 µm and composed of CuO (see Figure 3.2a). However, in the presence of $Mg(NO_3)_2$, a dark black color is formed on the Au substrate. The SEM micrograph shows a denser and a thicker deposit of CuO film, hiding the substrate, and

having a varying size between 0.3-0.5 µm. According to EDX analysis, the deposit is composed from Cu, Mg, O.

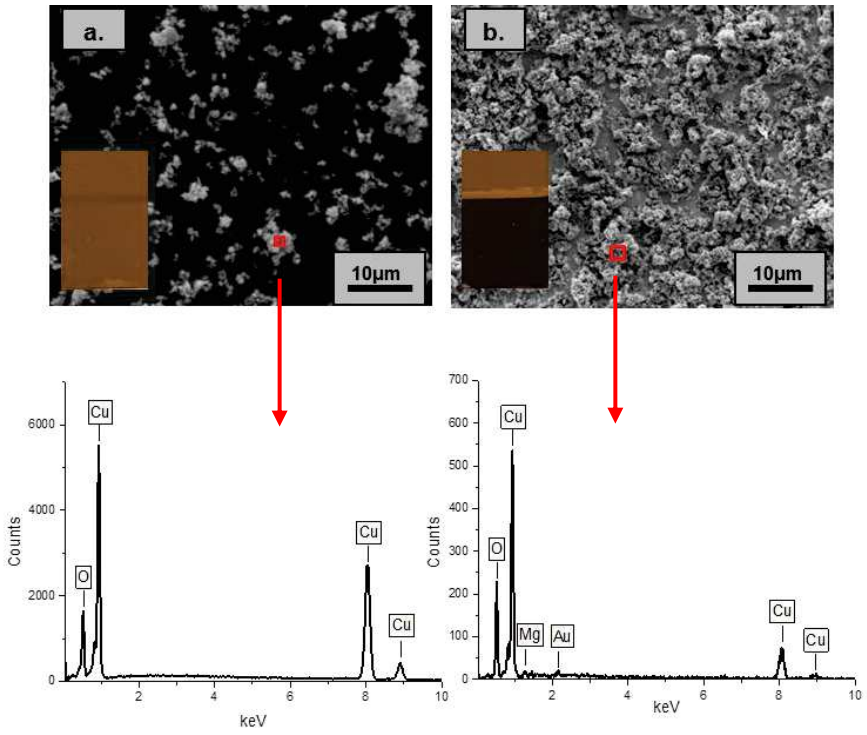

Figure 3.2: SEM top view image of the CuO deposits form CuO/IPA suspension ([CuO]= $5x10^{-4}g/cm^3$): (a) absence of $Mg(NO_3)_2$ and (b) in presence of $[Mg(NO_3)_2]$ = (1.5×10^{-4} g/cm^3) with the corresponding EDX spectrums: 50% O and 50% Cu (a) whereas 54.4% O, 1% Mg and 43.6 % Cu (b).

3.2.1.a. Analysis of the composition of the deposit

In order to verify the composition of the deposit formed on the AuSi wafer substrate, FTIR, elemental mapping and GIXRD were performed. The FTIR measurement determines the identity of Mg binder material, the elemental mapping localize the Mg binder in the deposit to understand the mechanism of deposition. Finally, the GIXRD allows the identification of the CuO phase present in the deposit.

3.2.1.b. FTIR measurement

The FTIR spectra of EPD deposits formed from: $CuO/Mg(NO_3)_2$/IPA suspension, $Mg(NO_3)_2$/IPA solution, and CuO/IPA suspension are represented in Figure 3.3. A characteristic OH band at 3700 cm^{-1}, the broad peaks at 1656 and 1403 comes from C-H stretches of the IPA and the OH in-plane bending of $Mg(OH)_2$ confirming its formation at the

cathode as reported by Talbot *et al.* [10]. The spectrum of CuO deposited shows a characteristic band at 527 cm^{-1} and 426 cm^{-1}, typical for CuO. The EPD deposit of CuO, in the presence of $Mg(NO_3)_2$ in the suspension displays a wide peak in the Far IR due to the presence of Cu-O and Mg-O (M-O bonds) in the deposit.

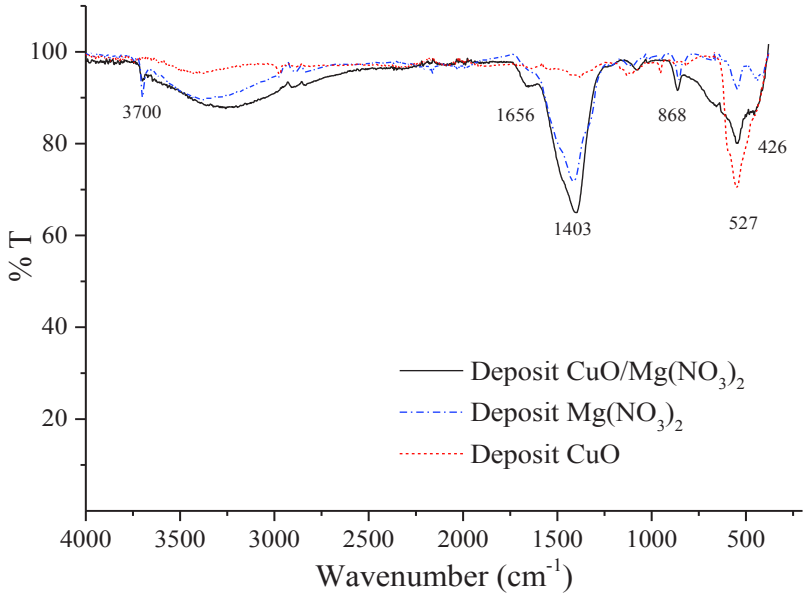

Figure 3.3: %T spectra of the EPD deposits of $CuO/Mg(NO_3)_2$/IPA suspension; ($CuO/Mg(NO_3)_2$); deposit obtained from $Mg(NO_3)_2$/IPA suspension and CuO/IPA suspension.

3.2.1.c. EDX-Elemental mapping

In order to localize the binder $Mg(OH)_2$ in the deposit, Surface Elemental mapping was performed by using EDX (see Figure 3.4). It clearly shows that Cu is more abundant than Mg species which are distributed between the particles in the deposit. The substrate (Au) is also observed, which is due to irregularity in the deposit. A small amount of N is also present could be coming from the residual suspension during the removal of the deposit. The final micrograph combining all the species together shows that Mg is dispersed in the deposit between the deposited particles of CuO.

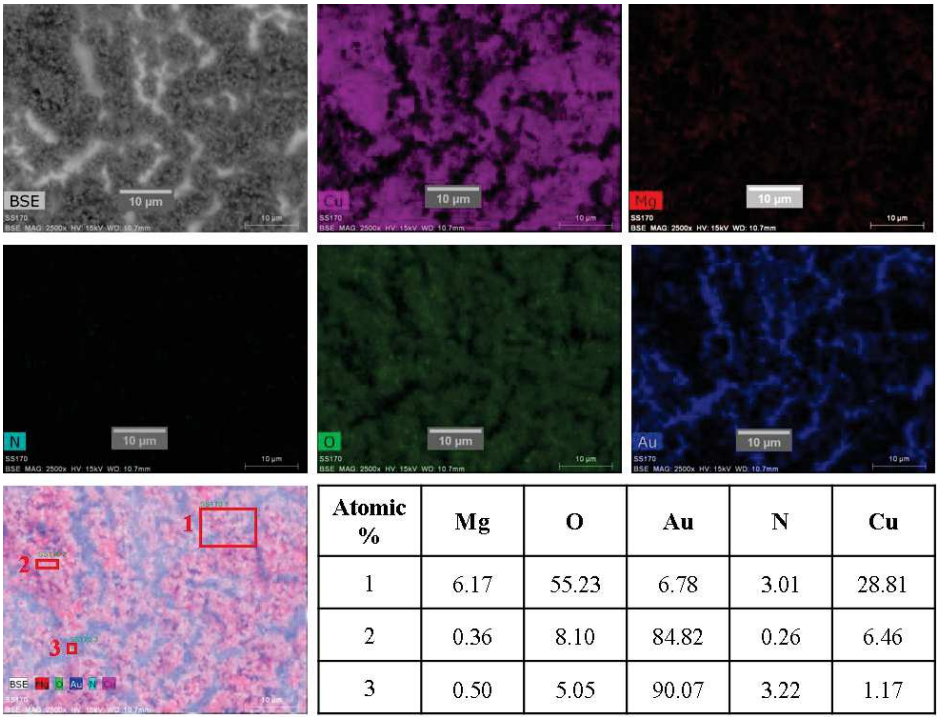

Atomic %	Mg	O	Au	N	Cu
1	6.17	55.23	6.78	3.01	28.81
2	0.36	8.10	84.82	0.26	6.46
3	0.50	5.05	90.07	3.22	1.17

Figure 3.4: Elemental mapping of Au-CuO/Mg film deposit by EPD of CuO/Mg(NO3)2/IPA suspension (15 mins, 50 V/cm^{-1}).

As a result, we suppose that upon the dissociation of $Mg(NO_3)_2$, the $Mg(NO_3)^+$ ions surrounding the negatively charged CuO results in a positively charged particle allowing then the cathodic deposition. $Mg(NO_3)_2$ plays a double role first as a charging agent and second as a binder material for the CuO, which is in agreement with the reported studies by Talbot et al on the EPD of phosphors/IPA suspensions in the presence of $Mg(NO_3)_2$ [11].

3.2.2.c. Grazing Incidence X-ray Diffraction of the deposit

X-ray diffraction measurements of thin films using conventional Θ/2Θ scanning methods usually produces a weak signal from the film and an intense signal from the substrate. In these conditions, it is difficult to identify the CuO phase. Thus, to avoid such phenomena, a 2Θ scan is performed with a fixed grazing angle of incidence, known as GIXRD. Figure 3.5 shows the comparison between a conventional Θ/2 Θ scan of 0.05 wt% CuO deposit and a GIXRD scan collected with a varying grazing incidence angle between 0.3-1°. As expected, the scan obtained from the conventional XRD reveals an intense peak at 38.3° corresponding to the gold substrate (111) plane and little information of the film which could not be distinguished from the noise coming from the analysis. While the GIXRD scan of the same deposit shows two intense peaks at 35.5° and 38.8° corresponding to single phase

CuO with a monoclinic structure. In this case the major phase (011) of $Mg(OH)_2$ at 2Θ=38.0° (JCPDS 84-2164) could not be indexed by XRD since it is masked by CuO (111) phase. The peaks of the Au substrate are not observed since the grazing incidence angles used are lower than the critical angle (Θ_c) of gold which in general is equal to 0.35. However, the critical angle of the substrate is usually shifted to higher values depending on the thickness, the density and the type of the deposit covering it. This explains why the peak of Gold is not observed clearly even at Θ=1°.

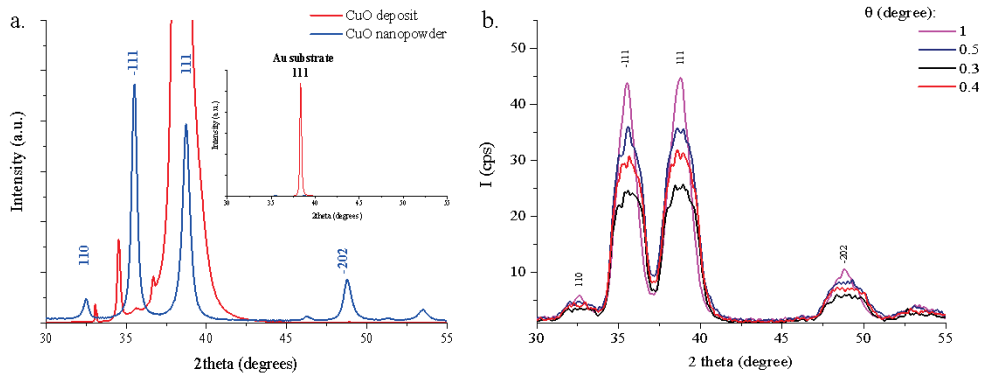

Figure 3.5: X-Ray diffraction analysis of the deposit obtained from of 0.05 wt % CuO deposit: a) conventional XRD; b) GIXRD.

3.2.2. Effect of CuO concentration

After fixing [$Mg(NO_3)_2$] at 1.5 x 10^{-4}g/cm^3, three different suspensions were prepared for three different CuO concentrations 0.05%, 0.01%. and 0.005%. EPD was then performed at 50 V.cm^{-1} for 15 mins. We observed that as the solid loading of CuO in the suspension increases, the deposit color is darker which corresponds to the amount of CuO deposited.

SEM analysis of the surface and cross-section view of the corresponding deposits are represented in Table 3.1. It is observed that as the amount of CuO increases in the suspension, the density and thickness of CuO increases.

Table 3.1: top and cross-section view SEM images of CuO deposits for a deposition time of 15 mins and applied electric field of 50 V.cm^{-1}

%W / time	0.001	0.01	0.05
Top-view	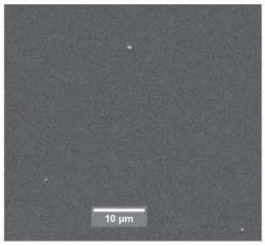	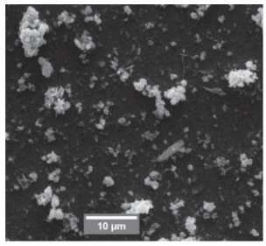	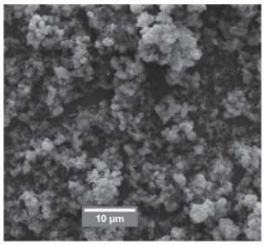
Cross-section		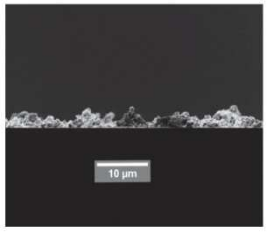	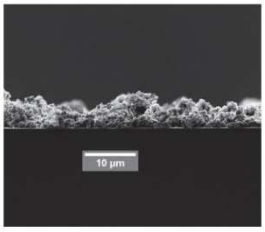

The SEM cross-section micrographs, allow the thickness measurement (see Figure 3.6) which is found to vary between 0.5µm for the lowest and 4.8 µm for the highest concentration, respectively. It is also evident from the graph of thickness vs %wt of CuO that the standard deviation of the thickness decreases with the increased concentration. This due to the deposition of higher amount of CuO as the amount of CuO increases in the suspension, which is also in agreement with Hamaker equation. As a result, the concentration of CuO is fixed at 0.05 wt% for the studies that follow.

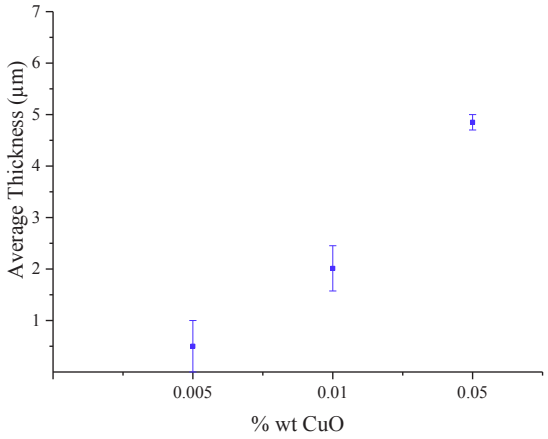

Figure 3.6: Average measured thickness of CuO deposits formed from: [CuO]= 5x10^{-4}, 10^{-4}, and 5x10^{-5} g/cm^3,in 1.5x 10^{-4} g/cm^3 $Mg(NO_3)_2$/IPA solution. EPD conditions: E=50 V.cm^{-1}, t=15 mins

3.2.3. Effect of applied electric field

In order to explore the effect of applied electric field on the deposit thickness and morphology, the deposition time and the suspension concentration were fixed and the applied electric field was varied (see Table 3.2).

Table 3.2: Parameters used to explore the effect of applied electric field

Suspension		EPD Setup and parameters	
[CuO] (g/cm^3)	$5x10^{-4}$	E ($V.cm^{-1}$)	5-10-20-30-40-50-100
		Deposition time (mins)	15 mins
[$Mg(NO_3)_2$] (g/cm^3)	$1.5x\ 10^{-4}$	Surface Area	2.5 x 2 cm^2
		Inter-electrode distance	1cm
Solvent (100 mL)	IPA	WE/CE WE/RE/CE	Au Si wafer / Pt AuSi/Ag,AgCl/KCl(3.5M)/Pt

The morphology and the microstructure of the deposits could be observed from the SEM top-view micrographs (see Table 3.3,Table 3.4, and Table 3.5). As E increases the deposit becomes denser and more particles are deposited covering completely the substrate. Moreover, at low magnification, the deposits look regular and the substrate shows the highest coverage at $100V.cm^{-1}$.

Table 3.3: SEM top view micrographs at E=5-20 V.cm^{-1}and t=15 mins.

5 V.cm^{-1}	10 V.cm^{-1}	20 V.cm^{-1}
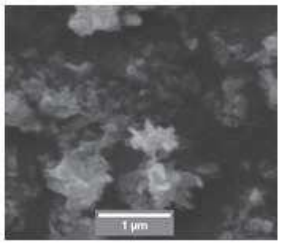	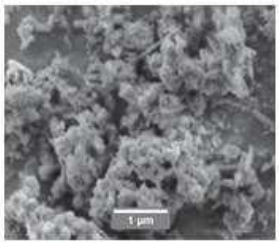	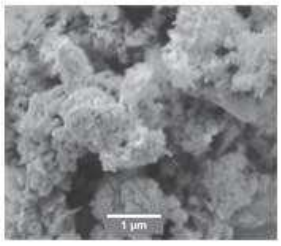
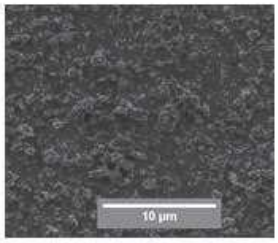	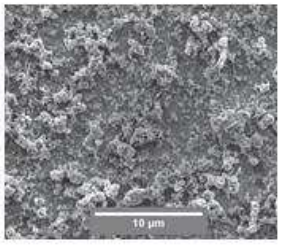	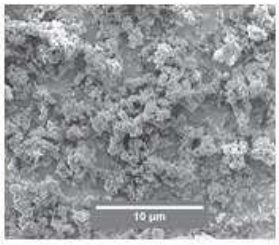
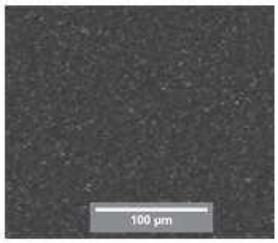	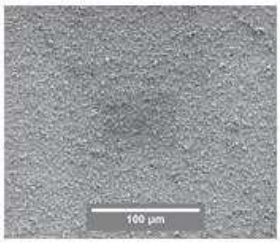	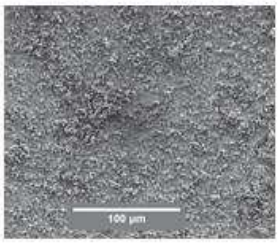

Table 3.4: Top-view SEM micrographs of deposits obtained at E= 30- 50 V.cm^{-1} and t=15 mins.

30 V.cm^{-1}	40 V.cm^{-1}	50 V.cm^{-1}
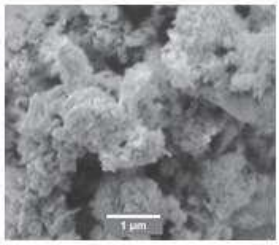	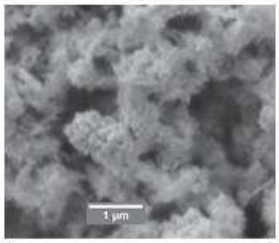	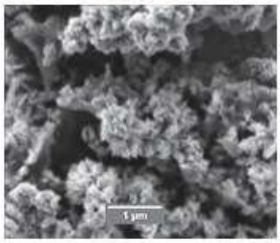

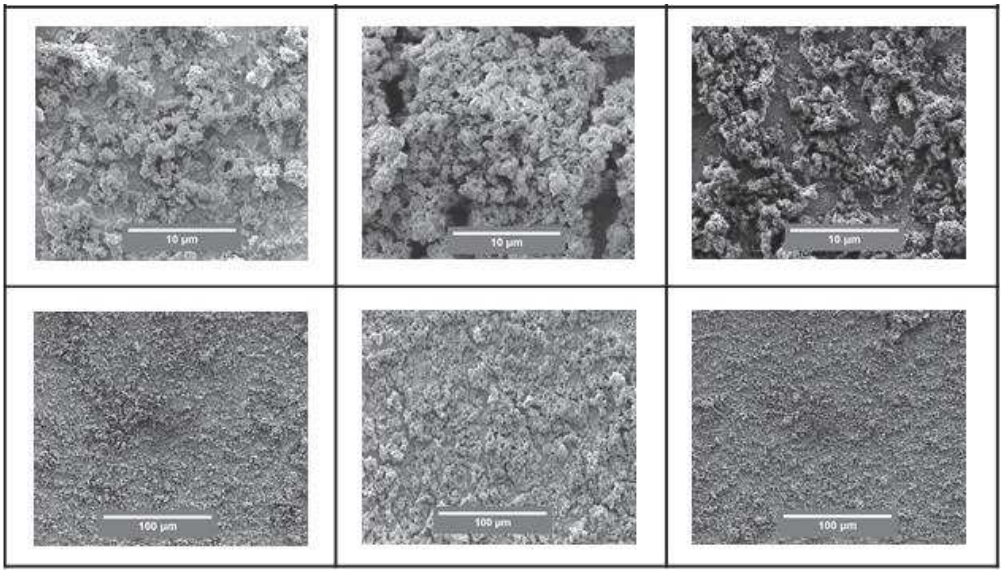

Table 3.5: Top-view SEM micrographs of deposits obtained at 100 V.cm^{-1}, at different magnification.

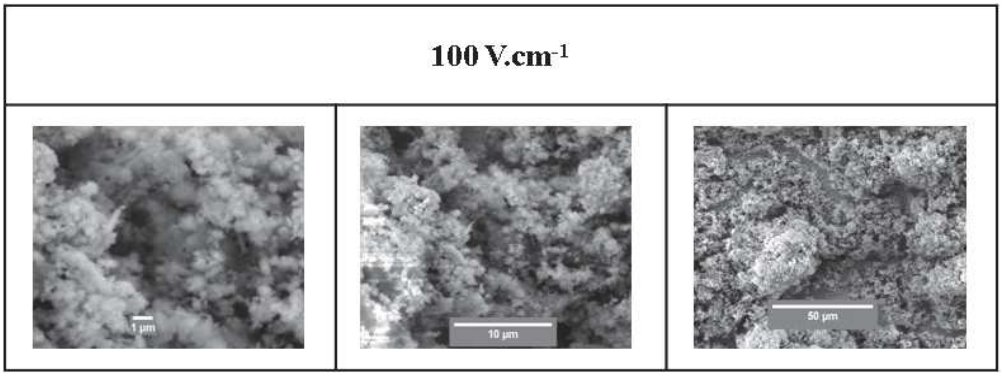

The deposit thickness is then obtained from the SEM cross section and traced against the applied electric field (see Figure 3.7).

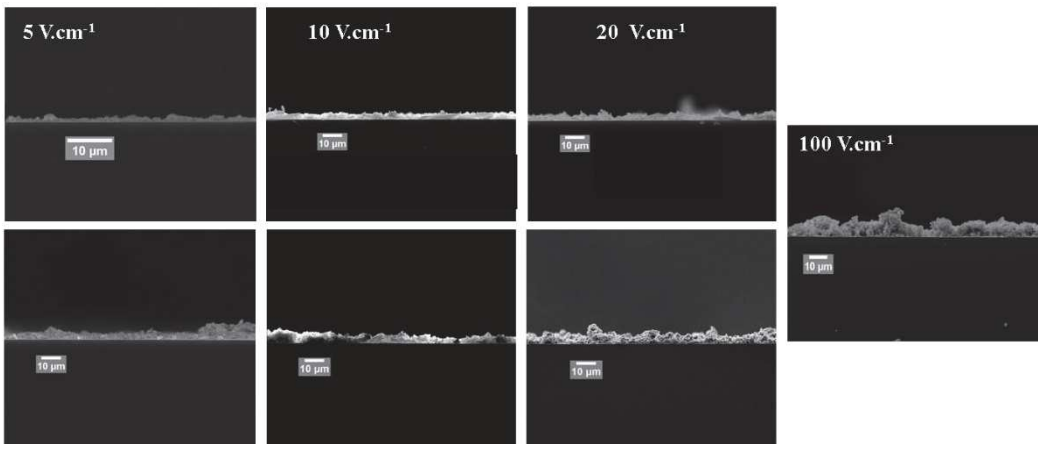

Figure 3.7: SEM cross-section micrographs of deposits obtained at 5-100 V.cm^{-1}

.

The average thickness of the deposit increases linearly with applied electric field, which is expected. The measured values vary between 1.8 to 9.5µm with a significant error bar. This is expected since the surface morphology and the size of deposited agglomerates varies with the applied electric field.

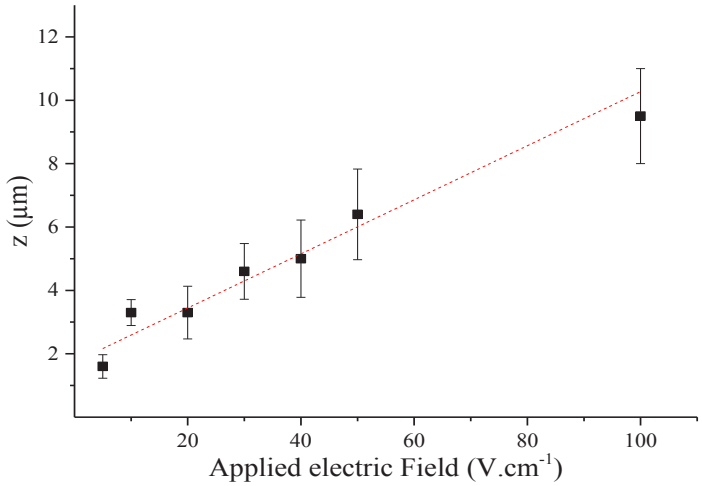

Figure 3.8: Average thickness (z), obtained from SEM cross section, as a function of E ($V.cm^{-1}$).

Moreover, the increase in the magnitude of the applied electric field pushes all the charged particles toward the electrode influencing their packing behavior. The quality of the film then depends on the accumulation rate of the particles beside the electrode. Basu and Das [12, 13] showed that only at moderate applied electric field a good quality coating could be observed. They explained that at high applied electric field, the particles migrate very fast and they do not deposit at positions forming ordered structures. The high electric field also causes a turbulence in the suspension by affecting the solvent stability during EPD. Negishi *et al.* [14] have also reported that the stability of n-propanol solvents is altered for applied electric fields higher than 50 $V.cm^{-1}$. On the contrary, at a low electric field, charged particles migrate very slowly and then agglomerate before reaching the electrode preventing their deposition. Knowing that there are several parameters influencing the deposition step during EPD, no rule of thumb could be adapted to determine the effect of applied electric field. So, each system has to be critically studied alone. In this context, we have chosen to study the effect of the deposition time at low voltage (5, 10 $V.cm^{-1}$), and moderate voltage (50 $V.cm^{-1}$). To avoid any turbulence in the suspension during EPD and ensure the stability of IPA, effect of deposition time at 100$V.cm^{-1}$ will not be studied.

3.2.4. Effect of deposition time

In order to study the effect of deposition time and understand the kinetics of EPD at the different applied electric field, the deposition time was varied between 1 and 30 mins for a fixed applied electric field (see Table 3.6):

Table 3.6: Condition for EPD deposition at different deposition time.

Suspension		EPD Setup and parameters	
[CuO] (g/cm^3)	$5x10^{-4}$	E ($V.cm^{-1}$)	5-10-50
		Deposition time (mins)	1-30 mins
[$Mg(NO3)_2$] (g/cm^3)	$1.5x\ 10^{-4}$	Surface Area	$2.5x2.cm^2$
		Inter-electrode distance	1cm
Solvent (100 mL)	IPA	WE/CE WE/RE/CE	Au Si wafer / Pt AuSi /Ag,AgCl/KCl (3.5 M)/Pt

The SEM cross-section of deposits represented in Table 3.7, shows that deposit thickness increases with time and the deposits are highly porous and loosely packed.

Table 3.7: Effect of deposition time on the deposits obtained at 5, 10, and 50V.cm^{-1}.

E / time	5 V.cm^{-1}	10 V.cm^{-1}	50 V.cm^{-1}
5 mins	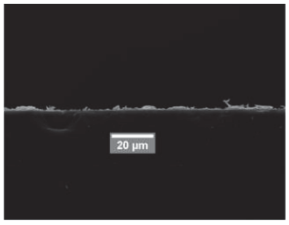	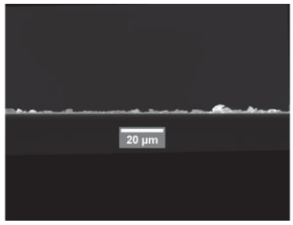	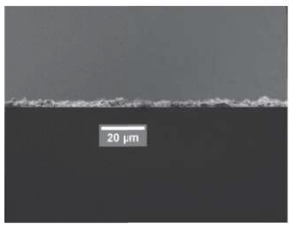
10 mins	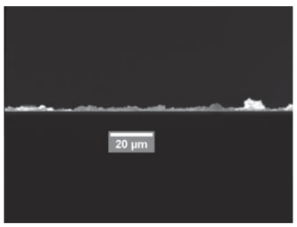	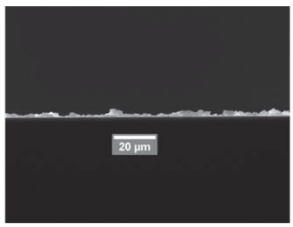	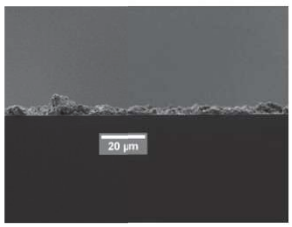
15 mins	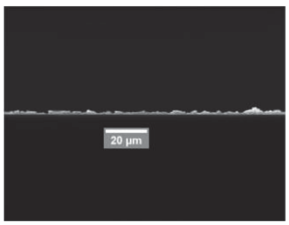	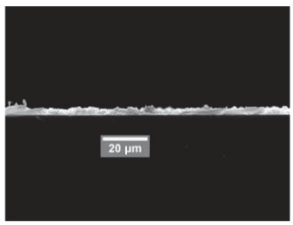	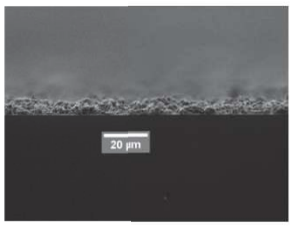
30 mins	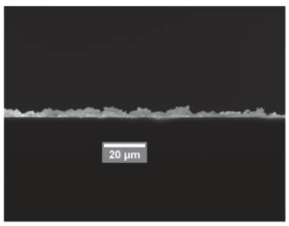	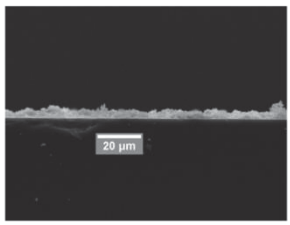	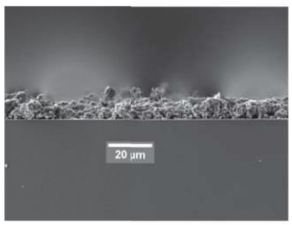

In order to calculate the effective density of the deposits, a Hamaker-Law type equation is used (see equation 3.4):

$$z = \frac{C_S.\mu_e.E.t}{\rho} \tag{3.4}$$

At a constant applied electric field "E"in V.cm^{-1}, solid concentration "C_s" in g/cm^{3}and electrophoretic mobility "μ_e" in cm^{2}V^{-1}s^{-1}, z is then considered directly proportional to the deposition time "t". After extracting the slope of the fit of the graph of z vs t then "ρ_e" is

directly calculated. From the SEM cross-section (see Table 3.7) the thickness "*z*" of the deposits are determined and plotted against the deposition time (see Figure 3.10). This plot shows a linear increased variation of *z* with time. After extracting the slope of the fit from the graph of z vs t, ρ_e is directly calculated. Note that the intercept is considered different from zero due to inherent dip coating effects based on unmatched clusters deposition induced by the different applied electric fields. For deposition at 5, 10 and 50 V.cm^{-1}, ρ_e is 0.35, 0.49, and 1.69 g/ cm^3, respectively. These values are considered very low compared to the theoretical density of bulk CuO (6.3 g/cm^3) but this was expected based on the micrographs obtained from SEM.

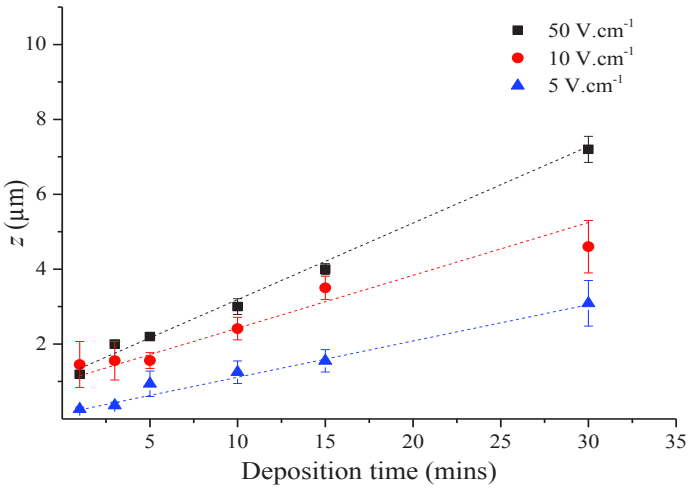

Figure 3.9: Thickness (obtained from a SEM cross section) as a function of deposition time from a 0.05%W suspension of CuO containing 10^{-3}g/cm3 of $Mg(NO_3)_2$.

The difference in density between the applied electric fields is attributed to the force the electric field applies on the particle while it migrates to form a deposit. When a sufficiently high electric field is applied agglomerates are forced to migrate and deposit with other smaller particles. This explains why bigger agglomerates are observed in the deposit as a function of increasing electric field (see Figure 3.10) which justifies the increasing effective density.

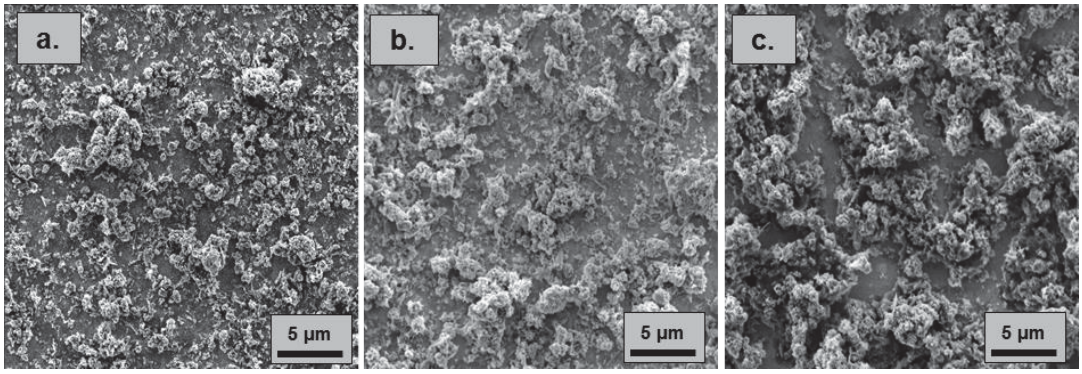

Figure 3.10: SEM top-view images of CuO deposited at AuSi wafer for a deposition time of 15 minutes: a) at 5 V.cm^{-1}; b) at 10 V.cm^{-1}; and c) at 50 V.cm^{-1}.

However, for deposition time greater than 30 minutes, deposits formed at 5 and 10 V.cm^{-1} detach from the substrate, while those obtained at 50V.cm^{-1} shows better adherence to the substrate up to a deposition time of 60 minutes. Then thick deposits of ~20 µm are formed. Thus, for comparison, this study was limited to 30 mins.

3.3. Spectral Selectivity

3.3.1. Effect of the deposition time on total reflectance (%R)

The spectral selectivity of the coatings investigated at different deposition times and applied electric field are represented in the Figure 3.12. The tandem system effect from the coating and the substrate is evidenced through the two distinct cut-offs or absorption edges (λ_c) of CuO and AuSi wafer appearing at 0.8µm and 0.47µm, respectively. As the deposit thickness increases, the substrate cut-off gradually disappears and the spectrum is shifted toward CuO cut-off. The total reflectance spectra show an apparent selectivity in the solar spectrum region (0.28-2.5 µm) and a sharp decrease in the total reflectance of the obtained coatings with the increase of the deposition time. In the IR region (2.5µm-16µm), the total reflectance is high at low deposition times and then decreases smoothly with the increasing thickness. It is noticeable that the applied electric field has a direct effect on the deposit thickness obtained and consequently on the spectral selectivity. The lowest overall %R is attained at 50 V.cm^{-1} compared to those obtained at 10V.cm^{-1} and 5V.cm^{-1}. This suggests that 50V.cm^{-1} is the condition which yields to the best tandem system having the lowest %R, for a deposition time of 30 minutes.

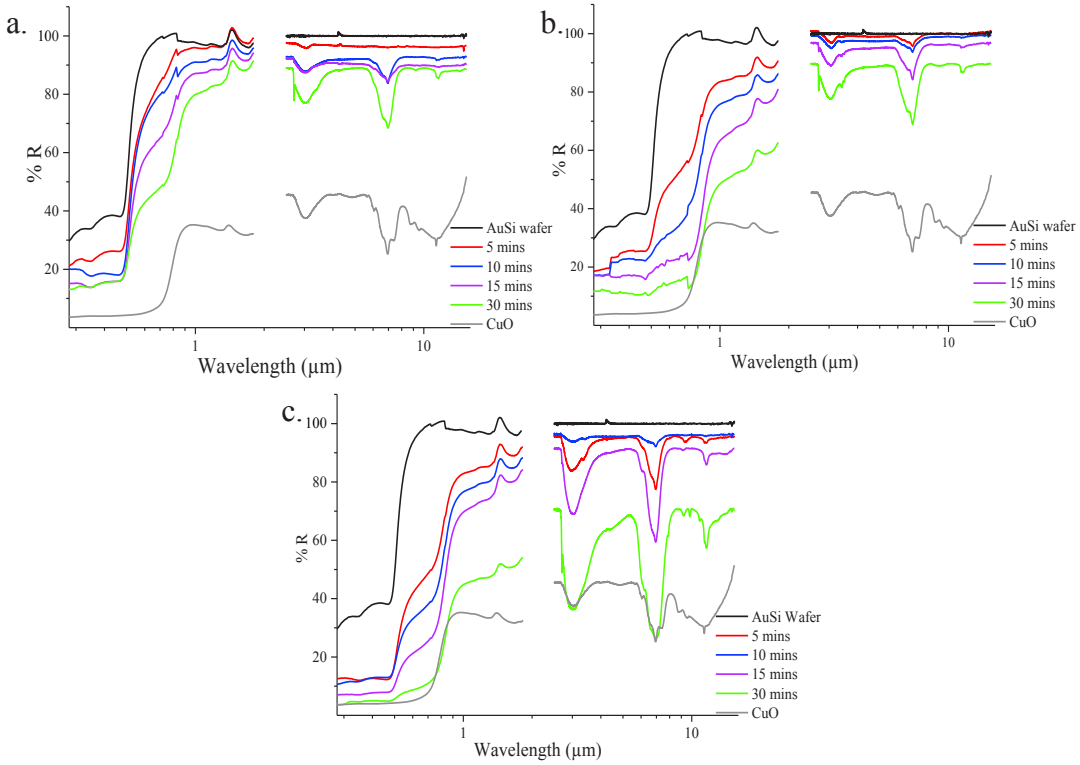

Figure 3.11: Spectral selectivity of the obtained films: a) at 5V.cm^{-1}, b) 10V.cm^{-1} and c) 50V.cm^{-1}.

3.3.2. Spectral Selectivity

The absorptance and the emittance calculated from the reflectance spectra against the deposited yield ($\rho_e z$, mg/cm^2) for a deposition time ranging between 3 and 30 minutes are represented in Figure 3.13, $\rho_e z$ in each case is calculated from the effective density values multiplied by the thickness obtained at each deposition time. The calculated absorptance and the emittance of the bare AuSi wafer and the starting CuO nanopowder are presented as dotted lines. The slight variation of the ε as a function of the deposited mass explains the low density of the films calculated for each applied electric field, compared to the bulk density of CuO (6.3 g/cm^3). Thus, the low emittance of the substrate is still conserved despite the high thickness, such as in the case of 7µm deposited at 30 mins and 50V.cm^{-1} ($\rho_e z$=1.22 g/cm^2). The α values obtained in the case of 5V.cm^{-1} increases between 0.25 and 0.55 for a $\rho_e z$ ranging between 0.01 and 0.11 mg/cm^2. While for 10 V.cm^{-1}, α ranges between 0.33 and 0.70 for a $\rho_e z$ ranging between 0.07 and 0.23 mg/cm^2. For 50V.cm^{-1}, α ranges between 0.46 and 0.80 for a $\rho_e z$ values between 0.20 and 1.22 mg/cm^2. Note that the absorptance increases with $\rho_e z$ but equivalent $\rho_e z$ from different applied electric fields yield distinct α value. This implies

that, the applied electric field affects the microstructure of the formed deposits hence the absorptance. A random micro-porosity is then obtained which is the main reason for the insignificant change in the ε values with the deposited mass. The previously analyzed SEM images of the formed deposits reveal their irregularity. The calculated surface roughness (RMS) for example, for a deposition time of 30 minutes, is 1.41 µm for 50 V.cm^{-1} and for 5V.cm^{-1} and 10V.cm^{-1} a similar roughness of 0.4 µm is obtained.

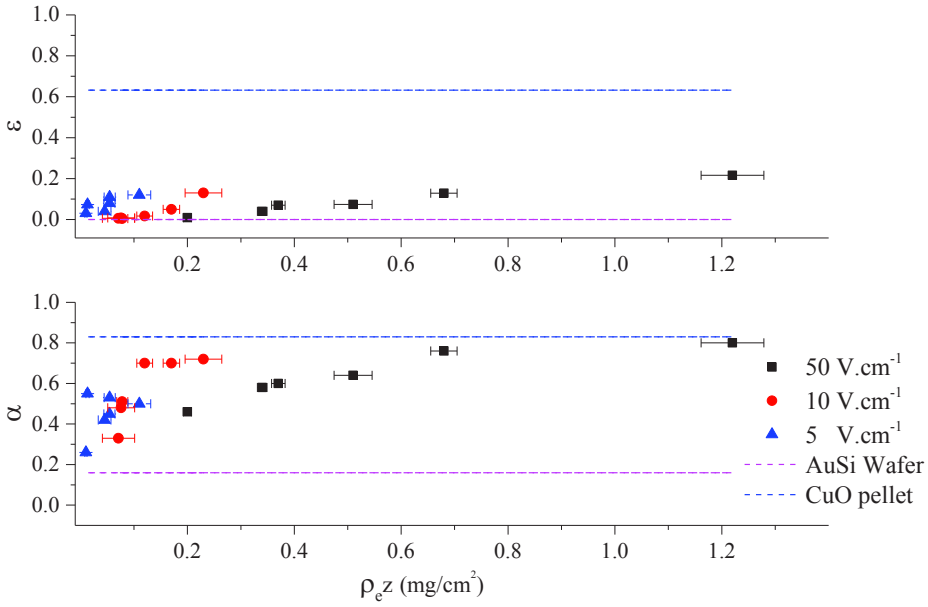

Figure 3.12 : Variation of α and ε w.r.t. deposition yield

The calculated selectivity of the tandem absorbers and their corresponding thickness as a function of deposition time are presented in Figure 3.13. As the deposit thickness increases, the selectivity of the deposits is found to decrease for all applied electric fields. At 30 mins the obtained selectivity is for 5, 10 and 50 V.cm^{-1} is 0.76, 0.82, and 0.73, respectively. It is true that the deposits obtained at 50 V.cm^{-1} have the lowest selectivity. But, this is due to the elevated emittance value as a result of increased thickness. However, deposits obtained at 50 V.cm^{-1} has higher effective density and better adhesion to the substrate.

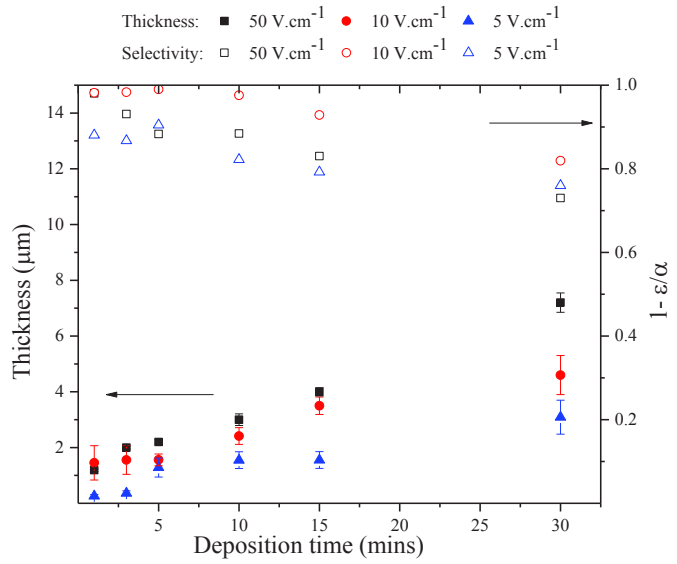

Figure 3.13: Selectivity and thickness of deposits as a function of deposition time

Conclusion

The formation of CuO-AuSi wafer tandem absorbers have been investigated by electrophoretic deposition in isopropanol, for selective optical properties. Dynamic light scattering coupled with laser doppler velocimetry experiments have evidenced that CuO nanoparticles are stabilized and positively charged by adding $Mg(NO_3)_2.6H_2O$ salt, acting also as a binder material. The zeta potential attains its highest measured value (35 ±5 mV) when $[Mg(NO_3)_2]$ is 1.5 x 10^{-4}g/cm^3. The applied electric field controls here both the thickness and the microstructure (e.g. roughness, porosity) of the coating. At low voltage (5V.cm^{-1} and 10V.cm^{-1}) the roughness is around 0.4µm and at higher voltage (50V.cm^{-1}) the roughness is 1.4 µm. The average thickness of the deposits, obtained by Scanning electron microscopy images analysis, as a function of time allowed the determination of the coating's effective density through a Hamaker law type equation. At high applied electric field, the effective density is 1.69 g/cm^3 and higher than the others, since at 10 and 5 V.cm^{-1} the measured effective density is 0.49 and 0.35 g/cm^3, respectively. At 50 V.cm^{-1} agglomerates are formed and are forced to migrate and consequently deposit with other smaller particles. The coatings obtained at 50 V.cm^{-1} showed better adhesion to the substrate compared to 5 and 10 V.cm^{-1}. Since as E increases nanoparticles are more pressed to the working electrode resulting in better adhesion and higher density. The spectral selectivity of the coating has been scrutinized by reflectance spectra measurements in order to determine the tandem

absorbers selectivity. The tandem obtained at 50 $V.cm^{-1}$ possess a selectivity 0.7 for a deposition time of 30 mins.

References:

[1] L. Fedele, L. Colla, S. Bobbo, S. Barison, F. Agresti, Nanoscale Research Letters, 6 (2011).

[2] D.A. Palmer, Journal of Solution Chemistry, 40 (2011) 1067-1093.

[3] T. Kida, T. Oka, M. Nagano, Y. Ishiwata, X.-G. Zheng, Journal of the American Ceramic Society, 90 (2007) 107-110.

[4] Z.-J. Wang, Z.-J. Wang, S.-C. Li, Z.-H. Wang, Y.-M. Lü, J.-S. Yuan, Chin. Phys., 13 (2004) 750.

[5] L. Miao, S. Cai, Z. Xiao, J. Alloys Compd., 490 (2010) 422-426.

[6] B.E. Russ, J.B. Talbot, Journal of the Electrochemical Society, 145 (1998) 1253-1256.

[7] B.E. Russ, J.B. Talbot, Journal of the Electrochemical Society, 145 (1998) 1245-1252.

[8] M.J. Shane, J.B. Talbot, R.D. Schreiber, C.L. Ross, E. Sluzky, K.R. Hesse, J. Colloid Interface Sci., 165 (1994) 325-333.

[9] R.W. Powers, J. Electrochem. Soc., 122 (1975) 490-500.

[10] B.E. Russ, J.B. Talbot, J. Electrochem. Soc., 145 (1998) 1253-1256.

[11] J.B. Talbot, J. McKittrick, ECS J. Solid State Sci. Technol., 5 (2016) R3107-R3120.

[12] R.N. Basu, C.A. Randall, M.J. Mayo, Journal of the American Ceramic Society, 84 (2001) 33-40.

[13] D. Das, R.N. Basu, Materials Research Bulletin, 48 (2013) 3254-3261.

[14] H. Negishi, H. Yanagishita, H. Yokokawa, Electrophoretic deposition of solid oxide fuel cell material powders, Electrochemical Society Inc, Pennington, 2002.

Chapter Four:

Electrophoretic Deposition of CuO in Water

4 Introduction

The use of organic solvents is popular as a suspending medium in EPD due to several advantages such as avoiding electrolytic gas evolution, joule heating, and electrochemical deterioration at the electrodes. Additionally, they possess higher density, good chemical stability and low conductivity. But their corresponding low dielectric constant limits the formation of charge on the particles due to their low dissociating power. Thus, high applied electric field is therefore required in order to promote their migration. On the other hand, there is a high interest in using aqueous systems which offer faster kinetics due to their high dissociating power, in addition to health, environmental, and cost benefits. Due to the high dielectric constant of water, particles are charged easily and thus low applied electric field is required [1].

In order to form CuO tandem solar absorbers by EPD, an appropriate stable dispersion of CuO in water should be prepared. Up to now several studies have been performed and results are mostly discouraging [2] while others have reported successful CuO dispersion using Catechol derivatives (such as Tiron) [3], Poly(vinyl alcohol)[4], PEG[5] in water. Nevertheless, none of these was reported for the aim of forming a charged suspension of CuO which could serve as a suspension for EPD.

The strategy of coating or grafting polymer to the surface of nanoparticles is often used to avoid their aggregation by inducing a surface-surface repulsion [6, 7]. Polyethyleneimine (PEI) is a cationic dispersant widely used in different sizes and structures for the preparation of stable suspensions of Ti nanoparticles [2], Ti_3SiC_2 [8], TiN [9], $BaTiO_3$ [10], ZnO [11]. The amine groups complex the surface of the metal oxide while the other free amine groups are pH sensitive leading to positive charge development. The size and the ramification of the polymer determines its mechanism of stabilization as steric or electrostatic stabilization or electrosteric stabilization (combination of steric and electrostatic stabilization) [8, 9].

In this chapter, we discuss the formation of CuO thin films by EPD, starting from an aqueous stable suspension. The stabilization of CuO in water using a cationic polymer (PEI) will be studied by varying suspension parameters such as the pH and concentration of polymer in order to select the best formulation. On the other hand, process parameters as the applied electric field and deposition time are investigated in order to form homogeneous and regular tandem absorbers by EPD. Finally, we present the surface analysis carried out to

determine the composition of the deposit and we discuss the influence of the process parameters on the spectral selectivity of the samples.

4.1. Stabilization of CuO in Polyethylenimine

In this part the stability and the dispersion of CuO by PEI is studied by light scattering zeta potential experiments (zetasizer) and AFM, respectively.

4.1.2. Effect of pH

The Zeta potential gives information on the charge of the particles which can result of the adsorption of a polymer at the particle surface, or from a reaction between the surface of the particles and the solvent. This parameter can also give information on the interaction between particles [9]. In aqueous media, the pH of a suspension of metallic oxide particles affects largely the zeta potential. On the other hand, the PEI used in these experiments is a highly branched polyamine (see Figure 4.1), composed of primary, secondary and tertiary amines achieving their cationicity through their protonation from the surrounding medium. However, primary amine groups which are the chain terminating units are the most basic and reactive. The ionization pH range of low MW branched PEI is between pH=2-10 [10].

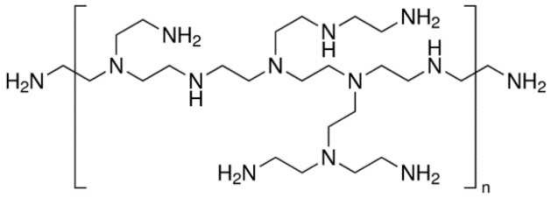

Figure 4.1: Polyethylene imine molecular structure (Mw=2000g/mol).

CuO nanoparticles are not stable in water, and sediment directly. Thus, to estimate the ZP value, 0.05 wt % of CuO was left to stir at pH=7 overnight. Then the ZP of the supernatant was measured and found to be positive of magnitude around 34 mV. This proves the presence of hydroxyl groups at the surface of CuO [4] leading to the formation of positive charge as a result of their ionization in water.

The subsequent sedimentation of CuO in water for different pH range renders the analysis by zetasizer of these samples approximative and ineligible for comparison even at very low wt% as 0.0001% (see Figure 4.2b). PEI is soluble in water and the addition of CuO to PEI solution results in blue solution having UV-VIS absorption band maxima at ~270 nm

and ~640 nm showing the formation of dative bond or a complex between surface Cu^{2+} and amine groups of PEI [12, 13]. A complete stabilization of CuO occurred for the working range of pH=3, 9, and 11. At pH=6, black sediments of CuO were observed thus CuO was not completely stabilized (see Figure 4.2c). Thus, the stabilization mechanism of CuO by PEI will be concluded by comparing the ZP of PEI to that of CuO/PEI, excluding those of bare CuO.

The corresponding ζ of bare PEI and CuO/PEI as a function of pH are presented in Figure 4.2a. The measured ζ of PEI is positive for the whole pH range studied (3-11). The magnitude of the ζ increases with decreasing pH ranging between ~4 and 22 mV. Upon the addition of CuO, the ζ shifts to higher positive values varying between 5 mV for pH=11 and 35 mV for pH=3. This proves that the PEI is well adsorbed on the surface of CuO and repulsive forces are dominating. The low values obtained at pH=11 are due to the fact that PEI is not enough protonated. At pH=9, the corresponding ζ shifts from ~5mV for PEI into ~24 mV for the suspension of CuO/PEI which proves a build-up of charge and the existence of a dative bond. At pH=6, the ζ of PEI alone is the highest compared to other pH and only a difference of ~10mV is observed between the ζ of CuO/PEI and PEI. This shows that maybe the PEI is too charged and stabilized by itself to be efficiently adsorbed by CuO surfaces. This could explain why only at pH=6 the obtained suspension is not stable and sedimentation is observed. At pH=3 the highest ζ (+35 mV) is obtained. However, the interaction between PEI and CuO is due to the dative bonds formed between Cu(II) surfaces and the amino groups of PEI resulting in surface complexation of CuO. While the other free amino groups play the role of charging agents which explain the variation of ζ with pH.

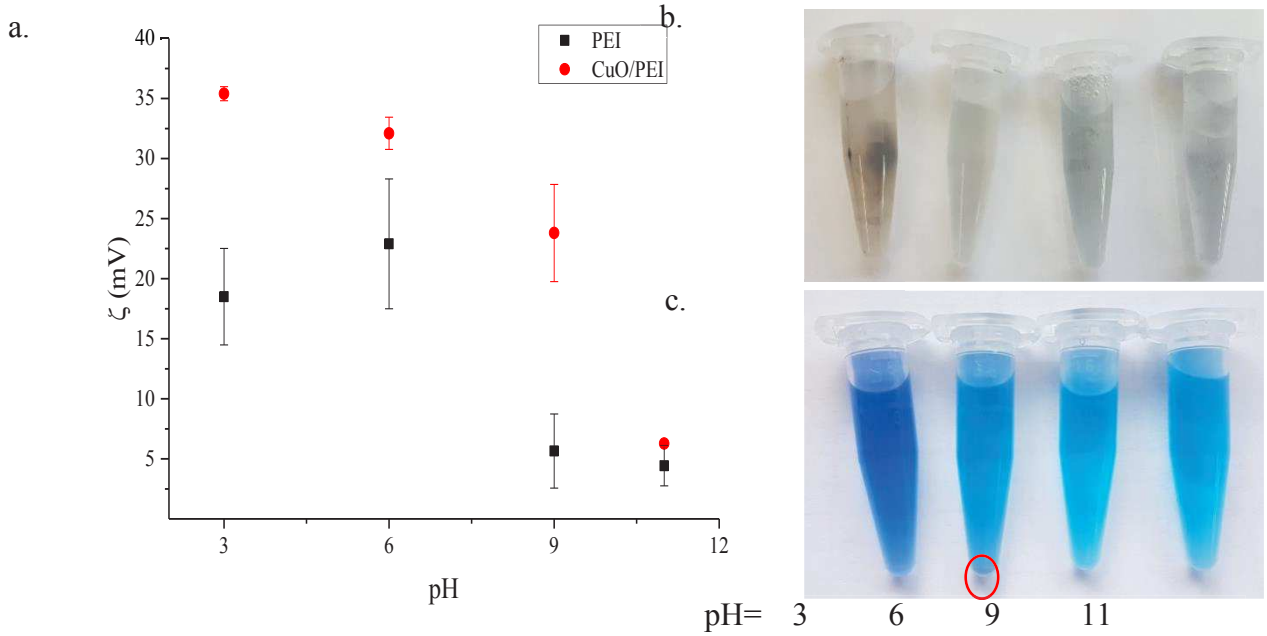

Figure 4.2: a) ζ of free polymer (0.88 wt% PEI) and CuO/PEI (0.05 wt % CuO/ 0.88wt% PEI) complex as a function of pH. b) CuO c) CuO/PEI suspensions at different pH.

4.1.3. AFM analysis of CuO/PEI suspensions as a function of pH

In order to observe the stabilized nanoparticles by PEI at different pH, the suspension of 0.05 wt% CuO was diluted 100 folds, and a drop was placed on a freshly cleaved "Mica" disc for each pH. Mica substrates provide a flat and even surface for high resolution AFM, so that the analyzed moieties could be observed clearly.

At pH 3, the size of CuO nanoparticles varies between 20 and 29 nm (Figure 4.3a). The depth profile shows a polymer having of 0.47 and 0.74 nm in height. Nanoparticles are found inside the polymers networks and some polymers could be observed isolated.

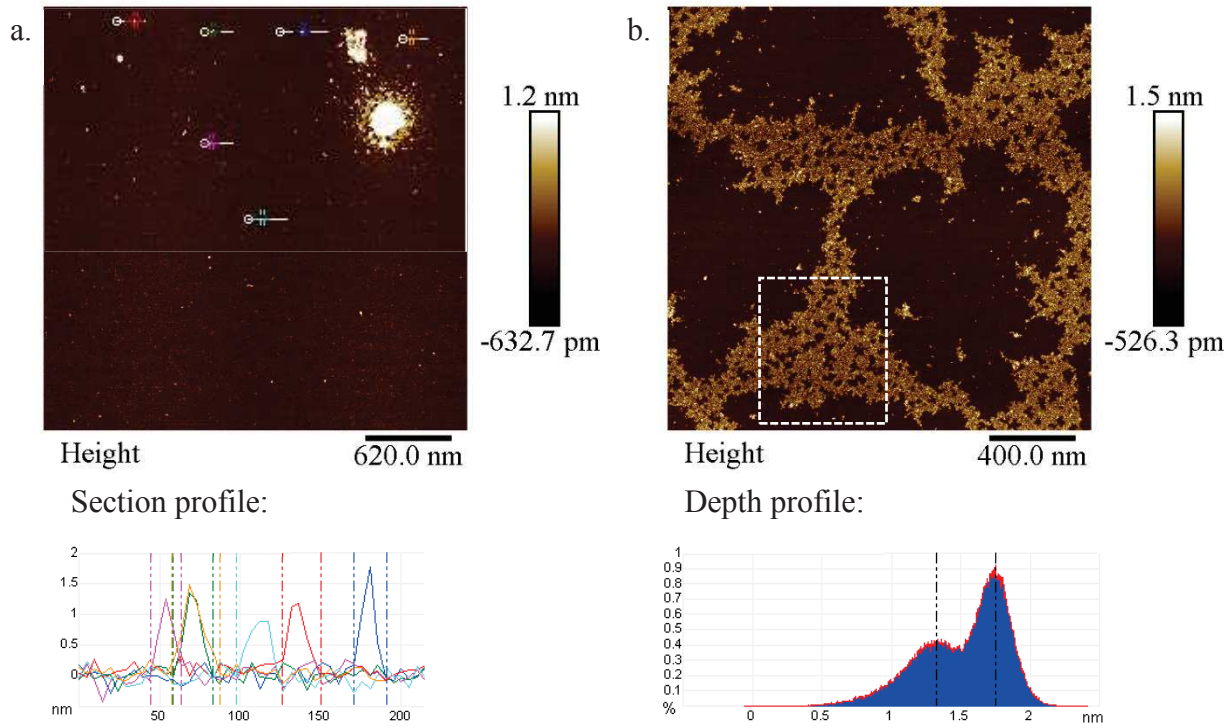

Figure 4.3: AFM micrographs at pH=3. a) section profile b) depth profile.

At pH=6 the NPs are located away from the polymers and are concentrated on the drying line and their size also varied between 20 and 29 nm. Big agglomerates of both very

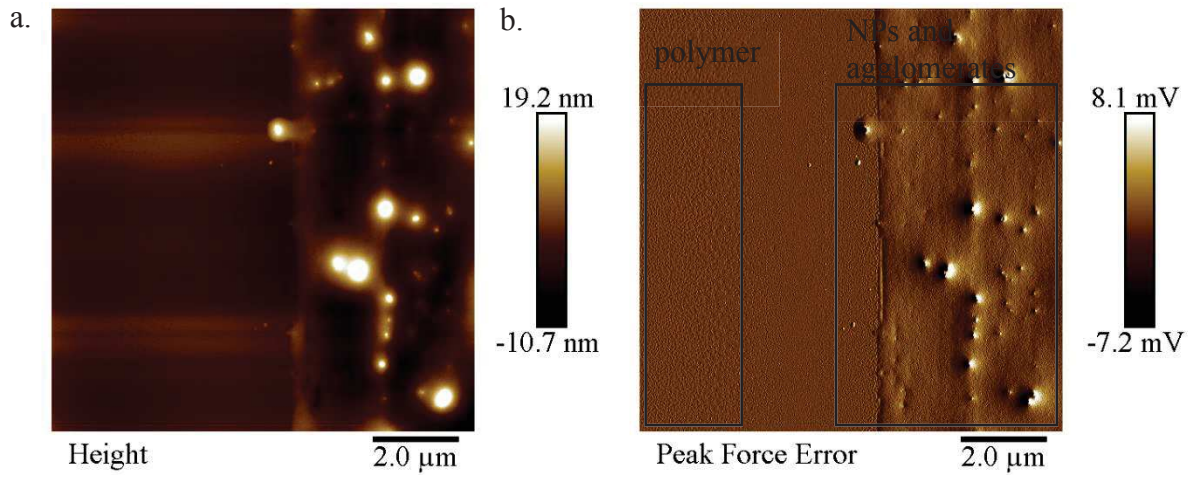

small filament forms and the monomeric form of polymers are observed (see Figure 4.4).

Figure 4.4: AFM micrographs at pH=6on the border of dried drop.

At pH=9 the defolded polymers combine into fibers and NPs are hardly observed showing higher interaction with polymers. The width of the polymer fiber measures ~4nm while the NPs have an average mean size of 53 ± 13 nm (see Figure 4.5a and b, respectively)

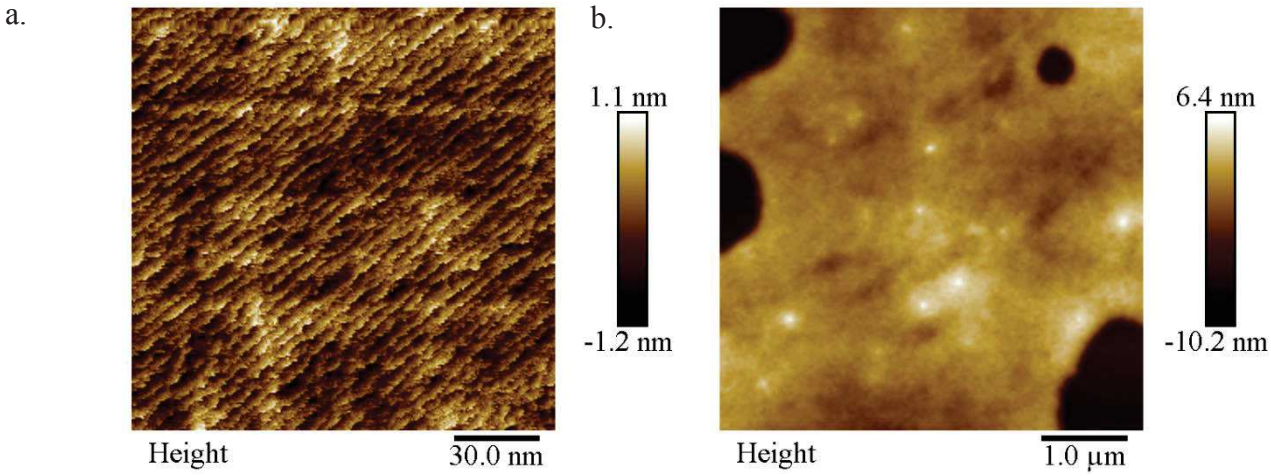

Figure 4.5: AFM micrograph of CuO/PEI drop in water at pH=9.

At pH=11 a fiber network is observed to be much bigger than at pH 9 and on the surface of this network there are polymer-covered NPs, which are displaced with the tip during imaging even when the tip interaction is minimized area. The mean size of the NPs is measured 15 ± 4 nm.

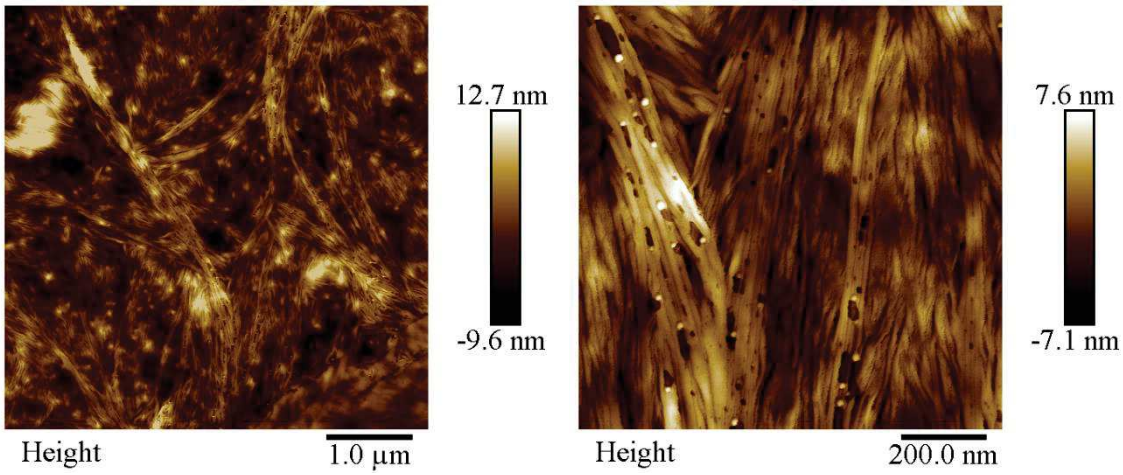

Figure 4.6: AFM micrograph of CuO/PEI/water drop at pH=11.

To observe more the nanoparticles, a more prolonged study was performed at pH=9. The obtained image at pH=9 is presented in Figure 4.7, which shows polymeric chains connecting CuO nanoparticles. CuO nanoparticles of sizes varying between 15 ± 4 nm. Large agglomerates of CuO/PEI of 100-200 nm in size are also observed.

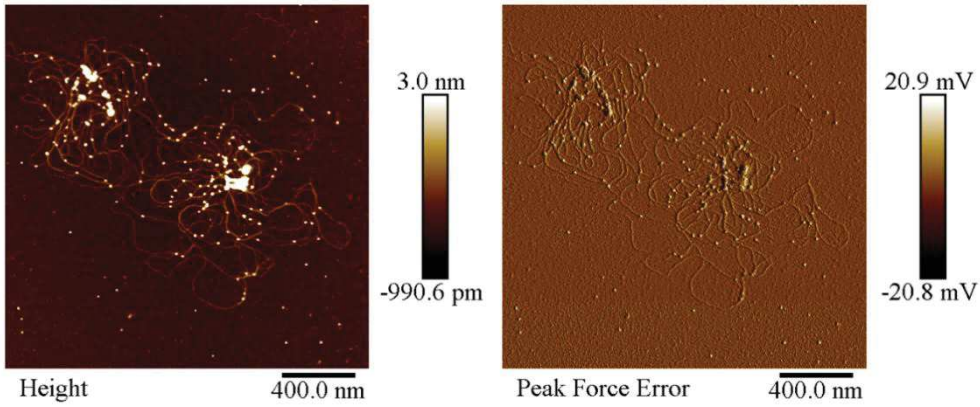

Figure 4.7: Height and peak force error AFM images.

However, the results obtained from AFM and DLS are in accordance. The high zeta potential obtained at pH=3 is due to high repulsive forces between individually charged polymers and between polymers and nanoparticles that lead to their subsequent stabilization. At pH=6 the stabilization of nanoparticles by PEI is not evident since upon drying of the drop, they are seen separated. At pH=9, nanoparticles show higher interaction with the polymer chains and are found connecting polymers together. Finally, at pH=11 a denser network of polymers and nanoparticles is observed. Polymers are adsorbed on the surface of CuO nanoparticles through the uncharged amine groups. The low ionization of PEI at this pH explains the low ζ value as well.

As a conclusion, the best stabilization conditions are at pH=3 and pH=9. At both pHs, the mechanism of stabilization could be described as electro-steric repulsion. At pH=3 fully protonated amine groups [-$(NH_3)^+$] of the polymer repel other similar groups and meanwhile the un-protonated amine groups form dative bonds with the surface Cu^{2+}. The former prevents the agglomeration of CuO while the latter maintains the stability of the suspension and prevents the sedimentation of CuO. At pH=9 stronger dative bonds are formed between the surface of CuO and the amine groups. The slight protonation results in inter-repulsion between of the protonated amine groups in the polymer chain. CuO nanoparticles surrounded by polymer are expected to be found in the suspension at pH=9 while at pH=3 individual protonated polymers will more probably exist and deposit alone during cathodic EPD.

4.1.4. Choosing a suitable pH for EPD

Four suspensions of 0.88 wt % PEI in water were left to stir for 30 mins then few drops of 1.5M of HNO_3 were used to attain the requested pH. Then 0.05 wt% of CuO were added to each suspension and left to stir for 2 days. One of the interesting features of PEI that it allows the stabilization of CuO through dative bonds and the charging occur at a wide range of pH. Since the amine groups of PEI readily adsorbs protons in the solution. From previous section we have noticed that decreasing the surface charge of PEI is pH dependent and the pH also affects the mechanism of stabilization.

Since cathodic EPD will be performed, it is also important to recall the influence of the pH on the electrolysis reactions occurring at the vicinity of the cathode, (equations 4.1-4.2) [14, 15]:

Electrolysis cathodic reaction:

$2H^+ + 2e^- \leftrightarrow H_2$ (E°= -197 mV vs. Ag/AgCL, 3.5M KCl) (4.1)

$2H_2O + 2e^- \leftrightarrow H_2 + 2OH^-$ (E° = -1027 mV vs. Ag/AgCl, 3.5M KCl) (4.2)

Electrolysis reactions usually affect the morphology of the deposit by the formation of gas bubbles, during EPD, leading to the incorporation empty holes/spaces into the final coating. However, according to reaction (4.1), as H^+ ions increases in solution, H_2 gas formation increases at the cathode and thus more bubble are incorporated as holes in the deposit. This activity could be observed in the SEM micrograph of the coating obtained at pH =3 (see Figure 4.8).

When comparing different pH, one should consider also the suitability of stabilization at a certain pH. For example, at pH= 6 the suspension obtained was found to sediment and from the SEM micrograph obtained at pH=6, it could be concluded that the suspension used is unstable and unsuitable for EPD, which was expected. For pH=9 we found that the deposit obtained is more homogeneous and no empty gas holes/spaces are present, compared to pH=3, since less H^+ are present in the solution thus the release of H_2 gas due to electrolysis reaction is reduced. At pH=11, the deposition of large agglomerates is observed, which is expected, since the nanoparticles are not sufficiently charged having the lowest ζ value (6.28 ± 0.22 mV). Thus, large charged agglomerates migrate to form the deposit, resulting in reduced homogeneity and uniformity.

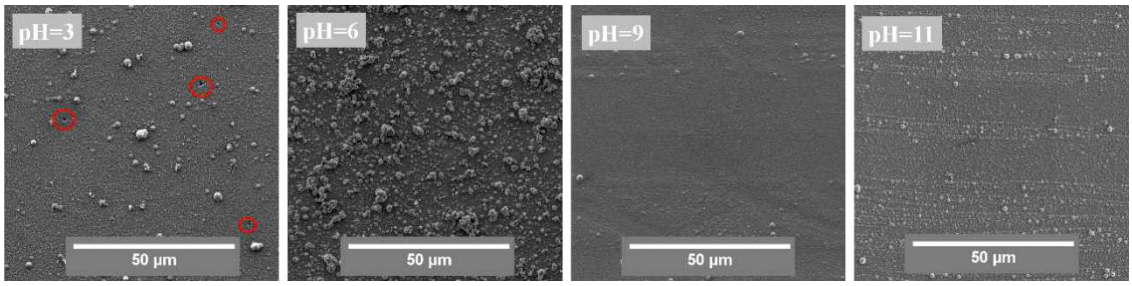

Figure 4.8: Top-view SEM micrographs of EPD deposit of CuO/PEI obtained at pH=3. holes generated from electrolysis reaction are shown in red

The phenomenon of EPD depends directly on the charge of the suspended NPs. Thus, the thickness of the deposit obtained should be proportional to that of ζ, which is the case. From the SEM cross-section micrographs of the deposits obtained at different pH, we can observe that the thickness varies between 1358±33 nm for deposits obtained at pH=11 up to 1627±44 nm for deposits obtained at pH=3. While for deposits obtained at pH=6, it is clear that the deposit suffers from high roughness which is due to the instability of CuO/PEI suspension, (see Figure 4.9).

From the top-view combined with cross-section view, A linear relationship between pH and thickness of the deposit is observed. The deposit thickness increases with decreasing pH and increasing ζ.

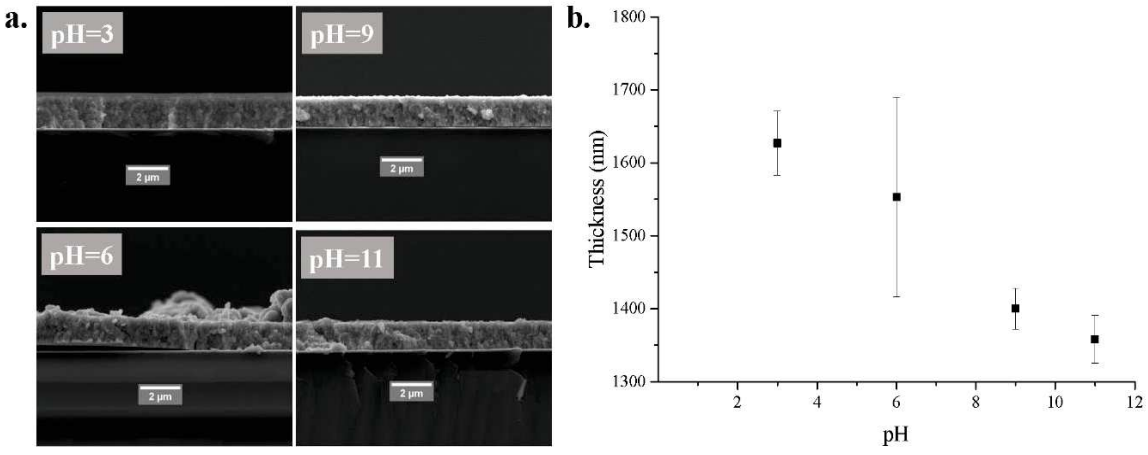

Figure 4.9: SEM cross-sections of CuO/PEI deposits at pH= 3, 6, 9 and 11, E=2V.cm^{-1}, t=120 mins.

For a more adequate analysis of the deposits, we have studied the surface morphology and measured more precisely the size of the deposited nanoparticles by AFM (see Table 4.1).

The average measured size by AFM has varied between 15 and 40 nm for the working pH range. However different surface morphology could be observed. Upon protonation, PEI polymer extend due to the inter-repulsion created between the protonated amine groups. Because low molecular weight PEI is used and even if it is hyperbranched, it cannot bend to complex the same CuO nanoparticle. at least 2 PEI chains containing two free amine groups are needed to complex to the surface of CuO. This could allow the formation of chains of (...CuO-PEI-CuO-PEI…) that arrange in this manner in the suspension but also found in the deposit (see Table 4.1). As the pH decreases higher repulsion is expected also between different polymer chains which explains why at pH=3 nanoparticles deposit farther away from each other. A deposit of agglomerates 80-200 nm in diameter was found at pH=11 while a compact and regular deposit was found at pH=9. Thus, for the following studies the pH of the suspension was fixed at 9, to ensure the deposition of dense deposits formed from well stabilized suspensions.

Table 4.1: AFM analysis of deposits obtained at different pH.

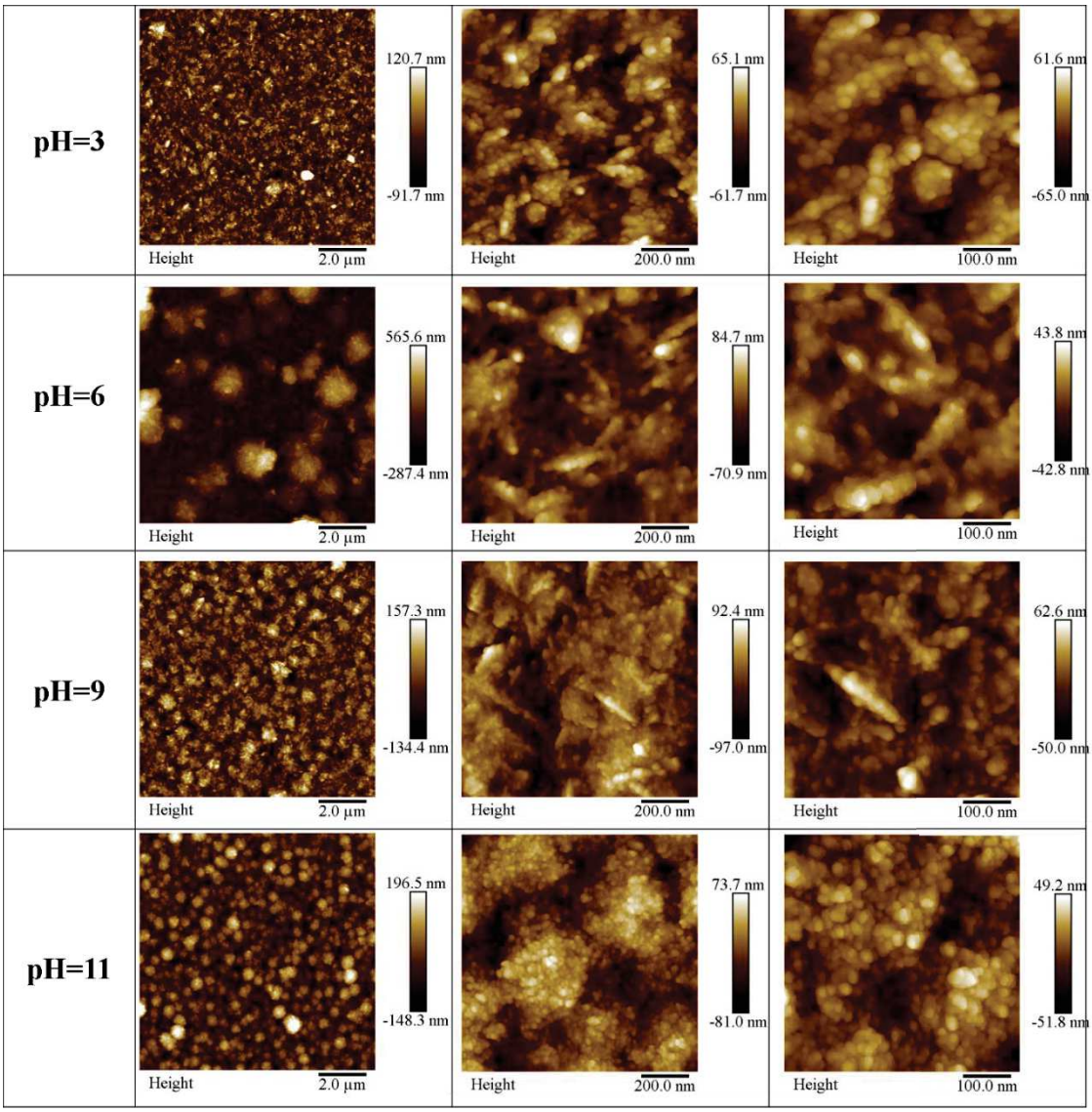

4.2. Effect of EPD parameters on the deposition process

4.2.1. Post deposition: Enhancing the quality of the deposits

As a first attempt, several deposits were performed by EPD and then analyzed by SEM. As a first observation, a thin organic layer was found to cover the surface of the deposits and prevented a clear analysis by SEM and even AFM (see Figure 4.10a&c.). Thus, as a solution we have thought of removing this polymer layer by washing the obtained deposit directly after EPD in deionized water due to the high solubility of PEI in water. Then to facilitate the drying process and limit the residual interparticle water molecules, the deposit was dipped in ethanol and directly removed, left to dry completely for at least two days at the

room's temperature. As a result, we have noticed that the deposit could be clearly better observed and analyzed (see Figure 4.10 b &d).

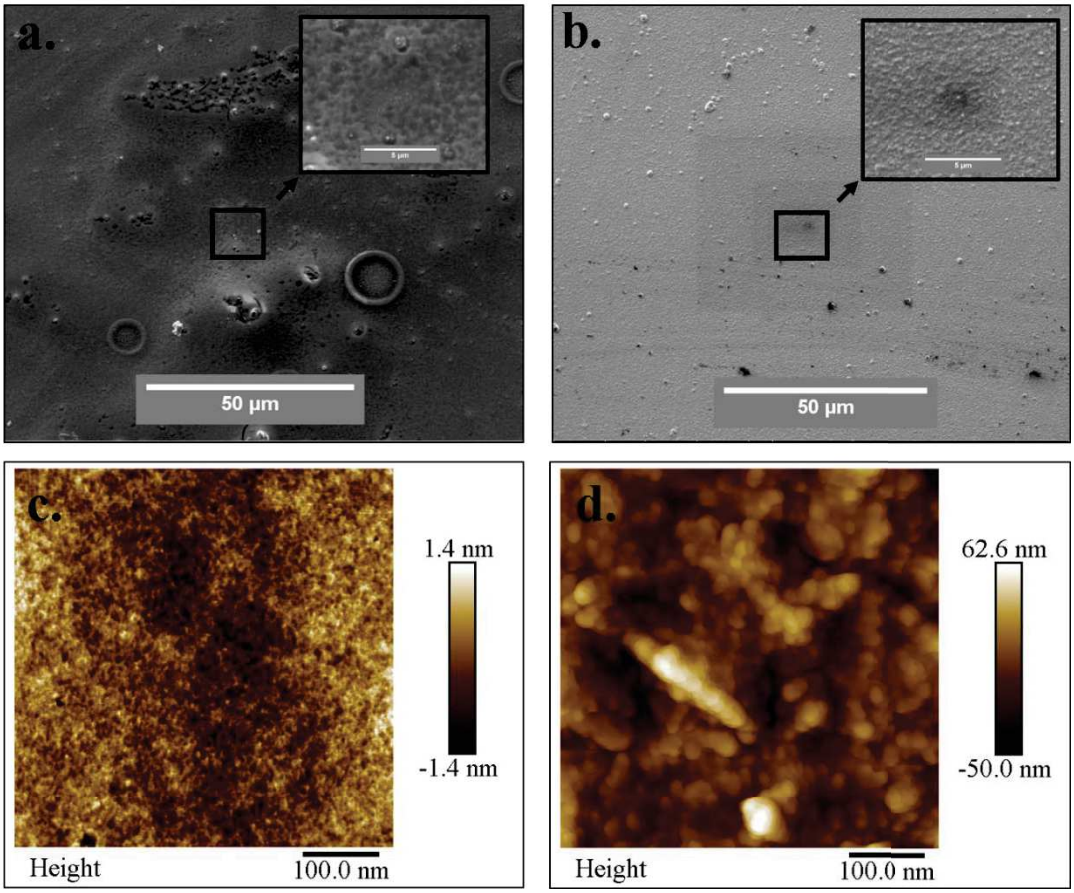

Figure 4.10: CuO stabilized EPD deposit at pH=9 (E=2V.cm^{-1}, deposition time=2 hours) SEM (up) and AFM (bottom) images. a&c) without washing. b&d) with washing.

4.2.2. Effect of applied electric field

In order to study the effect of applied electric field (E), the concentration corresponding to CuO:2PEI (1:2 molar ratio for attaining surface complexation), pH, and deposition time were fixed and E was varied between 1 and 5 V.cm^{-1} (see Table 4.2).

Table 4.2: parameters employed for the study of the effect of applied electric field.

Suspension		EPD Setup and parameters	
[CuO] (g/cm^3)	5x10^{-4}	Applied E	1, 1.5, 2, 3, 4, 5 V.cm^{-1}
		Deposition time	120 mins
[PEI] (g/cm^3)	0.019	Surface area (cm^2)	2.5x2 cm^2

pH	9	Inter-electrode distance	1cm
Solvent	H_2O (100 mL)	WE/RE/CE	PtSi/Ag,AgCl/KCl(3.5 M)/Pt

Figure 4.11 shows the SEM micrographs of the obtained deposits in cross section view accompanied by the measured thickness and top-view (to analyze the morphology). The deposit thickness increases linearly with the applied electric field between E= 2 and 4 $V.cm^{-1}$, for higher electric field the thickness of the deposit saturated for a value of ~2600 nm. For $E \leq 1 V.cm^{-1}$, no deposit was observed at the cathode. The origin of this is not fully understood, but it could be due to the fact that $1 V.cm^{-1}$ is not sufficient to form the first layer of CuO. For the slightly higher E=1.5 $V.cm^{-1}$, an irregular deposit of 108±11 nm thickness is deposited which also lies outside of the linear fit. This shows that an $E \geq 2$ $V.cm^{-1}$ is required to allow the deposition phenomenon (see

Figure 4.11b). While for E= 5 $V.cm^{-1}$ saturation is attained since as E increases, the deposition process is accelerated thus higher thickness is obtained in a shorter time increasing the resistance of the deposit preventing further deposition. The obtained deposit has low adherence to the substrate due to the increased formation of gas bubbles, which prevents further deposition and causes the detachment of the formed deposit.

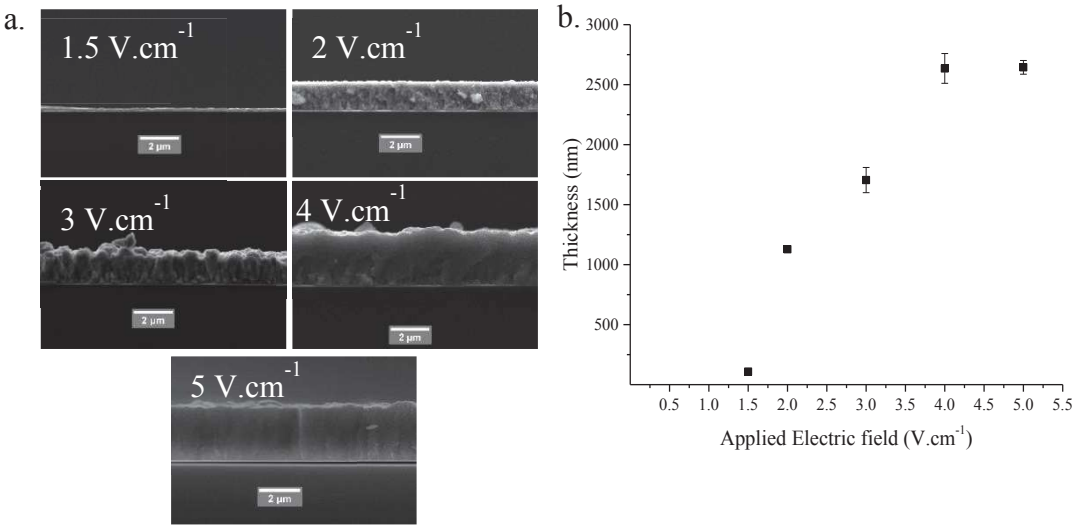

Figure 4.11: a. SEM cross section micrographs of the effect of applied electric field. b. average measured thickness as a function of applied electric field (t=120 mins).

Since EPD is a kinetic phenomenon, the accumulation rate of the particles around the electrode could influence their packing behavior. As a result, the choice of the applied electric field could be critical for EPD affecting the morphology of the deposits (as explained in chapter 3). On the other hand, high electric fields create high turbulence due to the increased gas bubbles formation around the working electrode altering the morphology of deposit formed. On one hand, the size of the agglomerate increases with the increasing applied electric field varying between 50-200 nm for 2V.cm^{-1}, ~500 nm for 3 V.cm^{-1}and 500-1000 nm for 4 V.cm^{-1} and 1000-2000 nm for 5V.cm^{-1} (see Figure 4.12). On the other hand, the morphology of the deposits varies as well with the applied electric field; where the charged nanoparticles migrate so fast without finding the right place to deposit and form close-packed structure. While at lower electric fields as 2 V.cm^{-1} deposits are formed from individual nanoparticles deposition, but with increasing the applied electric field nanoparticles are forced to migrate and deposit in the form of agglomerates (see Figure 4.12).

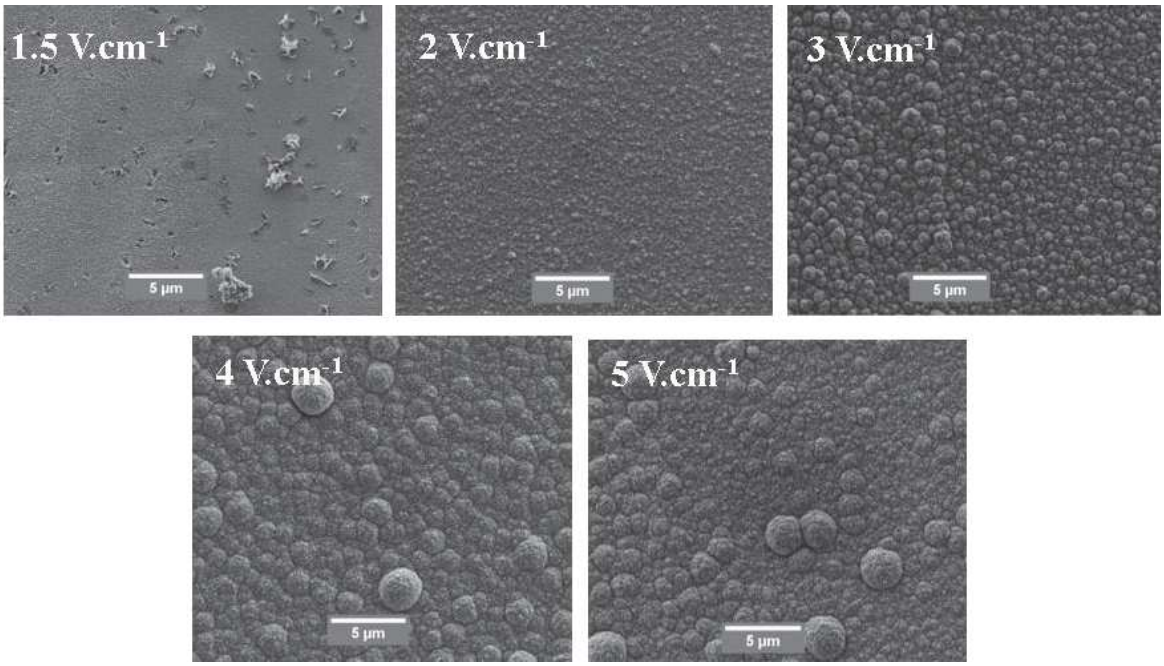

Figure 4.12: Top-view SEM micrographs of the obtained deposits for applied electric fields (1.5, 2, 3,4,5 V.cm^{-1} respectively.

4.2.3. Effect of deposition time

To study the evolution of the deposit as a function of deposition time, the applied electric field was fixed at 2 V.cm^{-1} for the same suspension, corresponding to CuO:2PEI (1:2 molar ratio for attaining surface complexation) at pH=9.

Table 4.3: EPD parameters used to study the effect of deposition time at a fixed E (2V.cm^{-1}).

Suspension		EPD Setup and parameters	
[CuO] (g/cm^3)	5x10^{-4}	Applied E	2V.cm^{-1}
		Deposition time (mins)	5,10,15,30,45,60,90,120, 180
[PEI] (g/cm^3)	0.019	Surface area (cm^2)	2.5x2 cm^2
pH	9	Inter-electrode distance	1cm
Solvent	H_2O (100 mL)	WE/RE/CE	PtSi/Ag,AgCl/KCl(3.5 M)/Pt

Figure 4.13 presents the evolution of the deposit thickness obtained from SEM cross-section for different deposition time varying between 5 and 180 mins. In accordance with Hamaker equation, the deposit thickness increases linearly with deposition time between 5 and 30 mins and then deviates from linearity after 30 mins. However, the deviation from linearity is expected since the deposit formed with time creates a resisting layer that decreases the conductivity of the substrates preventing further deposition.

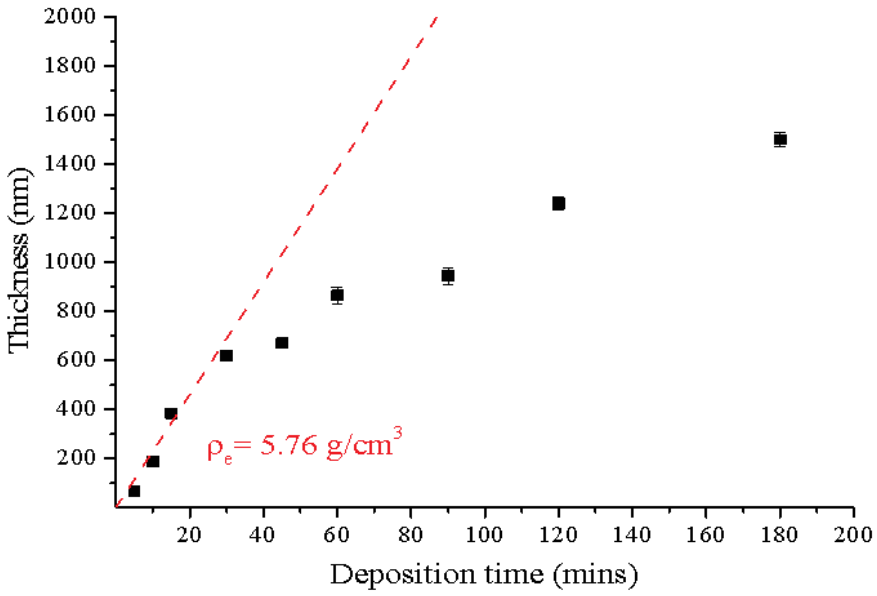

Figure 4.13: Average measured thickness as a function of deposition time (5-180 mins). The equation of the Hamaker fit, between 5-30 mins is also presented, from which ρ_e is calculated.

The SEM cross-section at different magnification also shows the high degree of particle packing achieved forming homogeneous and regular thin films (see Table 4.4).

Table 4.4: SEM cross section of the EPD deposits obtained for deposition time between 5 and 180 mins.

Deposition time (mins)	Cross-section	Cross-section	Cross-section
5	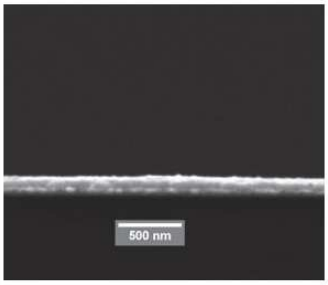	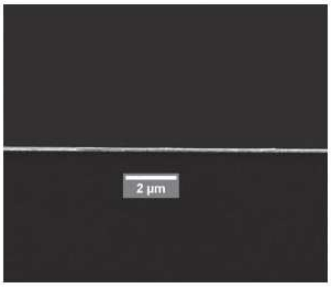	
10	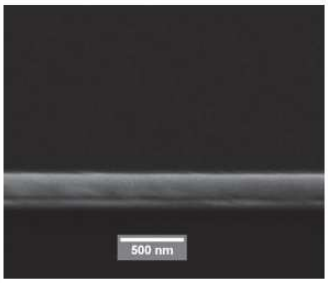	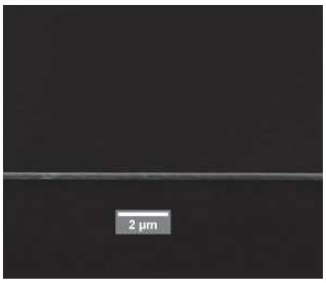	
15	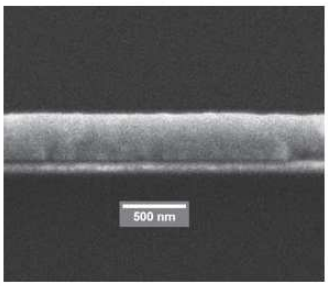	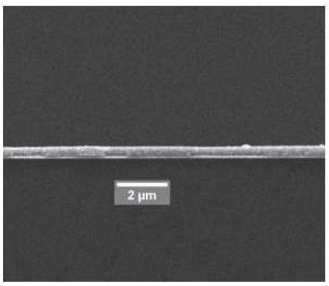	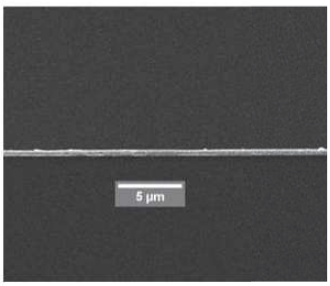
30	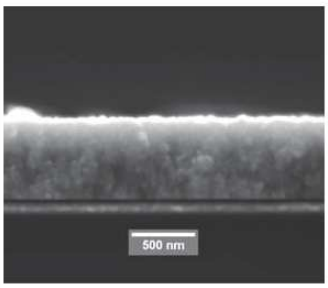	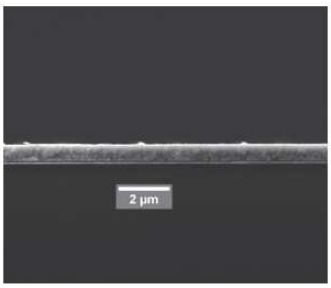	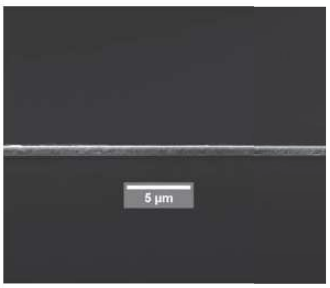
45	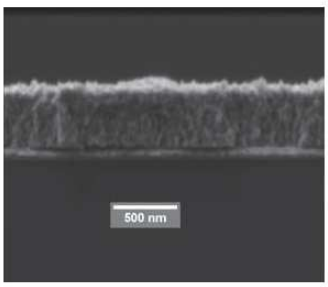	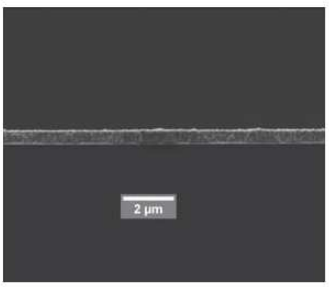	

Deposition time (mins)	Cross-section	Cross-section	Cross-section
60	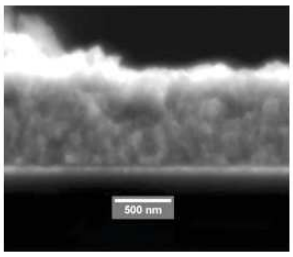	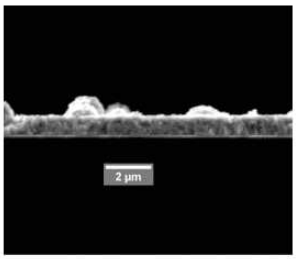	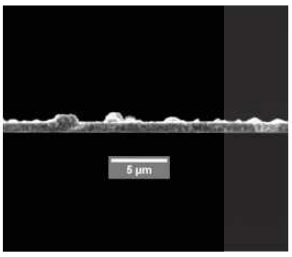
90	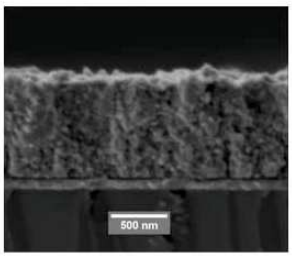	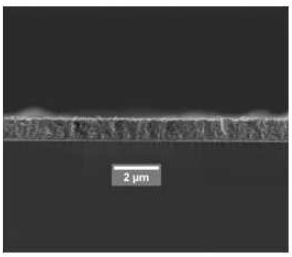	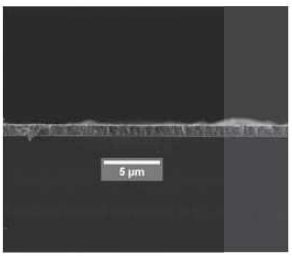
120	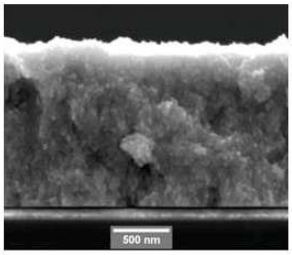	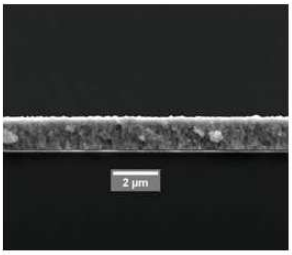	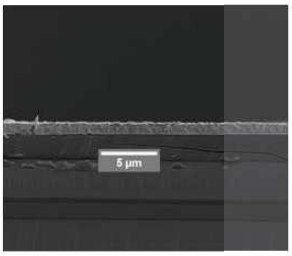
180	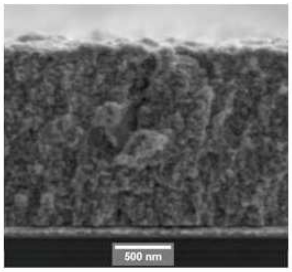	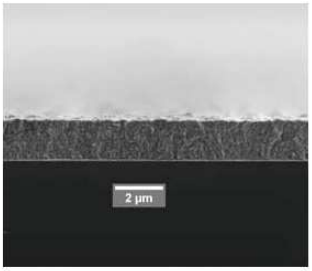	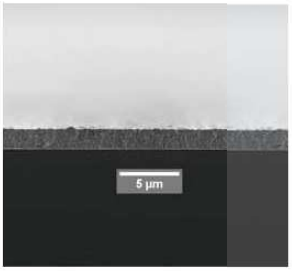

4.3. Composition of the deposits

4.3.1. Grazing incidence X-ray diffraction

In order to determine the composition of the deposit, we performed a conventional $\Theta/2\Theta$ XRD scan of bare Pt Si wafer and CuO/PEI deposit on Pt Si wafer. Two intense peaks were obtained at 2Θ of 39.9 and 69.4. These peaks correspond to the peaks of the substrate.

Upon deposition of CuO/PEI film, a slight shift in these peaks was observed and two new peaks appeared at 43.3° and 50.5°. These peaks were identified as Cu (111) and Cu (200) corresponding to face-centered cubic Copper (03-065-9026) (see Figure 4.14).

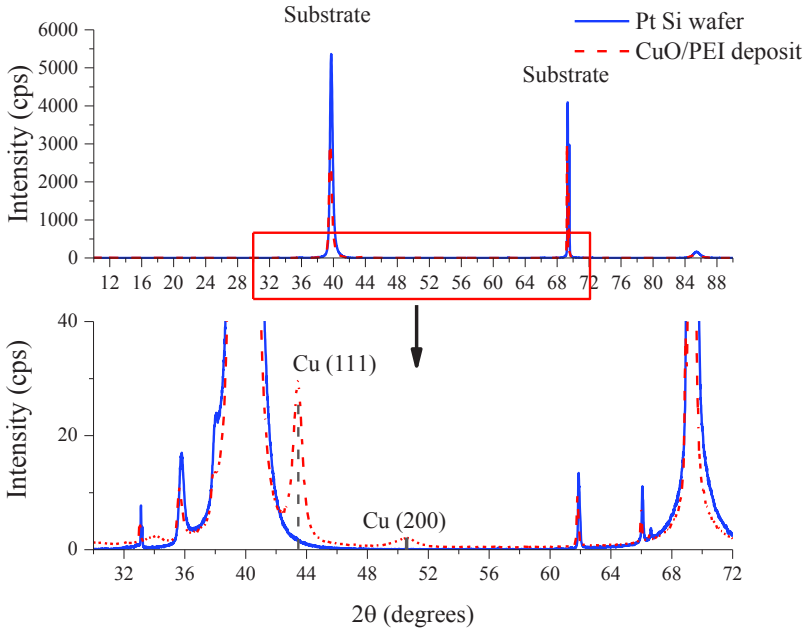

Figure 4.14: Θ/2Θ scan of XRD spectra of Pt Si wafer and CuO/PEI deposit.

Knowing that the main peaks corresponding to CuO, are located at 35.4° and 38.68° [4], could be masked by the substrate, we performed a 2Θ scan at a fixed grazing angle of incidence below the critical angle (Θ_c) of the substrate.

Then for the GIXRD analysis, incidence angle Θ_i is fixed to a value slightly above the critical angle of the material. In Figure 4.15a, the obtained GIXRD scan of the Pt Si wafer substrate shows a small hump at 39.9° corresponding to that of Pt and a strong peak at 69° corresponding to Si. Pt peak is observed more clearly when the Θ_i reaches 1°. While in Figure 4.15b, the scan of the deposit having a thickness of ~ 1500 nm is observed at Θ_i=0.4° a small hump between 35° and 40° which could correspond to CuO or Cu_2O planes and an intense peak at 44° and 52° corresponding to Cu are also observed. Varying the angle of incidence has resulted in varying the intensity of the peak which increased as we penetrated the deposit.

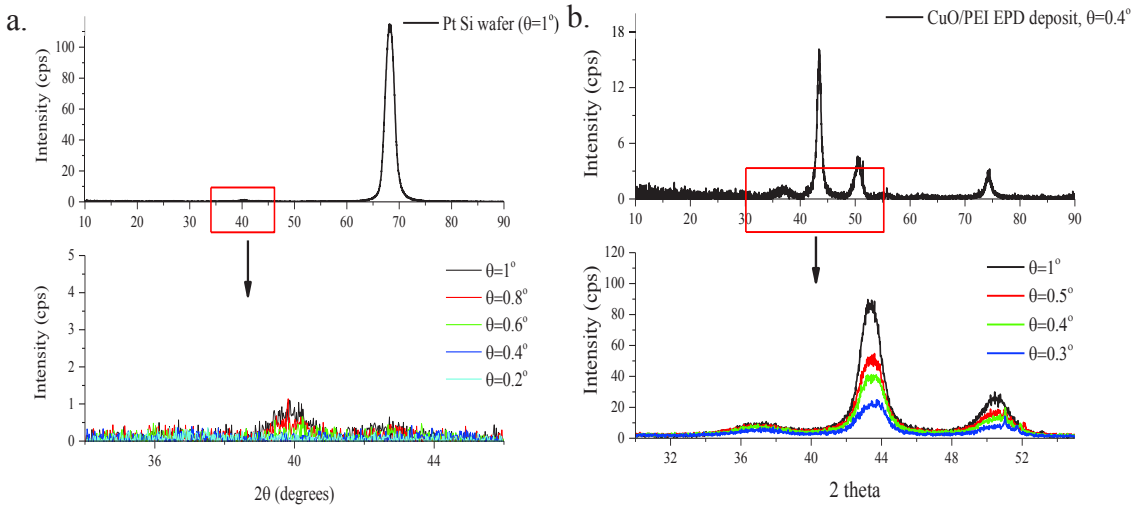

Figure 4.15: GIXRD scans of a) Pt Si wafer b) CuO/PEI EPD deposit. E= 2 V.cm^{-1}, t= 120 mins and inter-electrode distance=1 cm.

As a conclusion, the appearance of Cu (0) peaks in the XRD spectrum and the unresolved hump at ~36° suggests that CuO NPs have been reduced. This mechanism is, explained in literature by electrochemical reduction which could occur to bulk CuO nanoparticles or CuO films under cathodic applied electric field in alkaline conditions at 874 mV vs SCE [16, 17]. This reduction potential is equivalent to 913 mV for Ag/AgCl (3.5M KCl), which is inferior to the electric filed used for this study being 2V. Thus, the reduction of CuO is plausible in this case and further studies are required in order to determine if CuO was totally reduced.

4.3.2. X-ray photoelectron spectroscopy (XPS)

In order to identify the surface composition, the resulting CuO/PEI deposits were analyzed by XPS technique which analyzes the extreme surface (10-20 nm) (see Figure 4.16). The peaks in the Cu2p scan corresponds to the core level $Cu2p_{1/2}$ and $Cu2p_{3/2}$ transitions of Cu. The binding energy (BE) at 932.5 eV corresponds to Cu(I) while the peak at 934.1 and shakeup satellites correspond to Cu(II). However, the peaks of Cu(I) and Cu (0) in Cu2p scan are very close and the difference is around 0.2 eV. Thus, a CuLMM scan is performed to differentiate these two peaks since the difference will be higher. The peak observed at 916.7 corresponds to Cu(I) and that at 918.5 corresponds to Cu (0). Moreover, the O1s peak at 530.5 eV corresponds to Oxygen bonded to Cu (MO) while that at 532 could correspond to C-O bonds (adventitious carbon). The peaks obtained in the C1s spectra corresponding to 284.9, 286.2, 288.6 eV, respectively proves the presence of adventitious carbon since the

sample was dried in air. As a result, the data obtained from XPS, which analyzes only the extreme surface (20 nm) shows that the surface of CuO nanoparticles was reduced into Cu_2O or Cu (0) due to the release of H_2 gas formed at the cathode as a result of electrolysis of water.

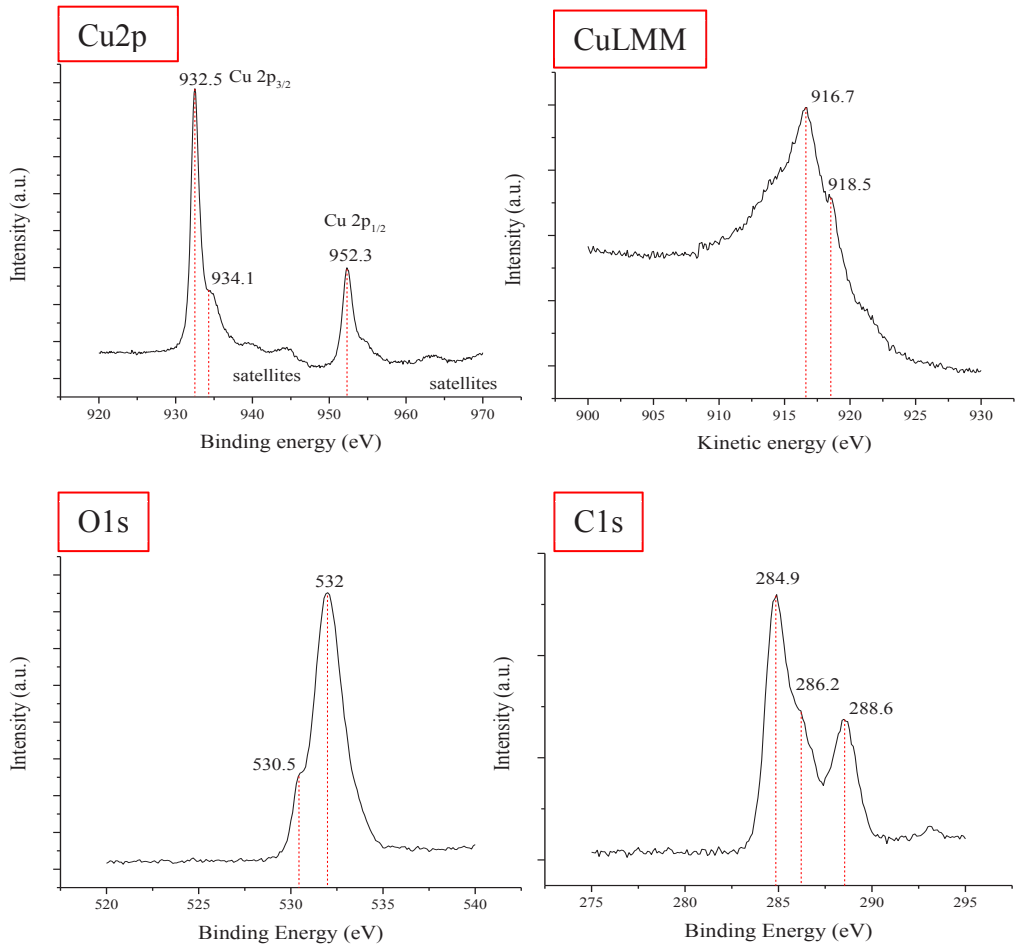

Figure 4.16: Cu2*p*, CuLMM, and O1s and C1s XPS spectra of CuO/PEI EPD deposit.

Combing the XRD, GIXRD and the XPS data we have concluded that CuO, Cu_2O and Cu coexist together in the deposit. This was also observed by the total reflectance spectra of the deposits, which showed a shift in the expected absorption edge of CuO. Compared to other reported work Cu has the least absorption in the UV-VIS-NIR region, while Cu_2O and CuO have higher absorption. Cu_2O has a better absorption in the UV-VIS while CuO absorbs better in the NIR region and a hybrid of CuO and Cu_2O results in an absorption and absorption edge intermediate between the two [18]. As a mechanism we propose that CuO is reduced by electrochemical reduction at the cathode forming a hybrid composite of Cu, CuO, and Cu_2O [17].

4.3.3. Estimating the density of the film at E=2V.cm^{-1}

Hamaker equation

For CuO deposits obtained at -2 V.cm^{-1}, the EPD kinetic study allowed the calculation of the effective density using Hamaker equation. This was achieved using the slope of the linear fit for the deposition time between 5 and 30 mins finding ρ_e to be 5.76 g/cm^3. This method was also followed in the previous chapter (Chapter 3) since very thick deposits were obtained having high roughness and not suitable for other film density measurement techniques. Since in this chapter homogenous and dense deposits are obtained, X-film measurement could be used to determine the real density of the deposit as well as the viability of using Hamaker equation for density estimation.

X-film measurements

X-film software allows the determination of thin film thickness and density using Energy Dispersive X-Ray. By varying the depth of the penetration into the material, the measurement of the K-ratio of the rays of various elements present in the multi-layer is achieved. Then by plotting curves "k ratio = f (E_0)" fit, the software gives the expression "ρz (mg/cm^2)". Then by substituting the measured experimental values of the thickness z (µm) obtained from the SEM cross-section, the density ρ (g/cm^3) could be calculated. The density of deposit obtained at 2V.cm^{-1}and pH=9 is found equal to 5.9 g/cm^3, which is lower than that obtained from Hamaker. This is expected since in the Hamaker equation used, the evolution of the thickness is considered with time and the composition is not taken into account. In fact, the polymer is present in the deposit around the nanoparticles and it could increase for example the thickness without increasing largely the density. Thus, another measurement of the density could also be complementary as the total organic carbon (TOC) which will give the theoretical density of the deposit taking into account the real amount of polymer present.

Total Organic Carbon

The theoretical and experimental density could be compared when considering two different deposits in which the amount of polymer is different. For example, for the same applied electric field of 2V.cm^{-1}, the %V of polymer present in the deposit obtained at pH=9, is found equal to ~17.1% while for pH=3 it is equal to 32.8%. These data confirm that at pH=3, a higher amount of polymer is present in the deposit. This could be explained by the higher zeta potential value of the suspension at pH=3 compared to pH=9, which increases the

rate of deposition resulting in a thicker deposit due to the higher positive charge acquired. However, the theoretical density of the film at pH=3 is 4.75 while for pH=9 it is 5.41. These values are calculated by considering bulk density ρ and volume fraction of the polymer and that of the CuO (e.g. At pH=9: ρ(theoretical)= ρ_{CuO} x V_{CuO} + ρ_{PEI} x V_{PEI}= (6.3x0.83 + 1.08x0.17) = 5.41 g/cm^3). The real/experimental density of the deposits by X-film is 5.02 and 5.90 g/cm^3 for pH=3 and pH=9, respectively. Both experimental and theoretical density values are close in magnitude. The slightly higher value obtained in X-film is expected, since the presence of Cu metal (ρ=8.96 g/cm^3) is not quantified and only the density of CuO is taken into account which is lower than that of Cu. Thus, a general lowering in the calculated density value is expected.

As a result, the density of CuO coatings obtained from E=2V.cm^{-1} at pH=9 is greater than 5 g/cm^3. The calculation of the coating density using Hamaker equation is thus reliable and leads to a close estimation of the real density of the deposit.

4.4. Spectral selectivity

4.4.1. Effect of applied electric field.

In Figure 4.17, the total reflectance (%R) and calculated α and ε of the EPD deposits obtained at different applied electric fields are represented compared to that of the substrate and CuO pellet. At 1V.cm^{-1} nothing deposited at the electrode while increasing E slightly allowed the slight deposition of CuO the α and ε values varied from that of the substrate. Increasing E to 2, 3, and 4 V.cm^{-1}, increased the α and ε to 0.88-0.02, 0.86-0.01, 0.8-0.03 respectively. For E=5V.cm^{-1} the α and ε values attained 0.95 and 0.4, respectively. However, the deposits obtained at 5V.cm-1, possess low adhesion to the substrate and detach easily from the Pt Si wafer. This is due to the increased formation of H_2 gas bubbles due to electrolysis in response to elevated E. As a result, the applied electric field increase doesn't enhance the α value, rather it is decreased for E = 2,3, and 4 V.cm $^{-1}$. While for E= 5V.cm^{-1} α and ε attain the highest values of 0.95 and 0.44 resulting in a tandem absorber of low selectivity due to the high calculated ε.

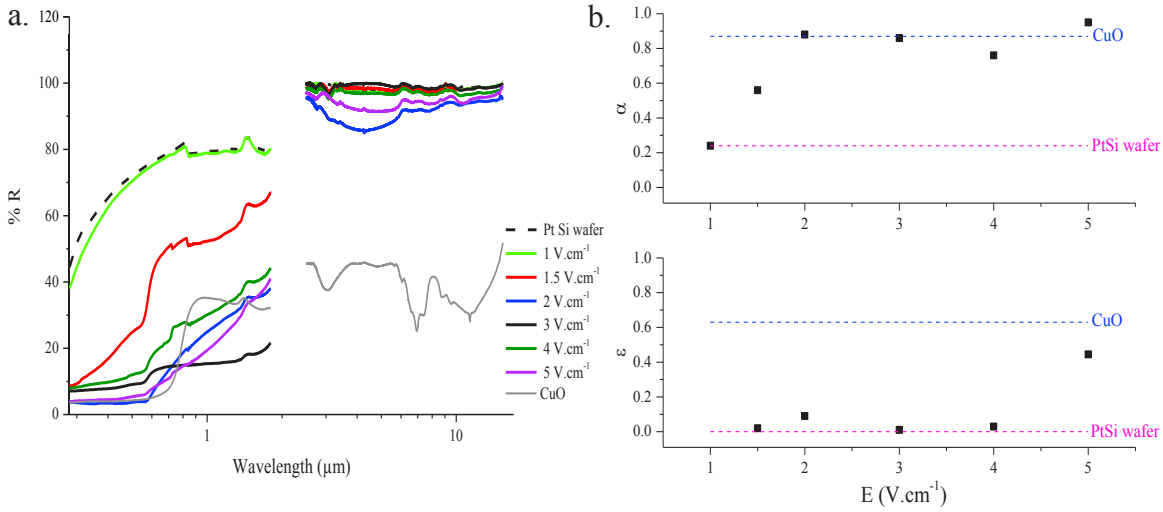

Figure 4.17: Total reflectance (%R) of the obtained deposits at 1, 1.5, 2, 3, 4, 5 V.cm^{-1}.

Besides, one can estimate the selectivity of the tandem solar absorber by the following formula: [19]

$$\frac{\alpha-\varepsilon}{\alpha} \qquad (4.3.)$$

This expression tracks the amount of power lost to the fraction of that gained. A selective tandem material will have a selectivity that approaches 1. The selectivity of the deposits as a function of applied electric field represented in Figure 4.17. The EPD process is found to be efficient to form optically selective deposits varying E (V.cm^{-1}). The deposit obtained at E=1.5 V.cm^{-1} presents high selectivity of ~0.9, which has an α value of 0.56. This shows the limitation of the selectivity equation criterion where a very low α and ε value could result in high selectivity.

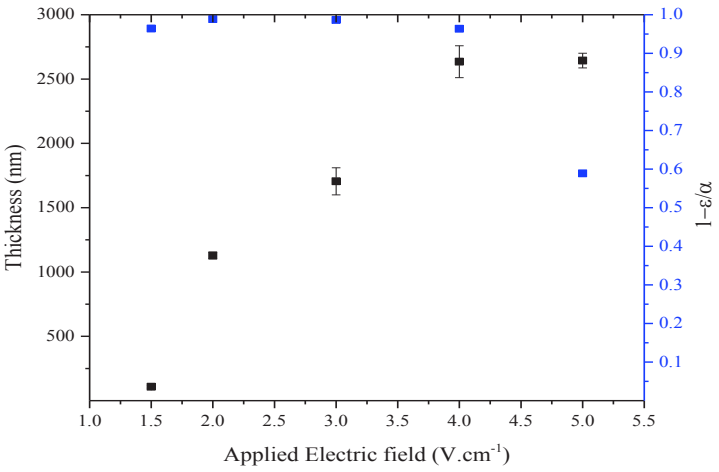

Figure 4.18: Spectral selectivity as a function of applied E for t= 120 mins.

4.4.2. Effect of deposition time

Figure 4.19a shows the total reflectance profiles of Pt Si wafer, CuO pellet and CuO/PEI deposits obtained at different deposition time for a constant applied electric field of 2 V.cm^{-1}. While Figure 4.18b shows the calculated α and ε as a function of deposition yield ($\rho_e z$) calculated for every deposition time (5, 10, 30, 60, and 120). It is also important to know that the deposition yield increases with deposition time. Small humps could be observed at 720 and 850 nm due to light source change over and stair correction while the hump at ~1500 is due to the water traces already in the chamber. The Pt Si wafer displays high reflection all over the spectrum and a corresponding absorptance of 0.24. Upon EPD for 5 mins a direct decrease in the total reflectance was observed with cutoff at 545 nm after which the % R increases with wavelength. The α value of the tandem absorber was 0.60. Then, as the deposition time increases the % R of the tandem absorbers decreases. The maximum calculated α of 0.87 was reached for a deposition time of 120 mins. A slight shift in the cutoff to higher wavelengths is also observed. On the other hand, the total reflectance of the Pt Si wafer in the Mid-Far IR region is high and exceeds that of the integration sphere; the calculated emittance of CuO tandems vary between 0.01 and 0.09 for a deposition time varying between 5 and 120 mins. Despite the formation of CuO thin film on the Pt Si wafer, the tandem absorbers still possess high total reflectance thus low emittance.

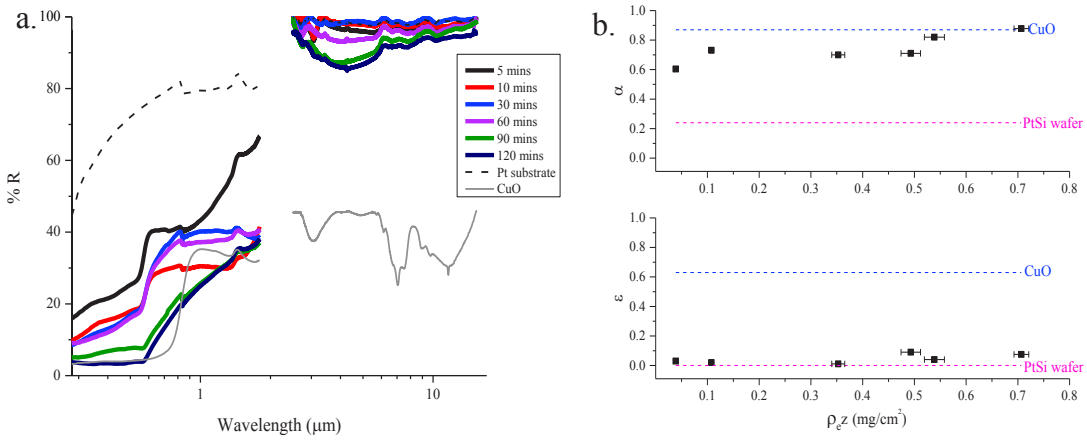

Figure 4.19: a) Total reflectance (%R) of the obtained deposits as a function of deposition time; b) calculated α and ε vs $\rho_e z$ (mg/cm^2).

Figure 4.20 shows the selectivity of the obtained tandem absorbers as a function of deposited yield (mg/cm^2). The obtained tandem absorbers possess high selectivity ranging between 0.9 and 0.98. It is expected that at very low deposited mass, the absorbers attain a very high selectivity which is due to the low emittance obtained. With the increase of deposited mass, the calculated α and ε increases which decrease the selectivity.

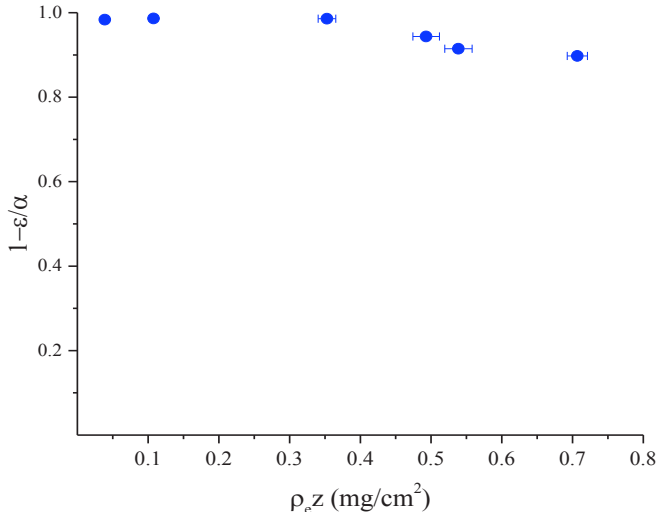

Figure 4.20: spectral selectivity of CuO/Pt Si wafer tandems obtained at E=2 V.cm^{-1} as a function of the "$\rho_e z$" or deposition yield at different deposition time.

Conclusion

The stabilization of CuO for the working range of pH 3-9 is possible. The best stabilization and EPD conditions together were obtained at pH=9 for 2PEI: CuO (surface) at a deposition time of 2 hours and applied electric field of 2V.cm^{-1}. The kinetics of the EPD at

these conditions were studied and Hamaker equation was used to calculate an effective density (ρ_e) of 5.7 g/cm^3. The amount of polymer present in the deposit was found equal to 17%V of the coating. The calculated value of effective density using Hamaker equation was verified using X-film and ρ_e corresponded to the real density value varying between 4 and 5.7 g/cm^3. The CuO tandems obtained presented low surface roughness (RMS= 40 nm) and good adhesion to the substrate. An α value of 0.84 and ε of 0.09 for an applied electric field of 2 V.cm^{-1} and deposition time of 120 mins was obtained. The presence of Cu metal and Cu_2O in the deposit was verified by GIXRD and XPS. They are incorporated in the coating as a result of electrochemical reduction of the CuO which could occur directly on the film or in the bulk suspension.

Finally, the presence of polymer in the CuO deposit renders the solar tandem absorbers vulnerable to degradation with time. In this context, the transformation of the organic carbon into carbon black or the deposition of an antireflection and protecting layer on the CuO/PEI deposit is in request to improve their durability and enhance their optical properties.

References:

[1] L. Besra, T. Uchikoshi, T.S. Suzuki, Y. Sakka, Journal of the American Ceramic Society, 91 (2008) 3154-3159.

[2] L. Fedele, L. Colla, S. Bobbo, S. Barison, F. Agresti, Nanoscale Research Letters, 6 (2011).

[3] M. Guedes, J.M.F. Ferreira, A.C. Ferro, Journal of Colloid and Interface Science, 330 (2009) 119-124.

[4] S. Mallakpour, M. Dinari, E. Azadi, International Journal of Polymer Analysis and Characterization, 20 (2015) 82-97.

[5] D.P. Kulkarni, D.K. Das, S.L. Patil, Journal of Nanoscience and Nanotechnology, 7 (2007) 2318-2322.

[6] R. Laucournet, C. Pagnoux, T. Chartier, J.F. Baumard, Journal of the American Ceramic Society, 83 (2000) 2661-2667.

[7] C. Pagnoux, J. Ceram. Process. Res., 3 (2002) 10-14.

[8] M. Mishra, Y. Sakka, T. Uchikoshi, L. Besra, Journal of the Ceramic Society of Japan, 121 (2013) 348-354.

[9] C. Mendoza, Z. González, Y. Castro, E. Gordo, B. Ferrari, J. European Ceram. Soc., 36 (2016) 307-317.

[10] M. Zarbov, I. Schuster, L. Gal-Or, Journal of Materials Science, 39 (2004) 813-817.

[11] M. Verde, M. Peiteado, A.C. Caballero, M. Villegas, B. Ferrari, Journal of Colloid and Interface Science, 373 (2012) 27-33.

[12] T. Wen, F. Qu, N.B. Li, H.Q. Luo, Arabian Journal of Chemistry, 10 (2017) S1680-S1685.

[13] J. Jia, A. Wu, S. Luan, Colloids and Surfaces A: Physicochemical and Engineering Aspects, 449 (2014) 1-7.

[14] M. Mishra, S. Bhattacharjee, L. Besra, H.S. Sharma, T. Uchikoshi, Y. Sakka, J. European Ceram. Soc., 30 (2010) 2467-2473.

[15] M. Ammam, Rsc Advances, 2 (2012) 7633-7646.

[16] W.-K. Han, J.-W. Choi, G.-H. Hwang, S.-J. Hong, J.-S. Lee, S.-G. Kang, Applied Surface Science, 252 (2006) 2832-2838.

[17] Y. Wan, Y. Zhang, X. Wang, Q. Wang, Electrochemistry Communications, 36 (2013) 99-102.

[18] Y. Yang, D. Xu, Q.Y. Wu, P. Diao, Scientific Reports, 6 (2016).

[19] G. Katumba, L. Olumekor, A. Forbes, G. Makiwa, B. Mwakikunga, J. Lu, E. Wäckelgård, Solar Energy Materials and Solar Cells, 92 (2008) 1285-1292.

Chapter Five:
Toward an Application

5 Introduction

The tandem selective solar absorbers studied in this work are made by a metallic reflecting substrate covered by a thin layer of an absorbing compound, leading to a high solar absorptance in the visible and near-infrared regions (0.3–2.5 μm), and a low emittance in the long wavelength (infrared) region (2.5–20 μm).

On the basis of bibliographic results presented in Chapter 1, CuO was chosen as absorbing compound. One of the objectives of the study was to assess whether it was possible to achieve this tandem absorber by EPD process and whether the properties of this material were competitive compared to those of other processes (Electrolytic deposition, spraying). It should be noted that, EPD process has similarities with electrolytic deposition (ELD), widely used for the production of such tandem absorbers. Coatings from ELD are formed from an ionic solution while coating formed by EPD are formed from a suspension of charged particles and in this case CuO nanoparticles will be used.

The substrate mainly used in this work is silicon wafer coated with gold or platinum. These model substrates are relatively expensive and have been chosen because they facilitate the characterization of the deposited layers by grazing incident diffraction, or SEM transverse cross section. However, it is clear that they can't be used for industrial application, and other industrial metallic substrates such as Stainless steel, Aluminum, Copper have to be evaluated.

Thus, in this chapter, the formation of CuO tandem solar absorbers using industrial metallic substrates by EPD, is discussed. On the other hand, the durability and efficiency of deposits was enhanced by the deposition of a protecting and anti-reflection layer or by calcination.

5.1. Choosing a Suitable metallic substrate

The EPD of $5x10^{-4}$ g/cm^{3}CuO and $1.5x10^{-4}$ g/cm^3 $Mg(NO_3)_2.6H_2O$ suspension for a deposition time of 30 minutes at 50 V.cm^{-1} was performed using Aluminum (Al), Copper (Cu) and Stainless Steel (SS) substrates (see Figure 5.1). The inserted pictures present the corresponding deposits formed on metallic substrates which shows black deposits of CuO. The SEM top-view micrographs show loosely packed and porous deposits. This is expected since the starting suspension is not sufficiently stable to result in regular and packed deposits.

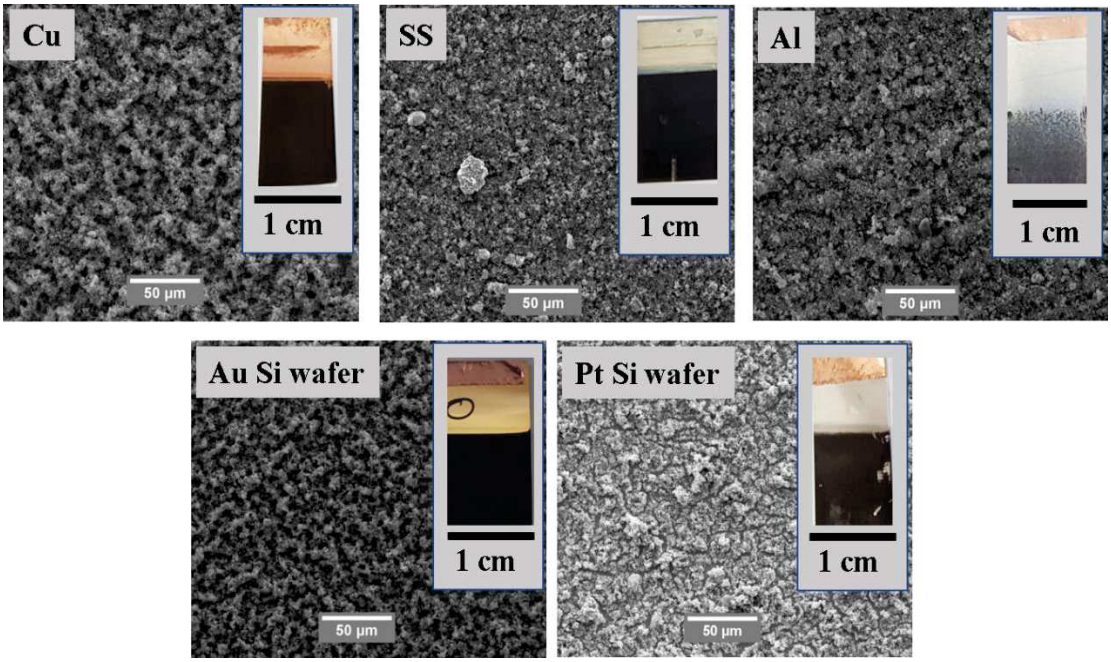

Figure 5.1: SEM micrographs of CuO/IPA deposits obtained by EPD using different substrates with their corresponding pictures.

The total reflectance (%R) of CuO tandems formed on different substrates is presented in Figure 5.2. All tandems are found to possess similar total %R with slight variation. This could be due to the variation of the morphology of the starting metallic substrate as well as the different resistivity that could alter the mechanism of deposition during EPD resulting in different deposit microstructure.

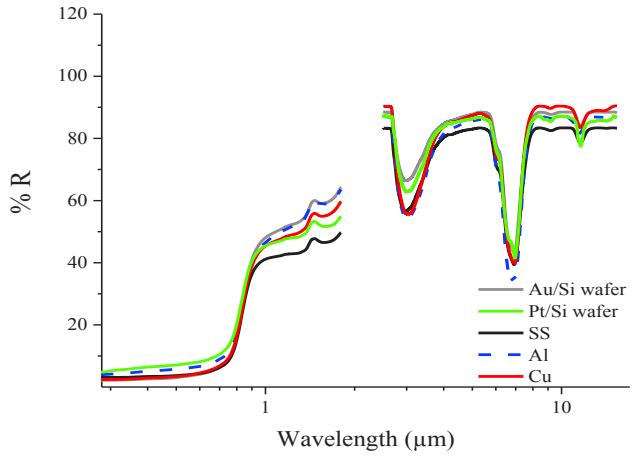

Figure 5.2: % R of of CuO/$Mg(NO_3)_2$ deposits obtained from IPA suspension using different substrates.

On the other hand, EPD on different metallic substrates using water based suspensions were also evaluated. These deposits were obtained from the EPD of $5x10^{-4}$ g/cm^3

CuO and 0.019 g/cm^3 PEI in water at pH=9. The corresponding pictures are inserted and the SEM micrographs of EPD deposits using different substrate are presented in Figure 5.3. The top-view of the deposits shows homogeneous, dense and regular deposits. Deposition at the Al substrate was prohibited due to substrate corrosion induced by the electrolysis reactions occurring at the electrode rendering Al substrate as not suitable for this system. Homogeneous and regular deposits were obtained for all metallic and metallized substrates used which proves the applicability of this system industrially.

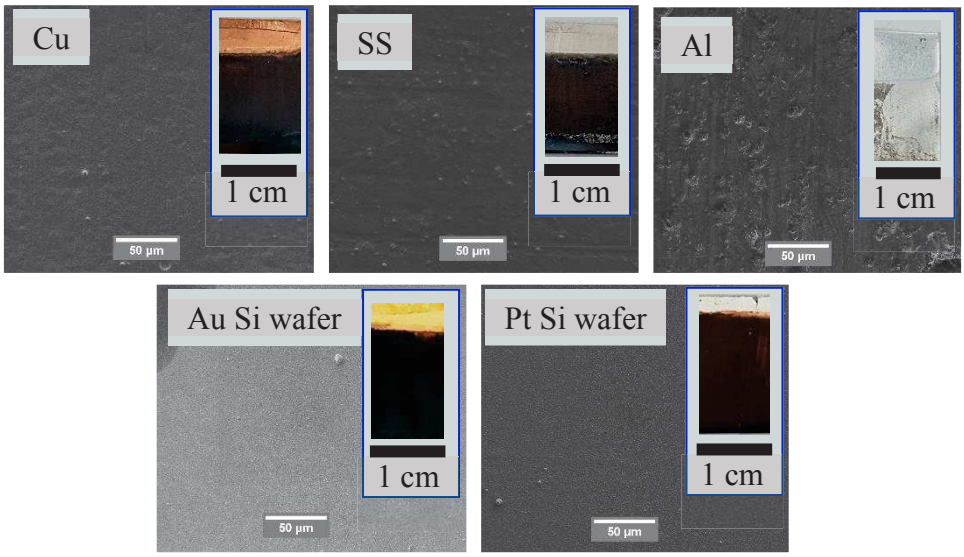

Figure 5.3: SEM micrographs of CuO/PEI in water deposits obtained by EPD using different substrates with their corresponding pictures

The total reflectance (%R) of the obtained tandems are presented in Figure 5.4. A slight variation also observed between different tandems using different substrates. However, this variation is also due to different properties between substrates. To understand all these effects, a more detailed study should be performed taking into account the state of the substrate (resistivity and morphology) before deposition and how it could alter the deposition process. Finally, a suitable and accurate system to estimate the deposited mass and thickness is also in request, since a cross section of the deposit couldn't be easily obtained.

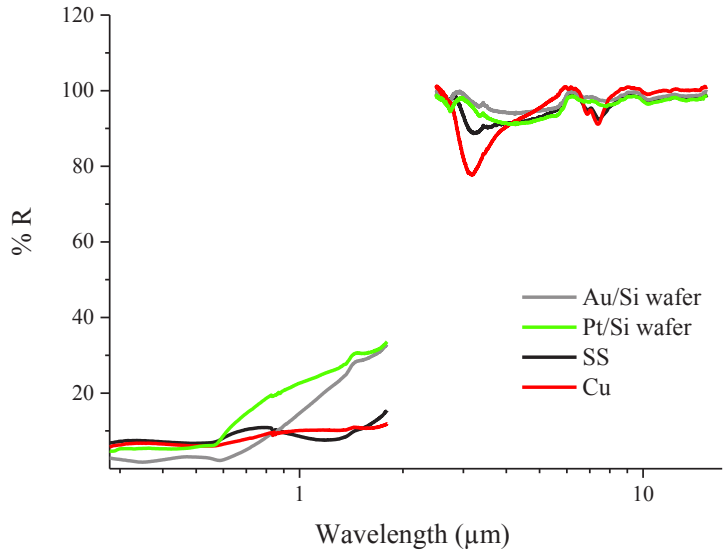

Figure 5.4: % R of CuO/PEI/metallic substrates tandem solar absorbers.

The calculated α (absorptance), ε (emittance) and η (efficiency) of the tandems obtained from both suspensions are presented in Figure 5.5a &b. It could be observed that the tandems obtained from water based suspension have the highest calculated α, ε and η for all substrates used, compared to IPA based suspensions. For water based suspensions α varies between 0.84 and 0.9, ε varies between 0.01 and 0.03 and η varies between 0.84 and 0.9. On the other hand, for IPA based suspension, the highest attained α is 0.8 for all substrates while ε varies between 0.1 and 0.2 and as a result η is 0.7 for all used substrates.

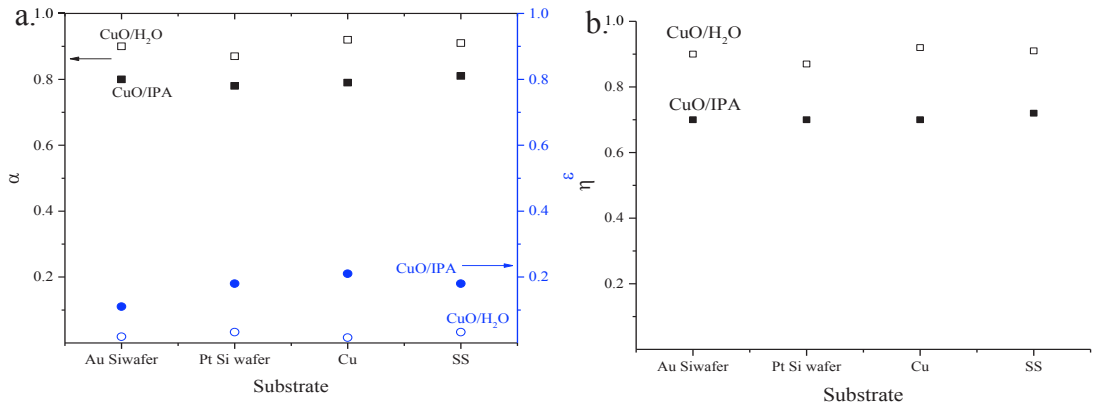

Figure 5.5: Calculated α, ε and η of CuO/PEI tandem absorbers on different metallic substrates of IPA and water suspensions

The morphology of the coatings obtained using aqueous suspension shows better homogeneity, uniformity and adhesion to the metallic substrate. The calculated efficiency using different metallic substrates is always higher in the case of aqueous based suspensions. This confirms that the stability of the dispersion prior to the deposition determines the uniformity and homogeneity of the coating formed.

5.2. Reproducibility

The reproducibility of the deposits was verified by repeating the same experiment for the same conditions by EPD for the two different suspensions used, IPA and water. The optimum conditions used and properties of obtaining selective tandem solar absorbers by both suspensions are presented in Table 5.1.

Table 5.1: EPD conditions and reproducibility results for CuO IPA and water suspensions.

Experimental Conditions	CuO/IPA	CuO/Water
CuO	$5x10^{-4}$ g/cm^3	
Stabilizing agent	$Mg(NO_3)_2$	PEI
Concentration (g/cm3)	1.5x10^-4	0.019
Stability	Stable up to40 mins	Stable
EPD Conditions	Cathodic EPD	
Applied E (V.cm^{-1})	50	2
Deposition time (mins)	30	120
WE	Au/Si wafer	Pt/Si wafer
Thickness	7.4±1.05	1.06±0.09
α	0.79-0.80	0.84
ε	0.22	0.01-0.03
η	0.7	0.84-0.89

For the same solid content of CuO in both suspensions, CuO/H_2O suspension is always more stable while in IPA suspension nanoparticles start to settle down after 40 mins which is slightly superior to the EPD experiment being 30 minutes. The average thickness is 7.4±1.05 µm for CuO/IPA suspension having high roughness and loose structure (see Table 5.2). In contrast, the thickness of CuO deposit obtained from H_2O suspension is 1.06 ±0.09 µm having a more compact and homogeneous morphology. The average thickness of the deposits obtained from CuO/IPA shows higher standard deviation (~1 µm) while the standard deviation of the thickness of the deposits obtained from CuO/H_2O is in order of ~100 nm. Thus, deposits obtained from CuO/water suspension presents more promising results for the formation of homogeneous and regular deposits.

Table 5.2: Reproducibility of deposits starting from IPA and water suspensions.

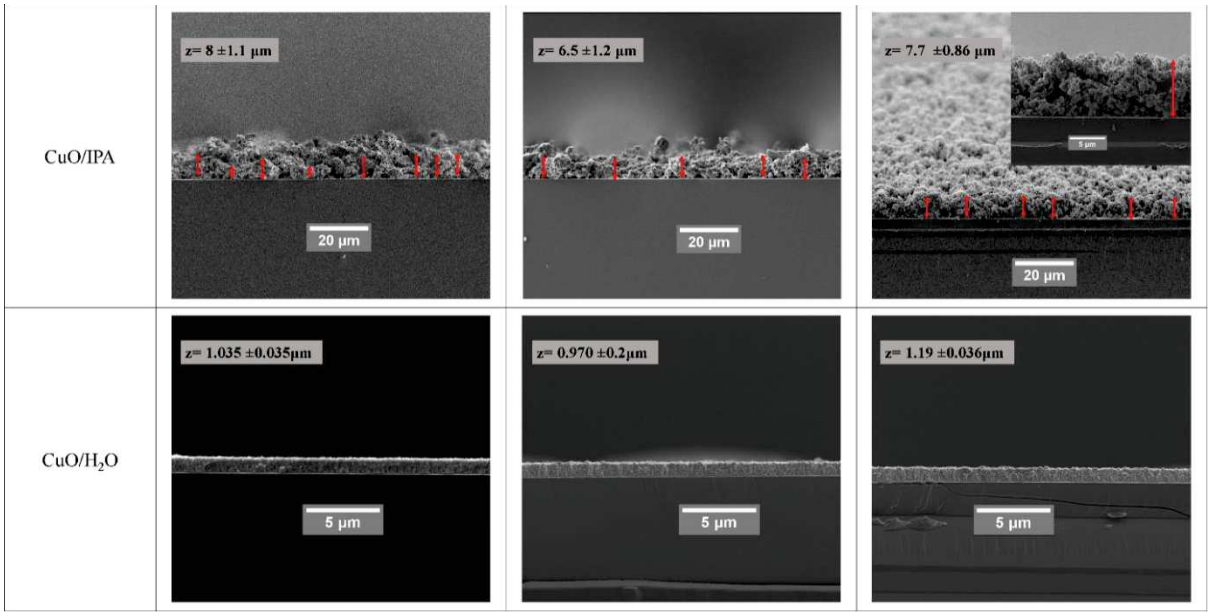

In Figure 5.6, the efficiency of CuO tandems obtained from both suspensions is compared w.r.t. the yield ($\rho_e z$ in g/cm^2) of the deposit for the same deposition time. It could be observed that for a deposit yield <0.2 g/cm^2, tandems obtained from CuO/H_2O have η=0.7 while for CuO/IPA suspension this value is obtained for a yield of 0.7 g/cm^2. The CuO tandems of CuO/H_2O suspension attain the highest efficiency varying between 0.85-0.89 according to the reproducibility results. As a result, further optimization is focused on the CuO tandems obtained from H_2O suspensions.

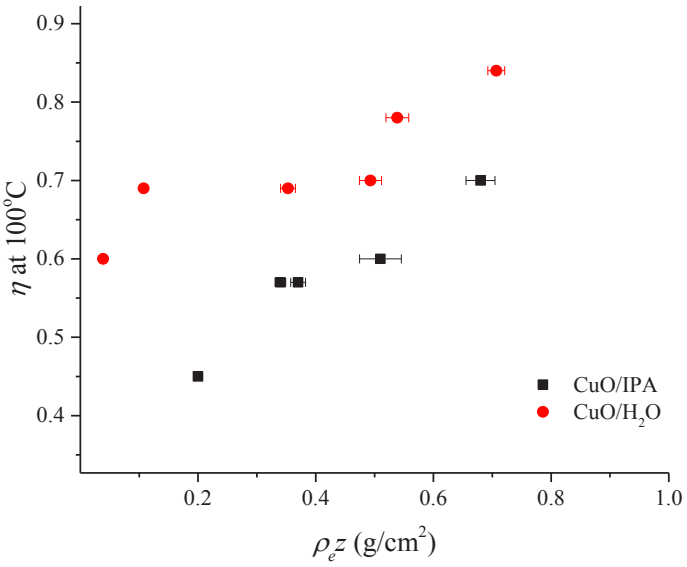

Figure 5.6: Efficiency of CuO tandem absorbers as a function o f deposition yield.

5.3. Protection of the deposit

5.3.1. Calcination

The calcination of the EPD deposits could act as a post deposition process to consolidate the deposit and result in a compact and dense film. On the other hand, calcination in an Argon atmosphere around the decomposition temperature of PEI could result in transformation of the polymer into carbon content. As a result, the presence of carbon is expected to enhance the calculated absorption value (α) of the tandem absorber and will prevent the degradation of the tandem absorber with time [1-3].

For that, two CuO/PEI deposits were prepared by EPD at 2V.cm^{-1} for a deposition time of 2 hours from 0.05 wt % CuO added to 0.019 g/cm^3 PEI solution at pH=9. After EPD, the deposits were left to dry overnight at room temperature then placed in a tubular oven under Ar atmosphere at 400°C for 1 hour at a rate of 3°C/min. Then the oven was left to cool down to 25°C before removing the sample. The total %R curve and picture of the deposits with and without calcination are shown in Figure 5.7. It could be observed that the deposit becomes darker in color which is due to the transformation of the polymer into carbon. On the other hand, the total reflectance decreases for the whole spectrum and the absorption edge wavelength (cut-off, λ_c) shifts from 0.560 µm into 1.8 µm as a result of calcination. The

calculated α and εincreases from 0.85 and 0.07 to 0.95 and 0.16 resulting in efficiency increase from 0.80 to 0.87.

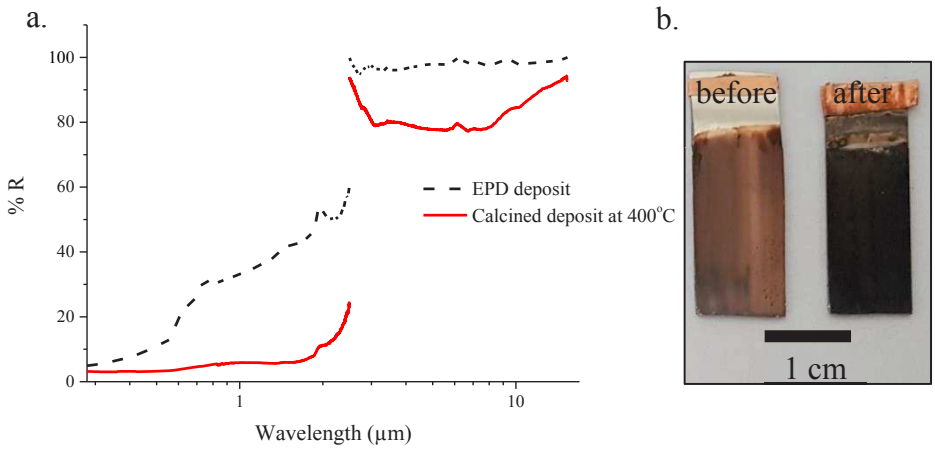

Figure 5.7: CuO/PEI/PtSi wafer deposit before and after calcination. b) Picture of CuO/PEI/Pt Si wafer tandem absorbers obtained by EPD before and after calcination.

The analysis of the cross-section of the deposit by SEM before and after calcination shows a variation in the morphology of the deposit (see Figure 5.8). The thermal treatment has resulted in the dilation of CuO and Pt layer and deformation in the substrate. The composition of the deposit was then analyzed by EDS, before and after carbonization (see Figure 5.9). The EDS spectrum of CuO/PEI deposit without calcination shows the presence of Cu and oxygen in the upper layer, Pt and Ti in the middle layer, and Si in the lower layer. While in the EDS spectrum of the calcined deposit, Cu and Si are present in all the layers especially in the middle ones. This shows that Cu, due to thermal treatment, was diffused into the Si wafer through the Pt/Ti layer. This effect has resulted in the dilation of the CuO/PEI deposit observed in the SEM cross-section.

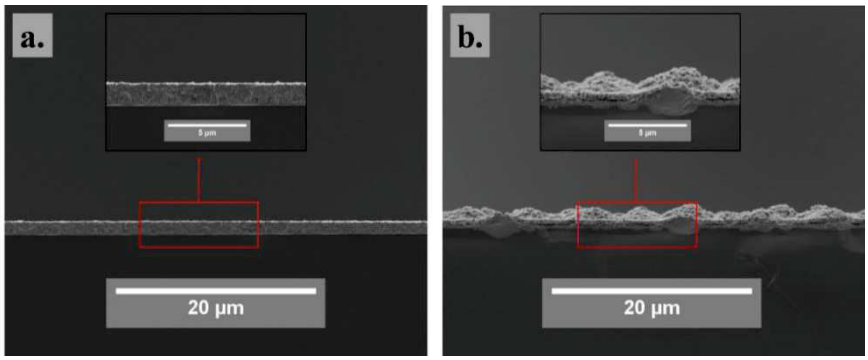

Figure 5.8: SEM cross-section of CuO/PEI/Pt Si wafer deposit a) with no calcination, b) with calcination.

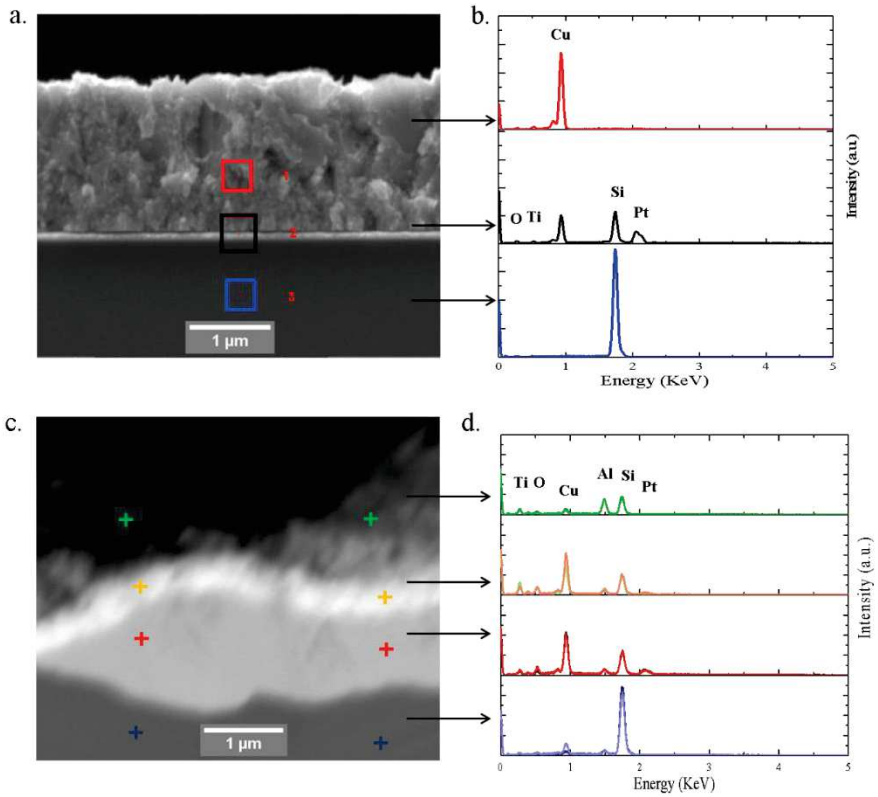

Figure 5.9: EDS of the SEM cross-section with and without calcination.

The XRD scan of CuO/PEI/Pt Si wafer of the as deposited and carbonized is presented in Figure 5.10. Except for the Si (004) peak corresponding to the Si wafer, new diffraction peaks are observed at 19.8°, 24.4°, 26.1°, 28.1 and 31.6° as well as other intense peaks at 42.8° and 45.13°. The peaks between 36 and 42 corresponding to Pt of the substrate and to the Cu in the deposit (at 43.30° and 50.62°) have also disappeared. The absence of a broad peak at 26° shows that carbonized polymer was not transformed into amorphous carbon and the absence of Pt film peaks and Cu confirms a major change in the structure and identity of the deposited material suggesting that the thin layer of Cu (as a result of reduction of CuO by H_2 gas arising by the carbonization of PEI) originally deposited to the Pt Si wafer is diffused into the Pt layer and Si wafer layer creating a cermet of Cu-Pt-Ti-Si.

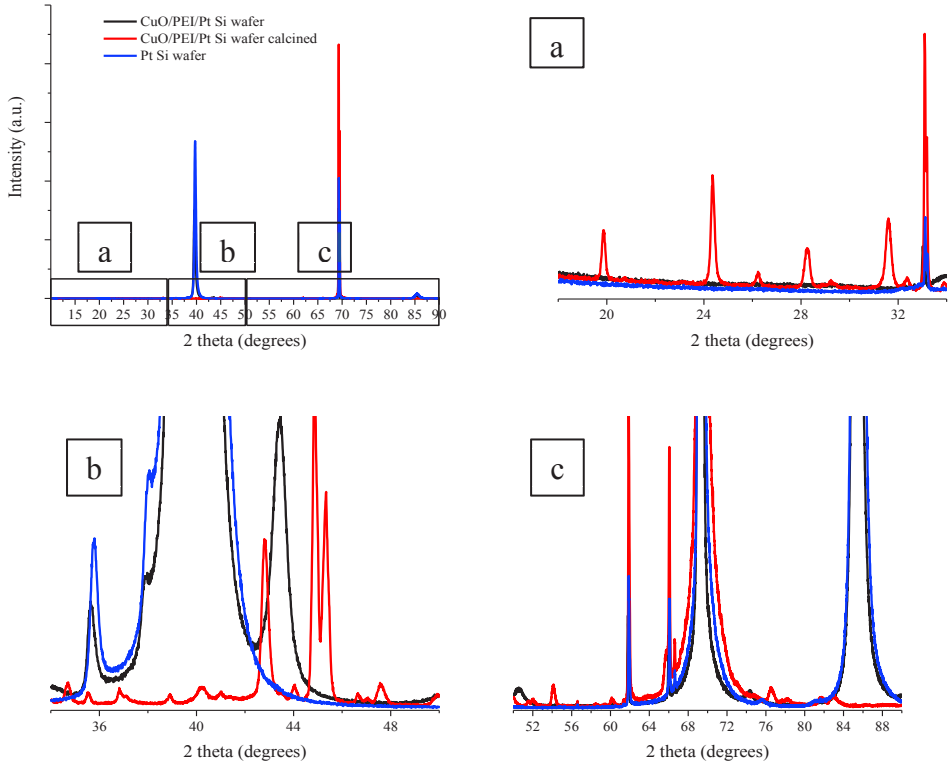

Figure 5.10: XRD scan of the substrate and tandem solar absorber before (black) and after (red) calcination.

As a conclusion, the calcination presents a potential post-deposition step that ameliorates the spectral selectivity of the deposit by increasing the calculated α value. But this step, at these calcination conditions, has also showed to modify randomly the chemical composition and the morphology of the deposit. Thus, a more adequate study should be done in the future to find the optimum calcination temperature that could be applied in order to transform only the PEI into carbon avoiding the diffusion of the Cu content into the substrate. In other cases, if the temperature is found to be the suitable temperature to be applied an anti-diffusion layer should be deposited on the substrate prior to the deposition. Finally, this step could present an innovative approach to form other dielectric films by EPD.

5.3.2. Anti-reflection layer

To reduce optical losses and enhance the durability of the absorber, various solar collectors employ transparent cover plates such as glass or plastic, and in a number of applications coatings which are highly reflecting in the infrared but transparent in the solar spectrum are used. These layers are defined as anti-reflecting layers such as SiO_2, ZnO, SnO_2, Al_2O_3. The deposition of thin layer of SiO_2 (100 nm) on the surface of the solar collector was

variously studied following a sol-gel route but never by EPD [4, 5]. Thus, the formation of a 100nm layer of SiO_2 was explored by EPD.

Setup

Several CuO/PEI deposits were formed on Pt Si wafer by EPD for a deposition time of 2 hours and $E=2V.cm^{-1}$. Then the deposit was left to dry for at least two days. On the other hand, 0.1wt % and 1 wt% of SiO_2 were prepared from LUDOX AS (24.4 nm), TM (23.8 nm) and HS (12 nm) suspensions by dilution in NaOH solution of pH=9 followed by stirring overnight. The LUDOX suspensions are known for their high stability and very low polydispersity (PDI=0.1). The LUDOX TM and HS have the same counter cation being sodium while the LUDOX AS has ammonium counter cation.

Then, 25 mL of SiO_2 suspension in request was poured into 25 mL beaker. A clean Pt Si wafer (CE), CuO/PEI/Pt Si wafer (WE) and Ag/AgCl (RE) were dipped and connected to the power supply. It is important to mention that SiO_2 suspensions are negatively charged, thus the CuO/PEI deposited substrate is placed at the anode and consequently anodic EPD will be performed.

For the deposits formed by EPD due to the difference in potential between different metallic substrates, same set-up was formed but without the application of an electric field. The deposition electrode was dipped in the SiO_2 solution, then removed at the same deposition time used for real EPD. Then the obtained deposits were left to dry at room temperature.

Effect of SiO_2 as antireflection layer

The total reflectance of the CuO/PEI/Pt tandem absorbers in the presence and absence of SiO_2 layer added by EPD and dip coating are presented in Figure 5.11 and Figure 5.12, respectively. It is observed that the presence of SiO_2 layer decreases the total reflectance of the tandem absorbers in all cases.

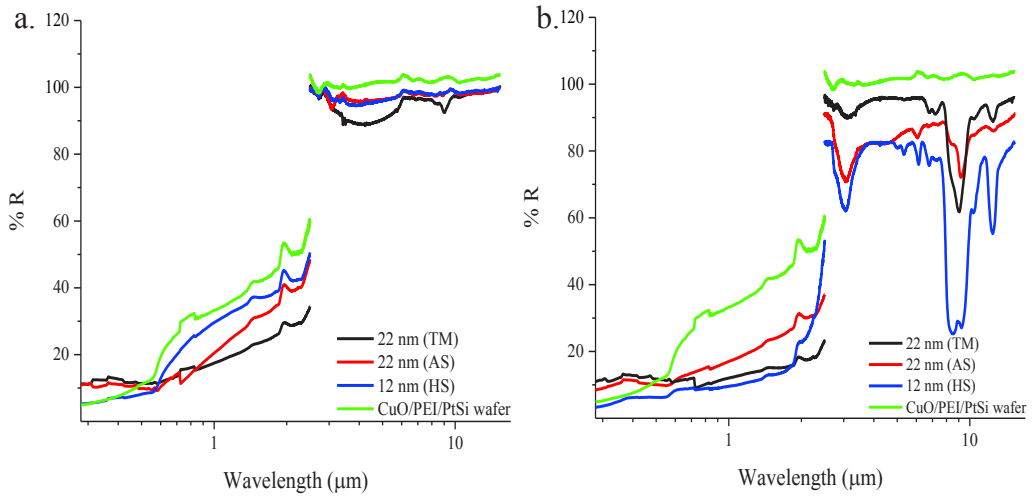

Figure 5.11: Total reflectance (%R) of deposits with SiO_2 layer added by EPD for E=2V.cm^{-1} and t=10 seconds: a) 0.1 wt% SiO_2, b) 1 wt% SiO_2.

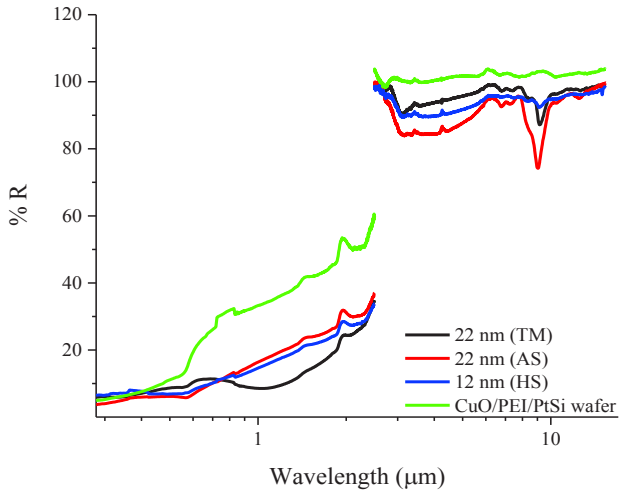

Figure 5.12: Total reflectance (%R) of deposits with SiO_2 layer added by EPD at no pplied electric field.

The SEM cross-section of the tandem solar absorbers shows a contrast between CuO layer and the top layer of SiO_2 (see Table 5.3). The increase in % wt of SiO_2 from 0.1 into 1 wt% resulted in the deposition of higher amount of SiO_2 and in the case of LUDOX HS a thick layer based of gel formed around the substrate. However, for the dip results, we have observed a difference in the morphology of the formed films when comparing different type of LUDOX used. LUDOX TM has showed to form the most homogeneous thin film of SiO_2.

Table 5.3:SEM cross-section of CuO/Pt Si wafers tandem absorbers with SiO coatings.

EPD	SiO_2 (24.4 nm)	SiO_2 (23.2 nm)	SiO_2 (12 nm)
0.1 wt% SiO_2 E= 2 V.cm^{-1} t= 10 s	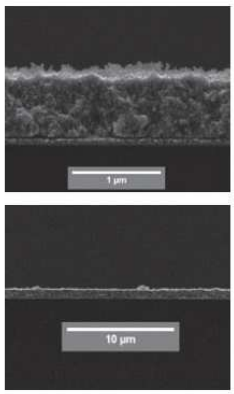	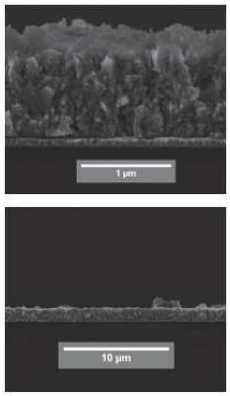	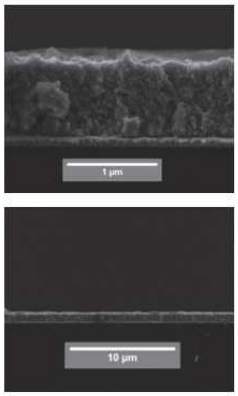
1 wt% SiO_2 E= 2 V.cm^{-1} t= 10 s	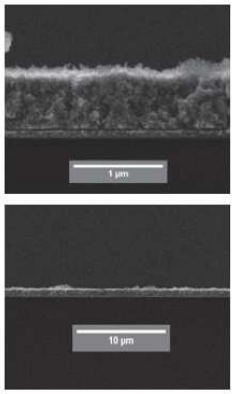	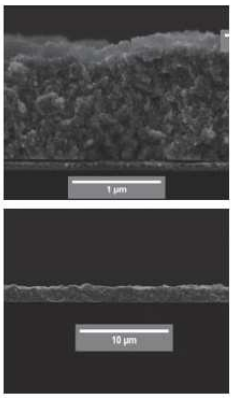	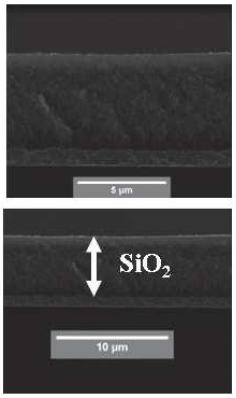
Dip	**SiO_2 (24.4 nm)**	**SiO_2 (23.2 nm)**	**SiO_2 (12 nm)**
1 wt% SiO_2 E= 0 V.cm^{-1} t= 10 s	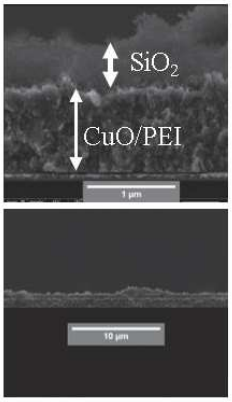		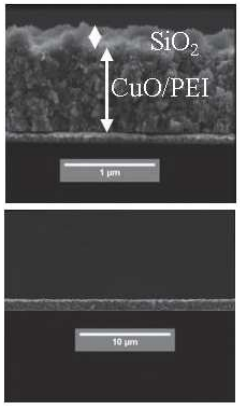

The measured thickness and calculated α, ε, and η are summarized in Table 5.4. The highest η was reported for the SiO_2CuO/Pt tandem solar absorbers obtained from a dip of LUDOX TM SiO_2 suspensions. It is also observed that for LUDOX HS and TM where the only difference is in the size of the nanoparticle, the absorptance is higher for larger size nanoparticles.

Table 5.4: Spectral Spectral selectivities of tandem absorbers and thickness of SiO2 layer.

Deposition electrode	CuO/PEI	CuO/PEI/SiO_2 (24 nm)	CuO/PEI/SiO_2 (23.2 nm)	CuO/PEI/SiO_2 (12 nm)
EPD 0.1% SiO_2 E=2 $V.cm^{-1}$, 10 secs				
Thickness (nm)	900 ± 100	121±35	~20	~12
α	~ 0.87	0.84	0.85	0.80
ε	0.04-0.06	0.08	0.06	0.11
η	~0.84	0.80	0.82	0.75
EPD 1% SiO_2 E=2 $V.cm^{-1}$, 10 secs				
Thickness (nm)	900 ± 100	150±20	93±22	5375±55
α	~ 0.87	0.85	0.88	0.91
ε	0.04-0.06	0.16	0.14	0.34
η	~0.84	0.77	0.81	0.74
EPD 1% SiO_2 E=0 $V.cm^{-1}$, 10 secs				
Thickness (nm)	900 ± 100	580±170	162 ± 13	185 ± 42
α	~ 0.87	0.88	0.90	0.88
ε	0.04-0.06	0.1	0.04	0.06
η	~0.84	0.83	0.88	0.85

As a conclusion, an anti-reflection layer of SiO_2 is deposited on the tandem CuO/Pt absorber by EPD at E=2 and 0 $V.cm^{-1}$. The layers deposited by EPD at $2V.cm^{-1}$ were not enough homogeneous and did not enhance the efficiency of the absorber. For higher concentration the SiO_2 suspension was destabilized during EPD and a gel was formed. While SiO_2 layers of 100 nm were successfully deposited by EPD at E=0 $V.cm^{-1}$ for only LUDOX TM and HS. Both presented a slight enhancement in the efficiency value but the most regular film structure was obtained using LUDOX TM of size ~24 nm, which raised the calculated α to 0.90 maintaining a low ε of 0.04. Thus, in order to deposit an anti-reflection layer of SiO_2 on the CuO/Pt Si wafer tandem, dip coating is employed using a 1% suspension of SiO_2 LUDOX TM nanoparticles for a deposition time of 10 secs.

5.4. EPD in Mixed Solvent

In order to avoid the tremendous effects of water electrolysis during EPD, a portion of an organic solvent as co-solvent could be added. This addition also decreases the dielectric constant of the medium which decelerates the speed of migration of charged particles. This facilitates the diffusion of gas bubbles formed at the vicinity of the electrode instead of their incorporation in the deposit. In Chapter 4, we have observed that the H_2 gas formed at the cathode leads to the surface reduction of Cu^{2+} into Cu (0) or Cu_2O, which prevents the formation of pure CuO thin films. Thus CuO/PEI suspensions were prepared as before but in water/IPA suspensions by using different proportions of IPA with respect to H_2O (see Table 5.5). The pH of the suspension was fixed to 9 by the addition of few drops of HNO_3 or NaOH.

Table 5.5: Prepared suspensions composition and EPD conditions.

Experimental conditions	H_2O: IPA	Stability
[CuO]= $5x10^{\wedge-4}$ g/cm^3 [PEI]=0.019 g/cm^3 E=2 $V.cm^{-1}$ t= 30 or 120 mins	0:100	Non-stable
	25:50	Stable
	50:50	
	75:25	
	100:0	

First, the stabilization of this suspension in the absence of water was not achieved which shows that the presence of water is crucial for the stabilization. The SEM micrographs and pictures of the obtained deposits are presented in Table 5.6. The presence of IPA in the suspension has showed to have a direct effect on the morphology and micro-structure of the deposits.

Table 5.6: SEM top-view of CuO/PEI deposits obtained from H2O: IPA suspension.

IPA (v/v%)	75	50	25	0
t= 30 mins	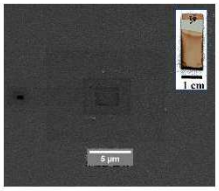	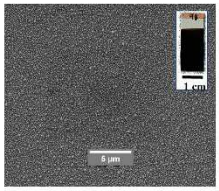	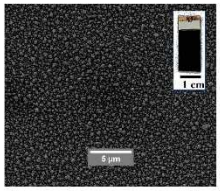	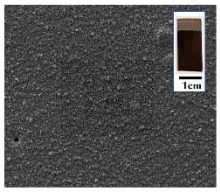
t= 120 mins	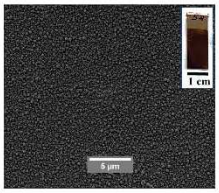	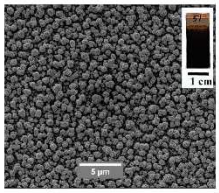	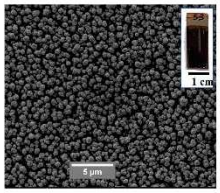	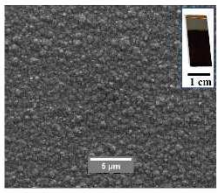

Table 5.7 shows the SEM cross-sections of the obtained deposits which allows the measurement of deposits average thickness (presented in Figure 5.13). The increase of amount of IPA decreases the thickness of the deposit which is expected. Since, as the amount of IPA increases the dielectric constant of the suspension decreases thus, reducing the electrophoretic mobility of the charged nanoparticles explaining the decreasing trend in thickness obtained with increasing amount of IPA.

Table 5.7: SEM cross-section of CuO/PEI deposits obtained from H_2O: IPA

IPA (v/v%)	75	50	25	0
t= 30 mins	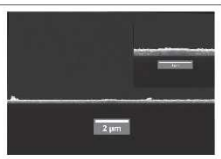	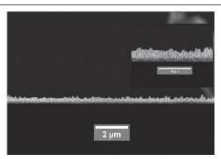	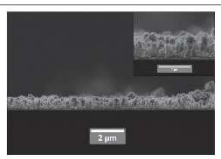	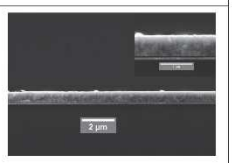
t= 120 mins	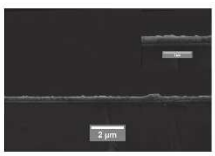	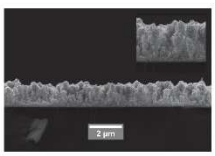	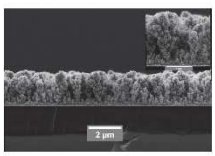	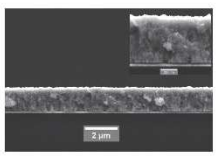

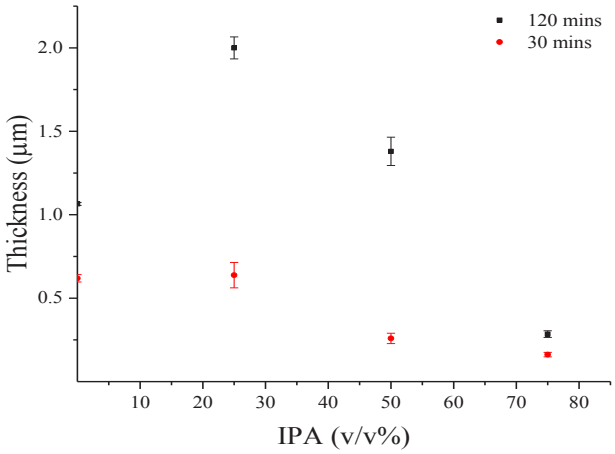

Figure 5.13: Average thickness obtained from SEM cross-section versus volume fraction (v/v%) of IPA for a deposition time of 30 and 120 mins.

Figure 5.14 a and b show the total reflectance of the obtained deposits at 30 and 120 mins. It is obvious that, as the thickness increases with deposition time, the total reflectance decreases when comparing a and b. The highest % R is reported for the 75 vol % suspension of IPA followed by 50 and 25 vol %, respectively.

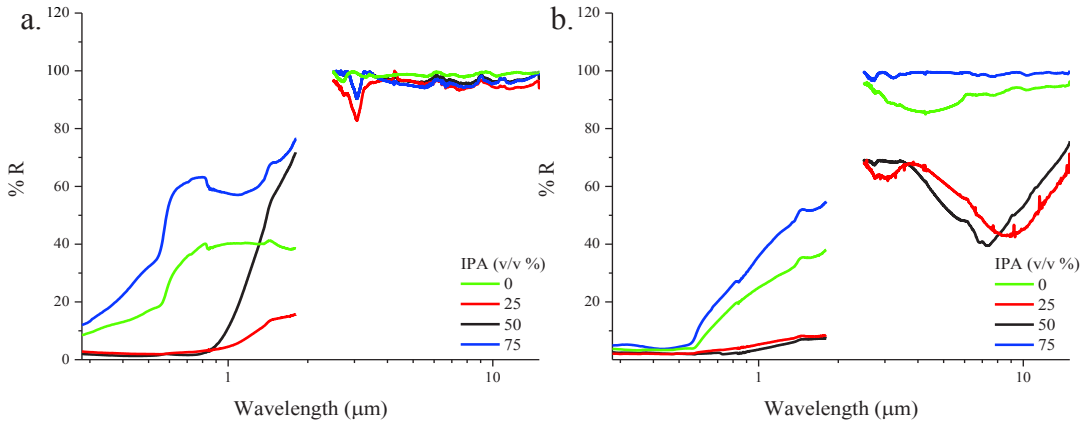

Figure 5.14: %R of the EPD deposits for a deposition time of: a)30 and b)120 mins

The calculated α, ε, and η are presented in Figure 5.15. Deposits formed at 30 mins are found to have similar emittance of ~0.01. On the other hand, the surface roughness and texturing plays an important role in allowing higher amount of light to be absorbed, which allows α to attain higher values for a mixed solvent compared to deposit obtained from pure water. An interesting observation is the deposit obtained from a suspension of 25 vol % IPA and 0 vol% IPA or in the absence of IPA, for a deposition time of 30 mins. Both has a similar

thickness of 0.638 and 0.619 µm, respectively but a different surface roughness. The former has a RMS surface roughness of 90 nm while the latter RMS=20 nm. A higher α of 0.95 is obtained for the deposit of higher roughness thus in the presence of 25 vol% of IPA. For deposits obtained at 120 mins the increase in the thickness results in an increase in the emittance value. On the other hand, the deposit obtained at 30 mins for 25 vol % of IPA attains the highest efficiency of 0.94 compared to the others.

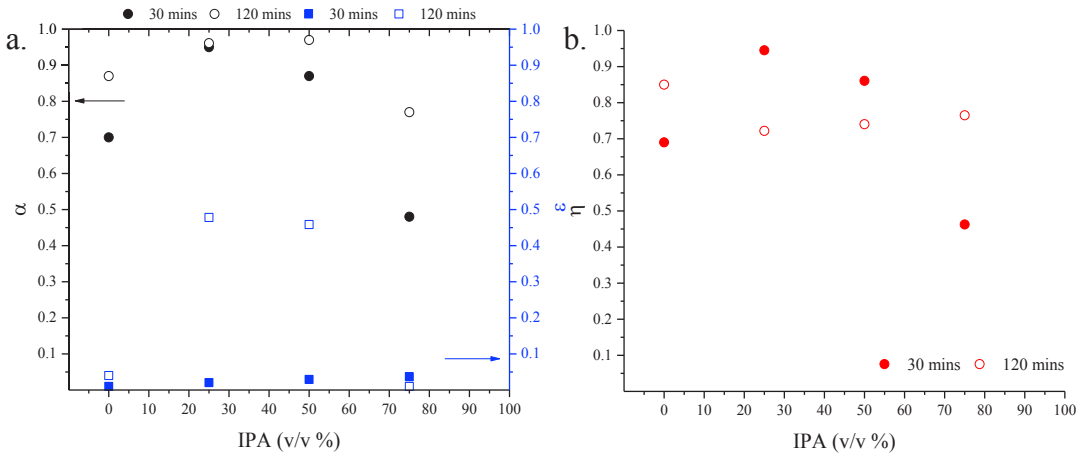

Figure 5.15: Calculated *α*, *ε* and η of the obtained deposits.

Thus, the addition of IPA as a co-solvent along with the water in the suspension decreased the phenomenon of water electrolysis. But the surface roughness of the deposit has varied as well. This surface texturing has enhanced the efficiency of the tandem absorber. However, a more adequate study is required in order to understand the mechanism of deposition and explain the surface texturing obtained.

Conclusion

Tandem solar absorbers of CuO on metallic substrates have been successfully obtained by EPD having an η ranging between 0.7 and 0.84. Deposits prepared from water-based suspensions prove to be more suitable as tandem solar absorbers since they possess higher efficiency and substrate adhesion compared to IPA based suspension. Carbonization of CuO/PEI deposits shifts the absorption spectrum to higher wavelengths resulting in higher α of 0.95 but higher emittance as well of 0.17 leading to an η of 0.86. Another effect of carbonization is the diffusion of Cu into the Pt-Ti-Si layer forming a cermet which opens the door toward new applications for EPD.

On the other hand, an anti-reflection layer of SiO_2 was added to CuO/PEI deposit by EPD. Forming a thin layer of SiO_2 by EPD at $2V.cm^{-1}$ was prohibited by the destabilization of LUDOX-SiO_2 suspension beside the electrodes leading to the formation of a thick layer of gel of SiO_2. While at E= 0 $V.cm^{-1}$, a 100-nm layer of SiO_2 was deposited and the efficiency of the tandem increased to 0.88. Finally, the surface roughness of the deposit has showed to increase the efficiency of the tandem attaining 0.96. This was achieved by the addition of 25 v/v% of IPA to water as a co-solvent to decrease electrolysis reaction occurring at the cathode. This has also changed the physiochemical properties of the suspension affecting largely the surface roughness as well. However, the physicochemical properties, mechanism of the deposition and reproducibility of such system is always in question and need more exploration.

References:

[1] D. Katzen, E. Levy, Y. Mastai, Applied Surface Science, 248 (2005) 514-517.

[2] G. Katumba, L. Olumekor, A. Forbes, G. Makiwa, B. Mwakikunga, J. Lu, E. Wäckelgård, Solar Energy Materials and Solar Cells, 92 (2008) 1285-1292.

[3] A. Charlot, O. Bruguier, G. Toquer, A. Grandjean, X. Deschanels, Thin Solid Films, 553 (2014) 157-160.

[4] T.K. Boström, E. Wäckelgård, G. Westin, Solar Energy Materials and Solar Cells, 84 (2004) 183-191.

[5] H.K. Raut, V.A. Ganesh, A.S. Nair, S. Ramakrishna, Energy & Environmental Science, 4 (2011) 3779-3804.

[6] L.C.-K. Liau, Y.-P. Chen, Colloids and Surfaces A: Physicochemical and Engineering Aspects, 429 (2013) 121-128.

General Conclusion

The work of this PhD was dedicated to form CuO/metallic substrate absorber/reflector tandem for low temperature photothermal applications using EPD.

The interest in using EPD was due to its versatility and the possibility of controlling the thickness and the composition of CuO thin layer by varying process parameters such as deposition time and applied electric field.

Traditionally CuO tandem absorbers were processed by several wet deposition techniques that involved ionic solutions of Copper (II) salts as starting precursors. These processes also involved an additional post-deposition thermal treatment essential to form the final CuO coating. This leads to the formation of Cu_2O or CuS that has lower absorptance or promote faster degradation of the absorber.

The EPD of CuO could be performed only if a suitable charged and stable suspension of CuO is available. The few studies made on the stabilization of CuO nanoparticles necessitate a better understanding of use of suitable stabilizing agents and stabilizing medium.

In an attempt to better stabilize CuO in IPA, $Mg(NO_3)_2.6H_2O$ was used as a positively charging agent and a binder material for CuO. A fundamental study was then performed by varying the deposition time and the applied electric field during EPD using Au/metallized Si wafer. The effective density of the deposited layer was calculated using Hamaker equation. The thickness of the deposit increased linearly with the deposition time and applied electric field. The density of the coating increased with the applied electric field, varying between 0.35, 0.49 and 1.69 g/cm^3 for 5, 10, 50 $V.cm^{-1}$, respectively.

On the other hand, the complete stabilization of CuO nanoparticles was successfully achieved in water using poly-ethylenimine as a cationic stabilizing agent allowing electro-steric stabilization. First, as a complexing agent for surface Cu^{2+} of CuO and second as a positively charging agent for pH working range between 3 and 11. The kinetics of EPD was then studied at pH=9 for different applied electric field and deposition time using Pt/metallized Si wafer. At $2V.cm^{-1}$the density of the coating was estimated to be 5.7 g/cm^3 using Hamaker equation and then more precisely measured using EDS-X-film software to be 5.9 g/cm^3.

Finally, both systems were found reproducible and applicable to different commercially used metallic substrates (Cu, SS, Al). The CuO tandems obtained from

CuO/water suspension showed to be more regular and uniform compared to the coating obtained from CuO/IPA suspension. The efficiency of the latter was 0.84-0.87 while that of the former ~0.7. The water-based systems showed better adhesion to the substrate and higher efficiency, thus presented a more promising system for further amelioration. On one hand, addition of an antireflective layer of SiO_2 of 100 nm thickness showed to increase the efficiency up to ~0.9. On the other hand, residual carbon was added to the coating by the carbonization of the deposited polymer which also shifted η up to ~0.9.

As a conclusion, CuO was successfully stabilized by PEI through electro-steric stabilization. The high stability of CuO/water suspension allowed the production of highly selective and efficient CuO tandem solar absorber of controlled thickness by EPD.

Table of Figures

Table of tables